CONTROL STRATEGIES FOR MICROGRID SYSTEM OF SYSTEMS

BY

MOHAMMED SAIF UR RAHMAN

A Thesis Presented to the

DEANSHIP OF GRADUATE STUDIES

KING FAHD UNIVERSITY OF PETROLEUM & MINERALS

DHAHRAN, SAUDI ARABIA

In Partial Fulfillment of the

Requirements for the Degree of

MASTER OF SCIENCE

In

SYSTEMS ENGINEERING

APRIL 2015

KING FAHD UNIVERSITY OF PETROLEUM & MINERALS

DHAHRAN- 31261, SAUDI ARABIA

DEANSHIP OF GRADUATE STUDIES

This thesis, written by **MOHAMMED SAIF UR RAHMAN** under the direction his thesis advisor and approved by his thesis committee, has been presented and accepted by the Dean of Graduate Studies, in partial fulfillment of the requirements for the degree of **MASTER OF SCIENCE IN SYSTEMS ENGINEERING.**

Dr. ADEL F. AHMED
Department Chairman

Dr. MAGDI S. MAHMOUD
(Advisor)

Dr. SALAM A. ZUMMO
Dean of Graduate Studies

Dr. FOUAD AL-SUNNI
(Member)

17/5/15
Date

Dr. MOHAMMAD ALI ABIDO
(Member)

DEDICATED TO
MY PARENTS AND MY BROTHERS

ACKNOWLEDGEMENTS

All praise to Allah, the Cherisher and Sustainer of the worlds, none is worthy of worship but Him. Peace and blessings be upon the beloved Prophet (SAWS), the mercy for all creatures. A big thanks to King Fahd University of Petroleum and Minerals for giving me an ideal environment for research and learning. I would also like to thank the Deanship for Scientific Research (DSR) at KFUPM for financial support through research group project RG-1316-1.

I am extremely thankful to my thesis advisor Dr. Magdi S. Mahmoud for his continuous support and encouragement. I would also like to thank my thesis commitee members Dr. Fouad Al-Sunni and Dr. Mohammed Ali Abido for their time and valuable suggestions.

I am extremely obliged to thank my parents Mohammed Najeeb ur Rahman and Fazeelath Amina for their unrelenting support and love. Their encouragement has been instrumental in my research work and career. I would also thank my brothers Mohammed Ibaad ur Rahman and Mohammed Zaid ur Rahman for their constant support and love. The contributions of my family towards my career have been immense and an indispensable part of my life. I also owe many thanks to all my friends here at KFUPM, for their cooperation and help.

Contents

ACKNOWLEDGEMENTS **v**

TABLE OF CONTENTS **vi**

LIST OF TABLES **xi**

LIST OF FIGURES **xii**

Abstract (English) **xvi**

Abstract (Arabic) **xvii**

1 INTRODUCTION **1**

1.1 Distributed Generation Systems 1

1.2 Introduction to System of Systems (SoS) 3

1.3 A System of Systems Perspective 5

1.3.1 Microgrid as System of Systems 6

1.3.2 SoS Framework 7

1.3.3 Microgrid SoS Control Hierarchy 9

1.4 Thesis Motivation 11

1.5 Proposed Objectives 11

1.6 Thesis Outline 12

2 LITERATURE SURVEY **15**

2.1 Introduction 15

2.2 Overview of SoS Applications 16

2.3 Review of Microgrid Architectures and Models 17

2.4 Microgrid Components 20

2.4.1 Microgrid Central Controller 21

2.4.2 Microsources and Load Controllers 23

2.4.3 Microturbines 24

2.4.4 PV Solar Cell 27

2.4.5 Wind Turbine 29

2.4.6 Fuel Cells 32

2.4.7 Storage Devices 33

2.5 Control Methodologies for Microgrid 33

2.5.1 Multilevel Control 34

2.5.2 Consensus Control 35

2.5.3 Decentralized Control 38

2.5.4 Networked Control 40

3 Networked Control of Microgrid System of Systems 42

3.1 Introduction 42

3.2 Microgrid Islanded System Modeling 49

3.3 Networked Control System 53

3.4 Closed-Loop Stability Results 59

3.5 Application Example 1 67

4 Networked Control Approach for Distributed Generation Systems 75

4.1 Introduction 75

4.2 Modeling of the Microalternator-PV system 76

4.2.1 Microalternator 77

4.2.2 Photovoltaic system 80

4.2.3 Power conditioning unit of PV system 83

4.3 Integrated Microalternator-PV System Modeling 91

4.4 Modeling of Networked Control System 99

4.5 Application Example 2 103

5 Event Triggered Control of Wind Turbine With Control and Communication Optimization 113

5.1 Introduction 113

5.2 Wind Turbine Model 116

5.3 Control Design 122

5.3.1 ET LQG Controller 126

5.4 Event Condition 130

5.4.1 Optimization of γ Using Particle Swarm Optimization . 132

5.4.2 Particle Swarm Optimization 134

5.4.3 PSO Algorithm and Analysis 135

5.5 Application Example 3 138

6 Conclusion and Future Work 144

REFERENCES 148

VITAE **170**

List of Tables

1.1 Functional levels of microgrid SoS 9

1.2 Variables of microgrid SoS 10

3.1 Parameters of the microgrid system. 53

4.1 Integrated system parameters [126] 99

4.2 Pattern of p_k 100

4.3 Pattern of s_k 103

5.1 Parameter values 121

5.2 Comparative analysis 142

List of Figures

1.1 Microgrid SoS structure 6

1.2 System of systems framework for microgrids 8

1.3 Control structure for microgrid SoS 9

2.1 Microgrid architecture 21

2.2 Microgrid with distributed sources and loads 22

2.3 Significant blocks of a microturbine model 24

2.4 Equivalent circuit of generator and rectifier in a microturbine . . 25

2.5 Simple PV cell model 27

2.6 Wind turbine model 29

3.1 (right) Direct structure of a two layer NCS, (left) Hierarchical structure of a two layer NCS 47

3.2 Microgrid with multiple parallel connected DGs 49

3.3 Single line diagram of the islanded system consisting of multiple DGs 50

3.4 Microgrid networked controlled sos 55

3.5 Simulink screenshot of the control design implementation 69

3.6 d component of load voltage 71

3.7 q component of load voltage 72

3.8 d component of DG1 current 72

3.9 q component of DG1 current 72

3.10 d component of load current 73

3.11 q component of load current 73

3.12 d component of DG2 current 73

3.13 q component of DG2 current 74

3.14 d component of DG3 current 74

3.15 q component of DG3 current 74

4.1 Microalternator connected to grid 78

4.2 Model of PV cell 81

4.3 DC/DC converter configuration 84

4.4 Inverter model 86

4.5 Combined system 92

4.6 Simulink screenshot of the control design implementation 107

4.7 Rotor angle of the microalternator 107

4.8 Rotor speed of the microalternator 107

4.9 Internal voltage of microalternator along q-axis 108

4.10 Field voltage of microalternator along d-axis 108

4.11 Photovoltaic cell current 108

4.12 Voltage across DC-link capacitor 109

4.13 Inverter output current along d-axis 109

4.14 Inverter output current along q-axis 109

4.15 Coupling line current of the filter along d-axis 110

4.16 Coupling line current of the filter along q-axis 110

4.17 Capacitor voltage of the filter along d-axis 110

4.18 Capacitor voltage of the filter along q-axis 111

5.1 Wind turbine system 117

5.2 Event triggered system block diagram 123

5.3 Timing diagram illustrating sampling times for ET systems with random transmission delays. 124

5.4 State response of the system 139

5.5 Sampling intervals and events 140

5.6 Normalized cost curves 140

5.7 State response of the system 141

5.8 Sampling intervals and events 141

5.9 Normalized cost curves 142

5.10 Optimized gamma (γ) 142

THESIS ABSTRACT

Name: Mohammed Saif ur Rahman.

Title: Control Strategies for Microgrid System of Systems

Major Field: Systems Engineering.

Date of Degree: April, 2015.

The microgrid has made its mark in distributed generation and has attracted widespread research. However, owing to the complexity of a microgrid system, the control design still remains a challenge. On the other hand, considering the applications of System of Systems (SoS) in a plethora of domains, and resemblance of microgrid to SoS characteristics, an intelligent SoS perspective is provided for microgrids in this thesis. A comprehensive review of microgrid architectures, models and control methodologies is compiled. A networked control methodology based on SoS is devised for the microgrid with multiple generation units acting as subsystems. An output feedback controller is designed to stabilize the system in presence of communication infractions such as packet dropouts and delays. The developed control design is applied to different models representing a microgrid. An event triggering scheme coupled with particle swarm optimization is also proposed for a wind turbine system in a microgrid. A comparative analysis highlighting the significance of optimization in event triggering sampling is also included. Effectiveness of the proposed control methodologies is illustrated through simulation results.

ملخص الرسالة

الأسم: محمد سيف الرحمن

عنوان الرسالة: استراتجيات السيطره للشكبه الدقيقه لنظام النظم.

مجال التخصص: هندسه النظم.

تاريخ الدرجه العلميه: ابريل 2015

شبكات القدره الدقيقه صنعت بصمتها في مجال المولدات الموزعه و اجتذبت بحوث على نطاق واسع. و لكن نظرًا لتعقيد شبكه القدره الدقيقه فإن تصميم المتحكم يشكل تحديًا. و من جهه اخرى، اخذ نظام كل النظم بعين الاعتبار في عدد كبير من المجالات و نظرا لتشابه خصائص الشبكه الدقيقه مع نظام النظم ، رؤيه لنظام نظم ذكي يتم نوفيره للشبكه الدقيقه. استعراض شامل للشبكه الدقيقه و تصنيف بنيها، نظم التحكم و كذلك النماذج. التحكم الشبكي على اساس نظام النظم وضعت للشبكه الدقيقه مع وحدات توليد متعدده تعمل كما الانظمه الفرعيه. تم تصميم متحكم ردود الفعل الخرج لاستقرار النظام في وجود قيود الشبكه مثل تأخير وصول الحزم و فقدها. المتحكم المطور يتعامل مع نمادج مختلفه من الشبكات الدقيقه. طريق حث اثار دمجت مع تحسين سرب الجسيمات لنظام تربينات الرياح في الشبكه الدقيقه. تحليل مقارن تسليط الضوء على أهمية الأمثل في الحدث اثار كما يتم تضمين أخذ العينات. فعالية منهجيات الرقابة المقترحة ويتضح من خلال نتائج المحاكاة.

Chapter 1

INTRODUCTION

1.1 Distributed Generation Systems

Economic challenges, technological advancements and environmental impacts are now demanding distributed generation in place of the conventional centralized generation [1]. Power operation companies are now confronted with unprecedented difficulties in terms of meeting load requirements, consumer satisfaction and environmental considerations. Thus, distributed generation has received good attention because of its potential to alleviate pressure from the main transmission system by supplying a few local loads [2]. The waste heat

generated from the fuel to electricity conversion is exploited by the distributed generation system with the help of microturbines, reciprocating engines and fuel cells to provide heat and power to the customers. This is accomplished by employing a small scale CHP (Combined Heat and Power) equipment. As a result of this, numerous applications of CHP have been used with significant progress [3].

Adding to the system Distributed Energy Sources (DER) like photovoltaic panels, wind turbines, energy storage devices such as batteries and capacitors, generators extracting energy from other renewable and controllable loads can provide momentous contributions to future energy generation and distribution. Another noteworthy feature is that the carbon emission is reduced to a large extent satisfying the commitment of many nations concerning decrease of carbon footprints [3]. However, the distributed generation faces technical issues regarding its connection to the intermittent renewable generation and feeble areas of the distribution network. Further, owing to the distinct behavior of the distributed generation unlike the conventional load, alteration in power flow results in problems. To introduce an intelligent electric network, the notion of the *smart grid* has recently emerged. Among desired characteristics of smart grid affecting the distribution level are improved reliability and sustainability. These attributes are mainly realized through microgrids which facilitate the effective integration of Distributed Energy Resources (DER) [4]-[8].

1.2 Introduction to System of Systems (SoS)

On another front, the gap between conventional technologies and the ever-growing needs of the society need to be bridged and hence development of systems engineering principles needs to undergo a transition. This is where, the extension of systems engineering to heterogeneous, interoperable and evolutionary System of systems becomes imperative. We need large scale, complex and integrated systems to tackle contemporary technical challenges and environmental concerns.

The concept of System of systems has opened up a new school of thought in Systems engineering.System of systems has emerged as a hot topic for research over the past few years. Although still in the infant stages, the concept of system of systems has managed to achieve substantial attention. It is a widespread notion now and has entered several domains including defense, IT, health care, manufacturing, energy and space stations and exploration to name a few [9], [10].

Many definitions have been proposed in the literature for System of systems, the more descriptive one being "systems of systems are large-scale integrated systems that are heterogeneous and independently operable on their own, but are networked together for a common goal" [11], where the goal is cost effectiveness, robustness and performance.

A System of systems comprises of numerous heterogeneous subsystems which are independently operable. These subsystems also possess the ability to continue

operating even if separated from the system of systems. Each constituent subsystem has no power over the other but communicate with each other through a network to effectively carry out tasks and collectively achieve a mission. However, one needs to understand the difference between large scale complex monolithic systems and actual system of systems. There exists certain characteristics or features which are unique to system of systems as given in [12]. The System of systems is expected to exhibit the following characteristics.

1. **Operational independence** : All the constituent systems within the SoS architecture operate independently and have no interference with other neighbor systems in their functionality.

2. **Managerial independence** : The constituent systems continue to operate on their own unperturbed by the SoS. In other words, they are responsible for their autonomous operation.

3. **Evolutionary development** : The SoS isn't designed as a single unit, and is rather flexible which can accommodate numerous new systems or do away with systems which are no longer necessary.

4. **Emergent behavior** : All the constituent systems function as a collective unit to accomplish a common objective, which cannot be achieved by a single component system.

5. **Geographic Distribution** : The distribution of the subsystems is sequential to facilitate flow of information among them.

1.3 A System of Systems Perspective

The microgrid has paved its way into distributed generation and looks promising for future aspects. It has the ability to respond to changes in the load, while decreasing feeder losses and improving local reliability. Basically designed to cater the heat and power requirements of local customers, it can serve as an un-interruptible power supply for critical loads.

However, conventional techniques and methodologies for designing microgrid systems seem inadequate. Further, due to the complex and dynamic nature of microgrids, we need contemporary and evolutionary SoS methods for the efficient design and operation of microgrids. Hence the motivation for using the SoS approach arises from the need to overcome prevalent issues in microgrid. The control system design is one of the most prominent of them. According to [13], there isn't still a consensus as to which architecture and control methodology is the best for microgrids. It is worth noting that the microgrid is a complex system comprising of variety of subsystems which are non-linear and possess strong cross-coupling between them. Therefore, analyzing the microgrid from an intelligent SoS perspective is the need of the hour. The SoS approach facilitates an unprecedented way of tackling problems in microgrids. Further, efficient control methodologies based on SoS must be established in order to solve the control design issue in microgrids.

1.3.1 Microgrid as System of Systems

The microgrid as described above is a complex system comprising of micro sources, loads and energy storage devices. Most of the elements are non-linear systems and possess strong cross-coupling between them. However, complexity is not the only thing that would be sufficient for the microgrid to qualify as a SoS, it must comply with other features of SoS presented by [12] mentioned in the previous section.

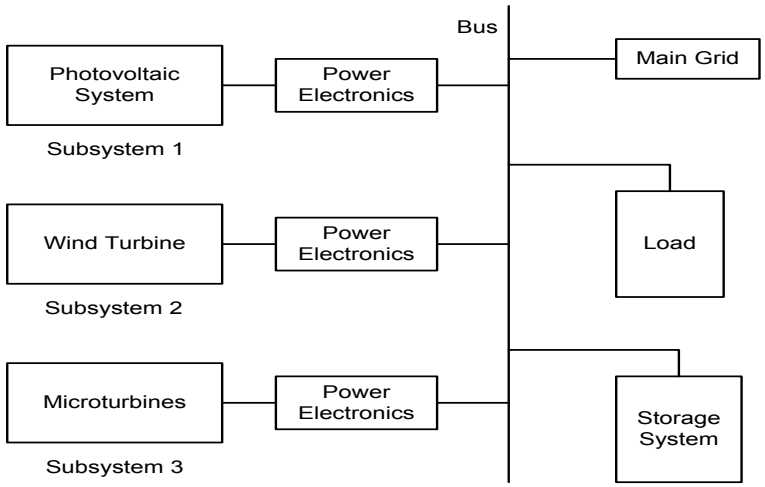

Figure 1.1: Microgrid SoS structure

The microgrid architecture as SoS is depicted in Fig. 1.1 As can be seen from the figure, the subsystems of the microgrid SoS are photovoltaic system, wind turbine and microturbine repectively. There could be other distributed generation units like fuel cells and unconventional sources of generation among the subsystems. The typical characteristics of microgrid SoS are

- The subsystems are independently operated and managed.
- The microgrid SoS is evolutionary. It can accomodate new subsystems when required and discard any of them from the structure.
- All subsystems are emergent. Collectively, they form the SoS which accomplishes the overall objective of supplying local loads and providing ancilary services to the main grid.
- The subsystems are geographically distributed.

Owing to the above characteristics which are similar to that of SoS, the microgrid falls perfectly on the lines of a SoS.

1.3.2 SoS Framework

A framework for the microgrid SoS is presented in Fig. 1.2 The objective of the Microgrid is best served when its constituent subsystems are well coordinated, organized and are able to communicate effectively among each other. This calls for a integrated framework which allows each subsystem to operate independently and establishes good communication among them to accomplish the desired goal. The emergent nature and geographic distribution of the microgrid makes it convenient to be architected in a System of systems framework. A

SoS framework addresses all the management, communication and control needs of a microgrid in a systematic manner.

The Microgrid Central Controller (MGCC) is connected to the main grid via a point of common coupling. All the constituent subsystems are integrated to the MGCC through a local control network. An electrical network and a communication network is used for the transfer of control signals and data collection respectively. Each subsystem has a dedicated local controller. These local controllers form the primary level of the microgrid SoS control hierarchy. Together, all the subsystems constitute the SoS framework.

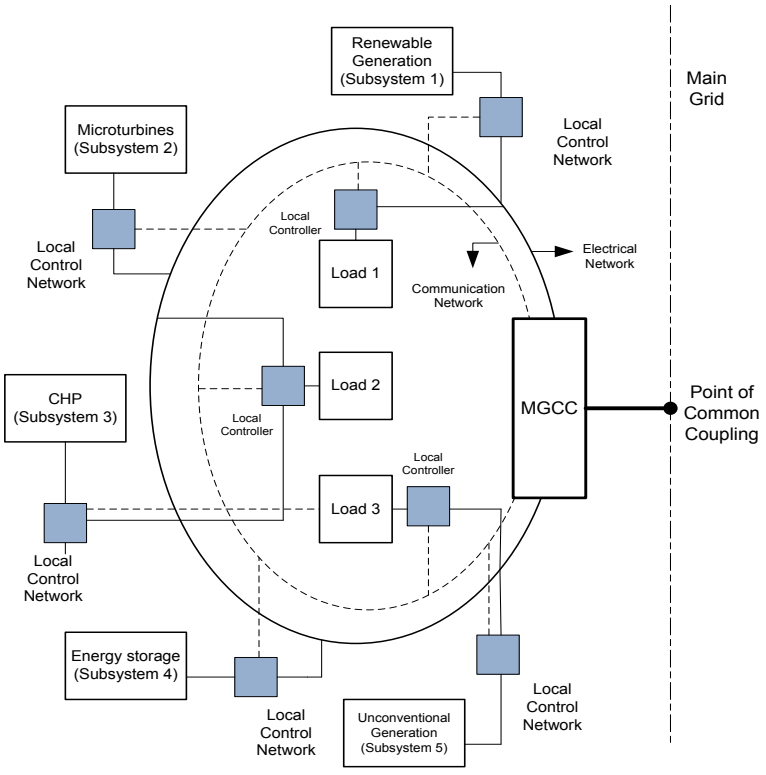

Figure 1.2: System of systems framework for microgrids

Table 1.1: Functional levels of microgrid SoS

Level	Function
Primary	Voltage and frequency stabilization after islanding
Secondary	Check for any deviations caused by primary control
Tertiary	Govern the power flow between microgrid and main grid

1.3.3 Microgrid SoS Control Hierarchy

The control design for microgrids is a major issue that needs attention. Based on the microgrid SoS structure and framework mentioned previously, a control methodology based on SoS is proposed for microgrids. A hierarchical control structure for the microgrid SoS is illustrated in Fig. 1.3. It can be seen that subsystems (DGs) of microgrid are integrated to the primary and secondary level of control. The tertiary level , however is connected to the SoS through a communication network. Table 1.1 summarizes the functions of each level. The variables for each level are described by Table 1.2.

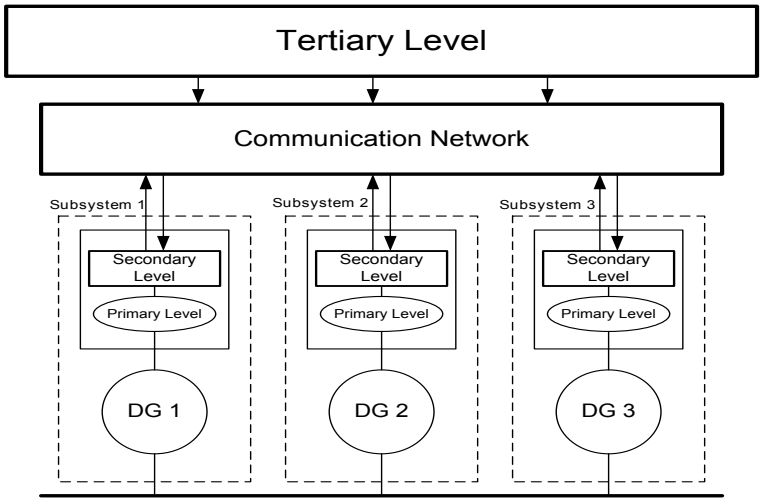

Figure 1.3: Control structure for microgrid SoS

Table 1.2: Variables of microgrid SoS

Level	Variable
Primary	Voltage (E), Frequency (ω) Power (P) Reactive Power (Q)
Secondary	Reference Voltage (E^{ref}) Reference Frequency (ω^{ref})
Tertiary	Reference Power (P^{ref}) Reference Reactive Power (Q^{ref})

1. **Primary Level**: The primary level is responsible to stabilize voltage and frequency after islanding. It consists of elementary control hardware. The current and voltage loops of the DERs are included in the control hardware.It adjusts the amplitude and frequency of the provided reference, voltage for instance. Further it also alleviates circulating currents which are a threat to the power electronic devices of DERs. It also distributes active and reactive power among DERs. Following an islanding event, a microgrid suffers from voltage and frequency instabilities due to power mismatch. Thus, voltages and frequencies need to be stabilized. This is accomplished by the primary level [7].

2. **Secondary Level**: The secondary level is responsible to compensate for any voltage or frequency deviation, which is caused by the primary level. It makes sure that the deviations are regulated towards zero, if any load or generation changes in the microgrid [14].

3. **Tertiary level**: The tertiary control level controls the flow of power from the microgrid to the main grid. This is accomplished by adjusting the frequencies and amplitudes of the DER voltages. It also ensures economically optimal operation of the microgrid [7].

1.4 Thesis Motivation

As mentioned above, the control design is a major issue in microgrids. Regulating voltages and frequencies of the microgrid during islanded operation and ensuring system stability is what needs particular attention. Therefore, devising control strategies for microgrid system is the primary aim of this research. Employing a networked control methodology, which incorporates communication infractions is the main task undertaken to address the aforementioned concerns in microgrids.

1.5 Proposed Objectives

The objectives of this thesis are as follows

- To present an extensive and in-depth survey of the published literature concerning modeling and control of both System of Systems and microgrid and to present a perspective of System of Systems on microgrid.

- To carry out modeling of the islanded system of microgrid constituting multiple distributed generation units and load from a System of Systems point of view.
- To devise control strategies based on System of Systems for controlling the islanded system of microgrid and elucidate the proposed control strategies through numerical examples and simulations in MATLAB and SIMULINK.

1.6 Thesis Outline

The thesis is organized as follows

Chapter 2

This chapter presents a survey of SoS applications in addition to an extensive review of microgrid architectures, models and control methodologies. Microgrid components are listed and mathematical modeling of components like alternator, solar cell and wind turbine is presented. Further, microgrid control is categorized into four main divisions and their applicability to microgrids with a SoS point of view is discussed.

Chapter 3

In this chapter, an output feedback networked controller is designed for a microgrid system of systems consisting of three distribution generation units as three subsystems supplying a load. The stability of the microgrid networked

system incorporating packet dropouts and delays is investigated in detail. The controller design is carried out and explained through theorems and LMIs. Simulation results are included to demonstrate the effectiveness of the proposed controller.

Chapter 4

An integrated system consisting of a microalternator and PV cell as two subsystems is considered in this chapter. Detailed modeling of individual subsystem and combined system is presented. Unlike a simple model considered in chapter 3, a comprehensive model of alternator and PV system having multiple components is proposed. The controller design of chapter 3 is implemented on two sets of integrated system with different parameter values. The controller performance is illustrated through simulation.

Chapter 5

In this chapter, an optimized event triggering scheme and a LQG controller design is proposed for a linearized wind turbine model in a microgrid system. The system is modeled as an event triggered system based on Asynchronous-sampled data system (ASDS) approach. Networked induced delays are considered in the communication channel. Particle Swarm Optimization (PSO) is employed to optimize control and communication cost, while reducing the event rate. Simulation results are included to elucidate the proposed controller design. A comparative analysis is also presented to demonstrate the significance

of optimization in event sampling.

Chapter 6

Finally, conclusions are drawn from the work carried out in the aforementioned chapters. The contributions of this thesis are highlighted and directions for further research and future extensions are discussed.

Chapter 2

LITERATURE SURVEY

2.1 Introduction

In this chapter, the first section deals with an overview of SoS applications. A review of SoS applications in various domains is presented. Then, a survey of microgrid architectures, models and control methodologies is done. Various control schemes proposed in the literature are included. Description and modeling equations for various microgrid components like microturbines, PV solar cell and wind turbine are presented. Finally, control methodologies for microgrid are classified into four broad categories, namely multilevel control, consensus

control, decentralized control and networked control and are surveyed.

2.2 Overview of SoS Applications

System of systems which was intially introduced and restricted to defense, has now entered a wide variety of domains. There can be a plethora of applications found in the literature in which the SoS methodology has been used. For instance, the application of system of systems framework to improve the capability of Unmanned Aerial Vehicles (UAVs) is presented in [15]. The system of systems approach to design an air defense weapon is discussed in [16]. In [17], the author proposes a system of systems method to enhance the effectiveness of the military system. In [18], the authors explore the application of a system of systems approach to supervise, control and diagnose subsea production and processing systems. Similarly, in [19], the authors demonstrate the use of SoS methodology and its effectiveness in production system design. The network architecture of the internet is anlayzed from a System of systems perspective in [20].

A System of systems approach for the enhancement of health care systems is presented in [21]. In [22], the authors illustrate a human health management system from a System of systems perspective. [23] puts forward the necessity of a SoS approach in aerospace industry. [24] utilizes SoS framework to assess the reliability of telecommunication networks. [25] presents the need for a SoS perspective to protect the environment from climate changes and its harmful

effects. [26] proposes a SoS framework to be implemented in the International Space Station (ISS). [27] views industrial automation from a SoS perspective.

2.3 Review of Microgrid Architectures and Models

The concept of Microgrid has received considerable attention owing to its potential to serve as an alternate power source, utilizing unconventional sources and supplying the most critical loads of the main grid in case of a network failure. Microgrids are low voltage networks or distributed energy systems which provide heat and power to a particular area by employing generators and loads. They have the ability to operate independently and isolate themselves from the main grid in case of a fault [28],[29]. If proper control techniques are implemented, they may improve the reliability of electrical energy supply. Microgrid comprises of microturbines, wind turbines, fuel cells, photovoltaic cells etc as sources of energy which are interfaced with the help of power electronic converters. All these units are connected to the main grid through a point of common coupling (PCC) and look as a solitary unit to the distribution network. No additional inertia is added to the system from the distributed generators.

However, because of this the power balance amid generation and load and the network frequency becomes complicated to maintain, especially when the microgrid is in islanded mode [13]. The islanded mode is an operating condition in

which the microgrid isolates itself from the main grid in case of a fault. However, the transition from the grid connected and the islanded mode must be stable [30]. If the microgrid is consuming or supplying power to the main grid before disconnection, a power imbalance occurs. This is compensated by the energy storage units because of the fact that the microsources have low inertia and slow dynamic response [31], [32].

A plethora of microgrid architectures can be found in the literature. Different layouts and models have been proposed to describe components of a microgrid. A review of the various architectures is provided in this section. A generalized structure of a microgrid is presented in [33]. The main features of a microgrid are discussed and the characteristics of control systems used are also described. In [34], microgrid design principles are discussed and a comprehensive review of microgrid is also presented. Application of industrial standards to microgrid is included, along with advanced control methods and storage systems. In [35], various structures of microgrid are presented. Ongoing demonstration projects in different countries are discussed. Layouts of the microgrid system in all these projects implemented worldwide are shown.

A review of numerous microgrid architectures and control methodologies is compiled in [36]. In [37], a survey is presented concerning the control of microgrids during islanded operation. Similarly in [38], a review is done on the various control strategies for voltage and frequency control of islanded microgrids. In [39], typical microgrid topology is considered and the modeling and control aspect is investigated in detail. In [40], a comprehensive review of the control methodologies and dynamic modeling of microgrid is presented. In [41], the modeling

and control aspect of microgrids is reviewed in detail. Recent developments in the area of microgrids is also presented.

In [42], a schematic of microgrid architecture is presented and modeling of microsources is explained. In [43], wireless configuration of microgrid is proposed, where communication exists among inverters. In [44], a multi-agent system approach is applied to the DERs in microgrids. The control architecture based on multi-agent systems is also designed and control strategies are proposed. An agent based microgrid management system is proposed in [45] and is applied to storage and generation devices connected to a microgrid. In [46], building blocks are considered as a part of control methodology for the microgrid and implemented on an experimental setup. The microgrid control issue is also addressed in [47].

In [48], a hierarchical control structure is proposed for a sample microgrid system. Further, modeling of a DG interface with the hierarchical control structure is also explained. In [49], a potential function based method is proposed for the control hierarchy in a microgrid. A generic schematic of a microgrid system is also presented. A distributed networked control scheme is proposed in [50]. In [51], a methodology to model the microgrid for small signal analysis is proposed in which the distribution is shared by power regulated and voltage-frequency regulated generation units. [52] focusses only on the secondary control layer of the microgrid. In [53] voltage source converter based model of a microgrid is considered and a novel control methodology is proposed. In [54], a unified model is proposed for a configuration based on voltage source converter for a microgrid and novel control techniques are devised. A comprehensive small signal state

space modeling is presented in [55]. [56] proposes hybrid modeling and predictive control for photovoltaic system and fuel cells which are integrated together as two generator subsystems. In [57], a hub model is considered for microgrid, based on which a predictive model is designed and optimized control is demonstrated. In [58], a networked controlled model is presented for multi-inverter systems. In [59], a power control scheme is implemented on a microgrid having distributed generation units with power electronic interface. In [60], robust control theory is applied to microgrids having gas turbines and batteries. Apart from these, many papers focus on the modeling of a microgrid and their control [61].

2.4 Microgrid Components

A generalized architecture of microgrid is shown in Fig. 2.1. As it can be seen from the figure the microgrid consists of Microgrid Central Controller (MGCC) or Central Energy Manager, microsource controllers, load controllers, microturbines, fuel cells,. battery storage, loads, renewable generators like the PV panel and a Combined Heat and Power (CHP) unit. The common coupling point can also be seen which connects the microgrid with the main grid. We shall now discuss each component to understand their role in the overall operation and performance of the microgrid.

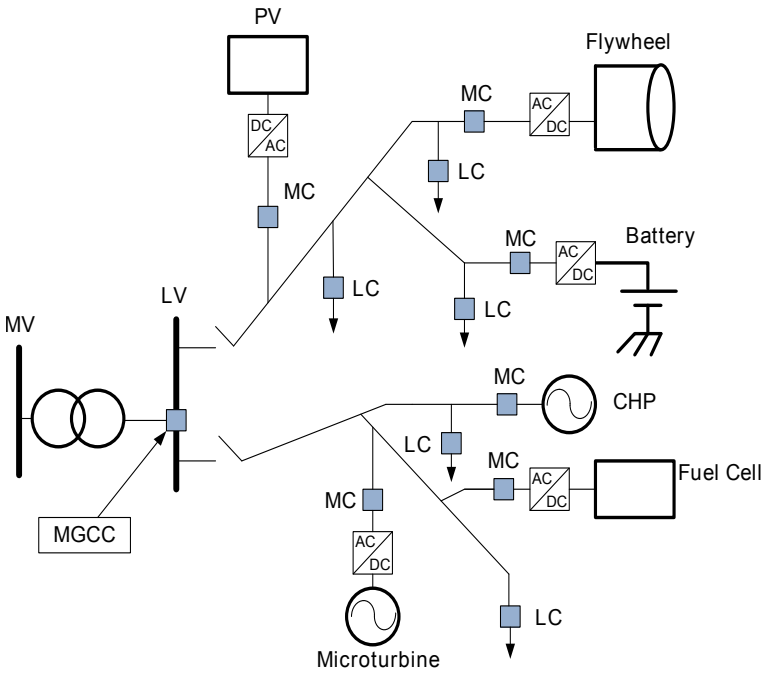

Figure 2.1: Microgrid architecture

2.4.1 Microgrid Central Controller

The Microgrid Central Controller (MGCC) acts as a connector between the medium voltage (MV) and low voltage (LV) side of the grid. The low voltage side of the grid is occupied by the microgrid and its components. The MGCC is responsible for allocating set-points to the load and micro source controllers and take care of the technical and management concerns of the microgrid. Also, it establishes communication with the distributed management system to perk up the operation of the medium voltage (MV) distribution system. Apart from this, the MGCC carries out numerous other functions including forecasting studies, scheduling of micro generation from an economic point of view, security as-

sessment and demand side management functions. All this is accomplished by collecting data from the loads and microsources. Additionally, during the islanded mode of operation of the microgrid, the MGCC acts as a secondary loop to facilitate a change in the output power control of micro-generators. Further, it must also devise interruption strategies and intelligently make use of the storage devices available to ensure reliability and reduce interruption time[62].

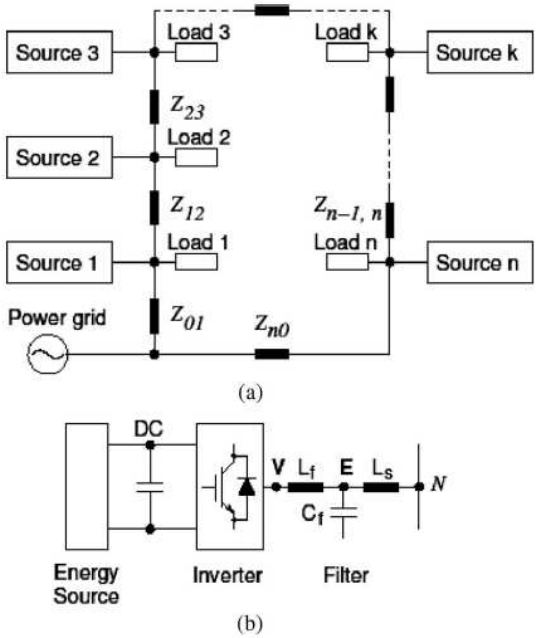

Figure 2.2: Microgrid with distributed sources and loads

Microgrids with distributed energy sources has a major feature in that the sources are dispersed over a wide area. These sources are tight to each other and to loads by a distribution network. In addition, the distributed microgrid may be coupled to the main power grid at some point as well. Fig. 2.2(a) shows a distributed microgrid structure connected to the main grid. It is also shown the microgrid line impedance ($Z_{01}, Z_{12}, ..., Z_{n1,n}$). The source is connected to the

microgrid distribution network by an inverter interface through a filter, that is, an LCL filter, shown in Fig. 2.2(b).

2.4.2 Microsources and Load Controllers

The microsource and load controllers are dedicated controllers for a particular component of the microgrid. By making use of local measurements of current and voltage, the microsource controller controls its assigned microsource. They are responsible to carry out load tracking and management, load control of the storage devices and economic scheduling functions. The primary functions of the microsource controller are regulation of power flow on a feeder where the operating points of the loads are varying, regulation of voltage at each microsource to accommodate the changing loads on the system and most importantly see that every microsource takes its load during islanded operation [63].

There exists several papers available in the literature where detailed modeling of various components of the microgrid can be found. For instance,[64] presents the modeling of microsources in a microgrid. Mathematical models are given for the diesel generator, batteries and wind turbine. Also, detailed models for fuel cells and microturbines having single shaft are available in [65], diesel generator having a prime mover, generator unit and governor is modeled in [66], [67].

In [68] and [69], the modeling of almost all significant components is explained including the PV systems, wind turbines, microturbines and fuel cells which

constitute the microsources. Further, basic models are also described for the power electronic interfaces. Similarly [70] deals with the detailed modeling of almost all components at steady state and studies their transient responses for input changes. The modeling of microgrid in islanding mode can be found in [71], [72], [73], [74].

2.4.3 Microturbines

Microturbines are single shaft, simple mechanical devices consisting of a generator which is a permanent magnet machine functioning at variable speed typically in the range of (50,000-100,000) rpm. The variable speed generation system is interfaced to the electrical system through power electronics. The microturbines are flexible to operate on different fuels such as natural gas and gasoline. Equipped with good reliability, they are also economical to afford [75].

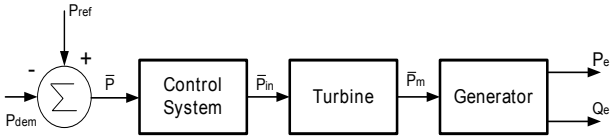

Figure 2.3: Significant blocks of a microturbine model

Fig. 2.3 shows the significant blocks forming a microturbine. The purpose of this simplified diagram is to perform the dynamic behavior analysis.P_{dem} is the demanded power, P_{ref} represents the reference power and P_{in} represents the power control variable which is to be applied to the turbine. The microturbine is equipped with recuperation, advanced materials and technologies enabling low

Nox emissions [76]. Further explanation and detailed modeling of the microturbines can be found in [77].

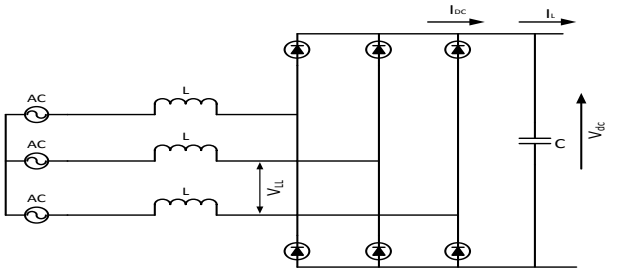

Figure 2.4: Equivalent circuit of generator and rectifier in a microturbine

Fig. 2.4 shows an equivalent circuit representation of the generator and the rectifier of the microturbine. Although the microturbine also consists of a recuperator, it has not been considered in modeling because it is used only for enhancing engine efficiency. The mathematical modeling presented below is taken from [70].

Considering the equivalent circuit in Fig. 2.4, the voltage induced in the generator terminal V_{LL} is given as

$$V_{LL} = K_v \omega \sin(\omega t) \tag{2.1}$$

where K_v is the voltage constant and ω is the electrical angular frequency. Now, the output DC voltage from the rectifier is given as [70]

$$V_{dc} = \frac{3}{\pi}|V_{LL}| - \frac{3\omega L}{\pi} I_{dc} \tag{2.2}$$

Substituting (2.1) in (2.2), we have

$$V_{dc} = \frac{3}{\pi} K_v \omega - \frac{3}{\pi} \omega L I_{dc} \tag{2.3}$$

Let us now define a no load voltage (DC) E as

$$E = \frac{3K_v}{\pi} \omega \tag{2.4}$$

Substituting in (2.2), we have

$$E = V_{dc} + \frac{3L}{\pi} \omega I_{dc} \tag{2.5}$$

Under the condition that the system does not suffer from any losses, the input power P_m can be defined as

$$P_m = V_{dc} I_{dc} \tag{2.6}$$

Substituting the value of V_{dc} from (2.3) in the above equation, we have

$$P_m = \frac{3}{\pi} K_v \omega I_{dc} - \frac{3}{\pi} L \omega I_{dc}^2 \tag{2.7}$$

For the same system, the mechanical shaft torque is given as

$$T_m = \frac{P_m}{\omega} = \frac{3}{\pi} K_v I_{dc} - \frac{3}{\pi} L I_{dc}^2 \tag{2.8}$$

And, the representation of mechanical part of the system is

$$\frac{d\omega}{dt} = \frac{1}{J_r}(T_m - T_t) \tag{2.9}$$

where J_r is the inertia of shaft and T_m, T_t are the mechanical and load torques respectively.

2.4.4 PV Solar Cell

Fig. 2.5 shows a representation of the solar cell through an electrical single diode model [78]. The inputs to the model are array voltage, ambient temperature and solar irradiance while the output is array current. Also, a lot of work has been done to design a comprehensive PV model by utilizing power electronic components. [79], [80].

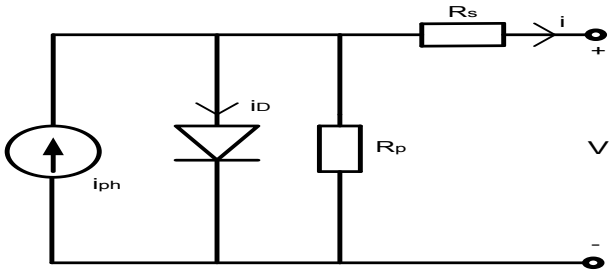

Figure 2.5: Simple PV cell model

Considering the equivalent circuit of the PV cell given in Fig. 2.5, the output current i is given by

$$i = i_{ph} - i_D - i_p \tag{2.10}$$

where i_{ph} is the current generated by light, i_D is the diode current and i_p is the shunt leakage current through resistance R_p. The open circuit voltage V_{oc} is given by

$$V_{oc} = V + iR_s$$

where V is the terminal voltage and R_s is the series resistance. Also, the diode current i_D is given by [81]

$$i_D = i_d[\frac{qV_{oc}}{A_{cf}KT} - 1] \tag{2.11}$$

where i_d is the saturation current of the diode, q is the electron charge, A_{cf} is the curve fitting constant, K is the Boltzmann constant and T is the temperature. Now the load current is expressed as

$$i = i_{ph} - i_{os}(exp[\frac{qV_{oc}}{AKT} - 1]) - \frac{V_{oc}}{R_p} \tag{2.12}$$

where

$$i_{ph} = \frac{G}{100}[i_{SR} + K_I(T - 25)]$$

and

$$i_{os} = i_{or}(\frac{T}{T_r})^3 exp[\frac{qE}{BK}(\frac{1}{T_r} - \frac{1}{T})]$$

Note that i_{os} is reverse saturation current of the PV cell, A, B are p-n junction ideality factors, G is solar irradiation, E is the band gap for Silicon, i_{SR} is the short circuit current at 25 degrees and 1000 W/m^2, K_I is the short circuit current temperature coefficient at i_{SR}, T_r is the reference temperature and i_{or} is the cell saturation current at T_r. More information about the modeling can be found in [70].

2.4.5 Wind Turbine

Fig. 2.6 represents a Squirrel cage induction generator based wind turbine. It has a conventional grid connected to a squirrel cage induction generator, which is connected to a rotor through a gear box. The function of the gearbox is to adjust the speeds of the rotor and generator, whose ranges are different. [82], [83]. There are different subsystems in the wind turbine that can be modeled separately. Out of which are the aerodynamic and mechanical subsystem whose modeling is presented below: The aerodynamic power is given by [84]

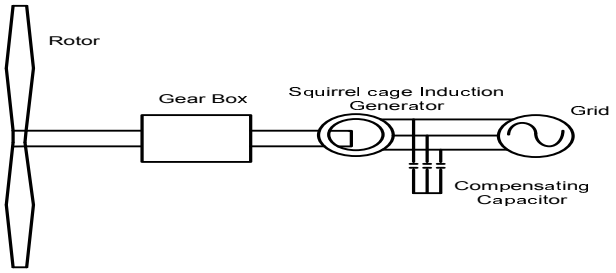

Figure 2.6: Wind turbine model

$$P_\alpha = \omega_r T_w = \frac{1}{2}\rho.A.C_p(\lambda,\beta).v_w^3 \tag{2.13}$$

where P_α is the aerodynamic power, ρ is the density of air, β is the pitch angle, A represents the rotor area, T_w represents the aerodynamic torque, ω_r expresses the blade rotating speed, λ is the tip speed ratio, v_w is the wind speed and $C_p(\lambda,\beta)$ is a dimensionless constant. Now, the mechanical subsystem can be simulated using three or six elastically connected masses. To represent the low-speed shaft torsional mode, a minimum of two masses are needed. Described below are the three mass equivalent state space equations of the model

$$\begin{aligned}\frac{d}{dt}\begin{bmatrix}\theta\\ \omega\end{bmatrix} &= \begin{bmatrix}[0]_{3\times3} & [I]_{3\times3}\\ -\frac{1}{2}[H]^{-1}[C] & -\frac{1}{2}[H]^{-1}[D]\end{bmatrix}\begin{bmatrix}\theta\\ \omega\end{bmatrix}\\ &\quad + \begin{bmatrix}[0]_{3\times3}\\ \frac{1}{2}[H]^{-1}\end{bmatrix}T\end{aligned} \tag{2.14}$$

where $\theta^T = [\theta_R \;\; \theta_{GB} \;\; \theta_G]$ represents the angular position vector, $\omega^T = [\omega_R \;\; \omega_{GB} \;\; \omega_G]$ denotes the angular speed vector and $T^T = [T_w \;\; 0 \;\; T_G]$ expresses the external torque vector including the electromagnetic torque T_G and aerodynamic torque T_w. $[H] = diag(H_R, H_{GB}, H_G)$ is the diagonal inertia matrix and C and D are stiffness and damping matrices respectively. C also denotes the high and low

speed shaft elasticities and is given as

$$[C] = \begin{bmatrix} C_{HGB} & -C_{HBG} & 0 \\ -C_{HBG} & C_{HBG} + C_{GBG} & -C_{GBG} \\ 0 & -C_{GBG} & C_{GBG} \end{bmatrix}$$

D represents the torque losses and internal friction and is given as

$$[D] = \begin{bmatrix} D_R + d_{HGB} & -d_{HGB} & 0 \\ -d_{HGB} & D_{GB} + d_{HGB} + d_{GBG} & -d_{GBG} \\ 0 & -d_{GBG} & D_G + d_{GBG} \end{bmatrix}$$

Note that the subscripts GB and G represent the gear-box and generator respectively. The induction generator is represented by a fourth order model in an arbitrary reference frame. From [68], using the generator convention for stator currents, we have

$$\begin{aligned} u_{sd} &= -r_s i_{sd} - \omega\psi_{sq} + p\psi_{sd} \\ u_{sq} &= -r_s i_{sq} + \omega\psi_{sd} + p\psi_{sq} \\ u_{rd} &= r_r i_{rd} - (\omega - \omega_r)\psi_{rq} + p\psi_{rd} \\ u_{rq} &= r_r i_{rq} + (\omega - \omega_r)\psi_{rd} + p\psi_{rq} \end{aligned}$$

where $p = \frac{1}{\omega_0}\frac{d}{dt}$ and ω_0 is the base cyclic frequency, ω represents the rotating speed of the arbitrary reference frame and the subscripts dq represent the dq

axis of the frame and s, r denote the stator and the rotor respectively.
Further, the fluxes ψ are related to the stator and rotor winding currents by the equations given below

$$\psi_{sd} = -X_s i_{sd} + X_m i_{rd}$$

$$\psi_{sq} = -X_s i_{sq} + X_m i_{rq}$$

$$\psi_{rd} = -X_m i_{sd} + X_r i_{rd}$$

$$\psi_{rq} = -X_m i_{sq} + X_r i_{rq}$$

And the electromagnetic torque is given by

$$T_e = \psi_{qr} i_{dr} - \psi_{dr} i_{qr}$$

2.4.6 Fuel Cells

The microsources include renewable sources of energy like solar, wind and hydro power. Mini hydro generators, wind turbines and PV panels are located geographically in a microgrid. The energy from these renewable sources is harnessed and converted to electricity. The only shortcoming of these sources is their intermittent nature.

Fuel cells are unconventional and produce electricity from hydrogen and oxygen. They release water vapor and the emissions are less. Also, they offer higher ef-

ficiencies when compared to the microturbines discussed above. However, fuel cells are currently uneconomical and quite expensive. From the environmental perspective, renewable sources and fuel cells are well suited for distributed generation in place of their conventional counterparts including the combustion engines, see Fig. 2.1.

2.4.7 Storage Devices

Storage devices have a crucial role to play in the microgrid. These are back up energy systems which provide energy to the critical loads much like the uninterrupted power supply. The storage devices include batteries, flywheels and ultra capacitors. With the advancement in technology, higher capacity storage devices are available which can provide considerable supply of energy.

2.5 Control Methodologies for Microgrid

Although extensive research has been carried out in designing control strategies for microgrids, there is still ambiguity regarding the best microgrid control strategies. [13] presents a survey of the various control techniques developed for microgrids. Several control strategies have been proposed for microgrids in [85], [86], [87], [88]. Robust H_∞ control is presented in [89] and [90] for the control of two distributed generation units. An optimal controller is presented

for controlling the frequency and voltage fluctuations during islanded mode in [91].

However, since we are looking towards the microgrid from a system of systems perspective, we need to use the control strategies devised for system of systems. The first hurdle lies in finding a mathematical model for the framework. The control paradigms given in [92] need a mathematical model for their implementation. Nevertheless, a few mathematical models of the microgrid are available in the literature which are complex and of high order. [93], [94]. Additionally, state space modeling has also been done for the microgrid [95], [96].

Once we obtain a mathematical model, we propose control strategies that might be applied to microgrids. One interesting control strategy would have been the multilevel control [97] ,[98]:

2.5.1 Multilevel Control

Functionally, the microgrid, can operate by using the following three main hierarchical control levels:

- Primary control is the droop control used to share load between converters.
- Secondary control is responsible for removing any steady-state error introduced by the droop control.
- Tertiary control concerning more global responsibilities decides the import

or export of energy for the microgrid.

Such kind of systems operate over large synchronous machines with high inertias and inductive networks. However, in power-electronics-based microgrids, there are no inertias, and the nature of the networks is mainly resistive. There are major differences between both systems that we have to take into account when designing their control schemes. A three-level hierarchical control can be constructed following [14]. The primary control deals with the inner control of the DG units by adding virtual inertias and controlling their output impedance. The secondary control is conceived to restore the frequency and amplitude deviations produced by the virtual inertias and output virtual impedance. The tertiary control regulates the power flows between the grid and the microgrid at the point of common coupling (PCC).

In what follows, we look at the basic elements of consensus-based control that can be possibly applied to the microgrid. This is an important class type of cooperative control paradigm [99]. Our view is to focus on the mutual agreement among the different units of microgrid as subsystems in a SoS.

2.5.2 Consensus Control

The consensus control problem has been discussed extensively in the literature owing to its applicability in the formation of robots, cooperative control of unmanned aerial vehicles and communication between sensor networks [100].

Consensus among a group of agents or subsystems means to arrive at a certain agreement concerning a particular value or quantity which is dependent on the states of every agent. A consensus algorithm or protocol is a rule that explains the interaction between an agent and its surrounding subsystems enclosed in the network. However, management of the shared information between the agents is a very critical issue which has to be resolved in order to carry out coordination among the subsystems. To address the consensus problems for dynamic networked agents, a theoretical framework was developed by [101].

A consensus protocol is introduced with x_i representing the information state of the ith agent, where the information state is responsible for the information that has to be coordinated among the agents, the consensus protocol for continuous systems can be formulated as [102], [103].

$$\dot{x}_i(t) = \sum_{j \in J_i(t)} \alpha_{ij}(t)(x_i(t) - x_j(t)) \tag{2.15}$$

where $J_i(t)$ is the group of agents whose information is available to agent i at time t, $\alpha_{ij}(t)$ represents a positive time-varying weighing factor.

Additionally, in [104], consensus among a group of networked agents or systems is obtained by using an optimal control design method. A set of agents are considered and each of them can be dynamically represented as

$$\begin{aligned} \dot{x}_i &= A_i x_i + B_i u_i, \quad x_i \in \Re^n, u_i \in \Re^m \\ y_i &= C_i x_i, \quad y_i \in \Re^q, i = 1, ...N \end{aligned} \tag{2.16}$$

where x_i represents the state vector, u_i represents the input vector and Y_i represents the output vector of each agent i. $n.m$and q give the dimension of the corresponding state,input and output vectors. However, the whole network of agents can dynamically be represented as

$$\dot{X} = AX + BU, \quad Y = CX$$

where X, U and Y represent the state, input and output vectors of the whole set of agents. All the respective individual agent vectors are concatenated in one vector as follows:

$$\begin{aligned} X_{Nn\times 1} &= [x_i^T, ..., x_N^T]^T, U_{Nm\times 1} = [u_i^T, ..., u_N^T]^T \\ Y_{Nq\times 1} &= [y_i^T, ..., y_N^T]^T \end{aligned}$$

Therefore, matrices A, B and C are given as

$$\begin{aligned} A &= diag[A_1, ...A_N],\ B = diag[B_1, ...B_N] \\ C &= diag[C_1, ...C_N] \end{aligned}$$

Consensus control of microgrids is proposed in [105]. Coordinated performance is achieved at the secondary level despite the units being out of synchronization in the beginning. The proposed scheme is tested for an islanded microgrid in various scenarios. Another distributed cooperative control mehtodology based on consensus is proposed in [106]. Power sharing is precisely realized among

DGs in addition to voltage regulation at the critical bus by the virtue of this methodology.

2.5.3 Decentralized Control

With reference to Fig. 2.2, the control of the inverter plus filter interfaces is crucial to the operation of the microgrid. Because of the distributed nature of the system, these interfaces need to be controlled on the basis of local measurements only. The decentralized control of the individual interfaces should address the following basic issues.

1. Interfaces should share the total load (linear or nonlinear) in a desired way.
2. Decentralized control based on local measurement should guarantee stability on a global scale.
3. Inverter control should prevent any dc voltage offsets on the microgrid.
4. Inverter control should actively damp oscillations between the output filters.

From the viewpoint of decentralized control, it is convenient to classify DG architectures into three classes:

- In *highly dispersed networks*, the interconnecting impedances are predominantly inductive, and the voltage magnitude and phase angle at different source interconnects can be very different.

- In *networks spread over a smaller area*, the impedances are still inductive with a significant resistive component. The voltage magnitude does not differ much, but the phase angles can be different for different sources.

- In very small networks, the impedances are small and predominantly resistive. Neither magnitude nor phase angle differences are significant at any point.

The main common quantity in all cases is the steady-state frequency which must be the same for all sources. In the grid-connected mode, the microgrid frequency is decided by the grid. In the islanded mode, the frequency is decided by the microgrid control.

In each of these classes, if every source is connected to at most two other sources, as shown in Fig. 2.2(a), then the microgrid is radial. Otherwise, it is meshed. If there is a line connecting Source 1 with Source k in Fig. 2.2(a), then it is a meshed microgrid. It is worth noting that the majority of work done on microgrid decentralized control has been for radial-microgrid topologies. The decentralized control of interfaces in meshed topologies is an area that needs further research.

2.5.4 Networked Control

Another control paradigm based on SoS which can be extended to the microgrid is Networked Control. Networked control of SoS has been introduced in [92]. A control system consisting of a real time network in its feedback can be termed as Networked Control System (NCS) [107]. As mentioned earlier, the microgrid can operate at multiple levels forming a control hierarchy. At the primary level, there is no need for a communication network, since the control is based on local measurements only. However at the secondary level, a communication network is required to accomplish global controllability of microgrids. The set points for the voltage and frequency to be maintained are generated by a higher control level and needs to be communicated to the primary level for the local controllers.

The stability of the communication network connecting the distributed generation units is a major concern. Ensuring network stability in this scenario is of paramount importance. Any packet lost or delays in the communication can cause severe power mismatches among the distributed units. On the other hand, the inverters connected to these systems operate under imbalance conditions due to sensitive loads. This leads to switching harmonics, voltage and frequency variations in the microgrid system and disturbs the stability of the system.

The primary challenge in SoS networked control design for a microgrid system is to build a distributed control system which can endure packet losses, delays

and partially decoded packets which affect system stability [92]. In other words it is expected to add robustness to the system. Alternatively, all characteristics of the ad-hoc network must be considered while designing a networked control system to check on communication infractions and ensure a robust and stable operation.

Chapter 3

Networked Control of Microgrid System of Systems

3.1 Introduction

As mentioned in previous chapters, microgrid comprises of micro-turbines, wind turbines, fuel cells and photovoltaic cells etc as sources of energy which are interfaced with the help of power electronic converters. All these units are connected to the main grid through a point of common coupling (PCC) and look as a solitary unit to the distribution network. No additional inertia is

added to the system from the distributed generators. However, because of this the power balance amid generation and load and the network frequency becomes complicated to maintain, especially when the microgrid is in islanded mode [13]. The microgrid operates in two modes namely the grid connected and the islanded mode.

Grid-connected mode: In the grid-connected mode, the microgrid is supposed to follow the rules of distribution network without being involved in the operation of main power system. The microgrid operation based on this approach is significant for the stable operation of power system. During this mode, the microgrid can draw power from the main grid or can supply its power to the main grid, thus functioning similar to a controllable load or source. By supplying or drawing power, the microgrid should be able to control the active and reactive power flows and have an eye on the energy storage [47]. However, in this mode due to the small size of distribution units the system dynamics have to be fixed by a wide extent. Another issue is the slow response at the control signals whenever there is a change in output power. Furthermore, due to lack of synchronous machines connected to low power grid, virtual inertias have to be incorporated in the control loops of the power electronic interfaces [97].

Islanded mode: The islanded mode is an operating condition in which the microgrid isolates itself from the main grid in case of a fault. However, the transition from the grid connected and the islanded mode must be stable [30]. If the microgrid is consuming or supplying power to the main grid before disconnection, a power imbalance occurs. This is compensated by the energy storage

units because of the fact that the microsources have low inertia and slow dynamic response [31], [32].

The microgrid must address the following issues when operating in the islanded mode:

1. Supply and demand balancing.
2. Acceptable power quality.
3. Voltage and frequency balance.
4. Communication among the microgrid components.

Controlling the islanded microgrid means balancing the generation and demand power to deliver high performance while maintaining acceptable ranges of frequency and voltage amplitude. The islanded operation of the microgrid will be the focus of this chapter.

Several control strategies for the microgrid have been proposed in the literature including PI controllers in [108], [85], [86], [87], [88], [109], [110], [111], [112]. Robust H_∞ control is presented in [89], [90] for the control of two distributed generation units. An optimal controller is presented for controlling the frequency and voltage fluctuations during islanded mode in [91].

Networked control of system of systems has been introduced in [10]. A control

system consisting of a real time network in its feedback can be termed as a networked control system (NCS) [107]. Extensive work has been published in the field of networked control systems. For instance, a predictive control algorithm is proposed in [113] for the stabilization of networked systems with random delays and packet dropouts. Similar work on networked predictive control with uncertain delays can be found in [114] which is more recent. Another recent work concerning robust tracking control for networked systems is presented in [115]. The consensus problem of multi-agent systems is another important topic in networked control. In [116], the consensus problem of multi-agent systems is considered with logarithmic quantization effect in the communication channel. In [117], the average consensus of multi-agent systems with communication noises and switching topologies is approached by a distributed protocol based on sampled data. Similarly, in [118], average consensus for multi-agent systems with delays in communication channel and limited data rate is considered. A mean square consensus of multi-agent systems with fixed topologies and noises in communication channels is explored in [119]. The consensus technique has also been extended to microgrid. Recently, a decentralized multi-agent system based frequency control methodology is presented in [120] for an autonomous microgrid having communication constraints. In [105], a consensus based decentralized secondary control scheme is proposed for islanded microgrids.

Apart from the aforementioned papers, a lot of work has been done in the networked systems domain. However, the application of networked control systems to microgrid is very limited. Hence, we propose a networked control strategy in

this chapter to be implemented to a microgrid from an intelligent system of systems perspective. The microgrid is considered to be operating in islanded mode where three distributed generation (DG) units supplying a load are considered as three subsystems. At the primary level, the islanded system is assumed to be equipped with PI controllers. While at the secondary level, the networked control system is designed for controlling the interconnected DG units, forming a networked microgrid system of systems. To the best of author's knowledge this is the first time, where the concept of system of systems, networked control and microgrid are integrated together.

As mentioned in [92], the need to design a SoS control system which can tolerate packet loss and delays is one of the prime challenges in SoS networked control. Hence, we consider a network which is subjected to bounded random packet losses where the controller stabilizes the system in the presence of packet losses.

Some key issues on the control of SoS are:

- Typically, in SoS control structure there is a sensor feedback of the individual systems in addition to wired or wireless sensor and/or data transmission from each neighboring system sensor to any given system controller/actuator.

- The two general configurations in network control systems are direct structure and hierarchical structure. In the NCS direct structure, see Fig. 3.1, the control network carries the data of the sensors to the loop controllers

that will calculate the control signal. This control values are transferred on the control network to the actuators. The network is also used to synchronize the sampling on sensors. As mentioned before, the advantage of such a configuration is the economy in cabling and remote commissioning of sensors and actuators.

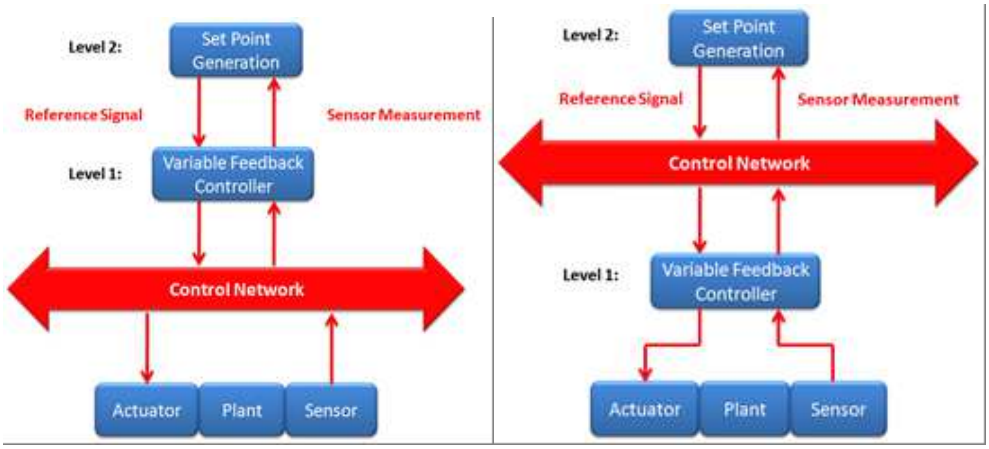

Figure 3.1: (right) Direct structure of a two layer NCS, (left) Hierarchical structure of a two layer NCS

The questions to be asked here are whether the microgrid falls under the SoS category and does it exhibit the characteristics of a SoS. For this, we need to consider the subsystems within the microgrid architecture and observe their operation and interaction among each other.

The elements of the microgrid, which in other words may be termed as subsystems include microsources which may be photovoltaic and wind generators, micro-turbines deriving energy from gas or bio-fuels, fuel cells and storage devices constituting batteries or flywheels. All of these subsystems operate inde-

pendently without interfering with each other. Thus, operational independence is seen in the subsystems of the Microgrid. Also, each subsystem depends on its own source to function and produce energy and is hence responsible for its autonomous operation. For instance, the micro-turbine runs on bio-fuel to perform its function of producing energy and has nothing to do with the microsource generators which harness energy from renewable sources such as the wind and solar power. The operation of the storage devices too is distinct and is concerned only with storing energy for use when required. Moreover, the microgrid supports evolutionary development and is supposed to accommodate new subsystems into its architecture whenever needed without affecting the complexity of the overall system. A new micro source may be added to the microgrid which utilizes hydro-energy for example, or a new storage device may be incorporated for better and efficient storage of energy. On the contrary, a subsystem may be discarded from the system or architecture owing to some reason. All this explains the evolutionary characteristic of the microgrid. Further, the emergent behavior of the microgrid is evident from the fact that the subsystems are all operating to collectively satisfy the main objective of providing combined heat and electric power to the local community even in the case of a failure of the main grid. This objective cannot be achieved by a single subsystem of the microgrid and requires a combined effort of all the constituent subsystems. Finally, the microgrid is geographically distributed and all of its subsystems are spatially distributed in a particular region. From the above discussion it can be concluded that the microgrid architecture satisfies the characteristics and falls perfectly on the lines of a system of systems.

3.2 Microgrid Islanded System Modeling

The mathematical modeling of the islanded system of microgrid is presented in this section. The islanded system having n distributed generation units and a local load is shown in Fig. 3.2. All the DGs and load are connected to the main grid via a Point of Common Coupling (PCC). A single line diagram of the islanded system consisting of multiple DGS and load is shown in Fig. 3.3.

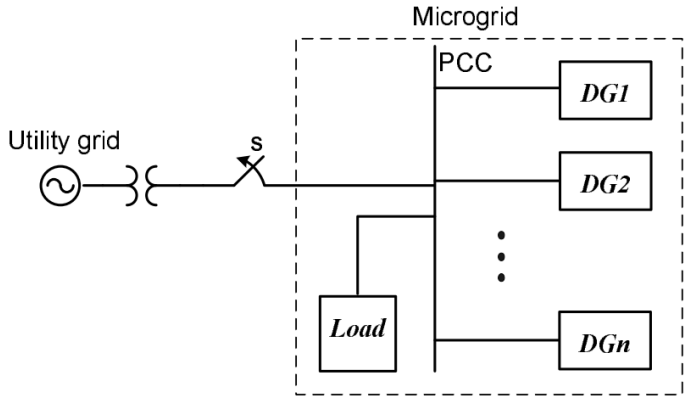

Figure 3.2: Microgrid with multiple parallel connected DGs

Each DG unit is modeled by a DC voltage source, a three phase voltage source converter and a series RL filter. However, we take into consideration three distributed generation units as three subsystems supplying a load. By applying KVL and KCL from the single line diagram in Fig. 3.3, we obtain the following equations:

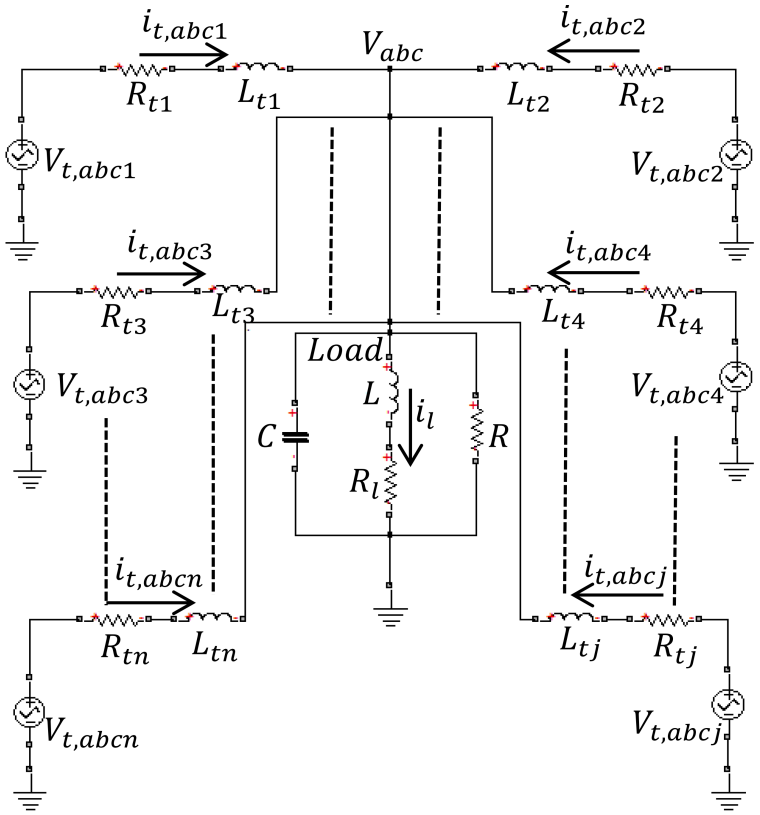

Figure 3.3: Single line diagram of the islanded system consisting of multiple DGs

$$
\begin{aligned}
v_{abc} &= L\frac{di_{L,abc}}{dt} + R_l i_{L,abc} \\
v_{t,abc_1} &= L_{t_1}\frac{di_{t,abc_1}}{dt} + R_{t_1} i_{t,abc_1} + v_{abc} \\
v_{t,abc_2} &= L_{t_2}\frac{di_{t,abc_2}}{dt} + R_{t_2} i_{t,abc_2} + v_{abc} \\
v_{t,abc_3} &= L_{t_3}\frac{di_{t,abc_3}}{dt} + R_{t_3} i_{t,abc_3} + v_{abc} \\
i_{t,abc_1} + i_{t,abc_2} + i_{t,abc_3} &= \frac{1}{R} v_{abc} + i_{L,abc} + C\frac{dv_{abc}}{dt}
\end{aligned} \tag{3.1}
$$

In (3.1), $v_{abc}, v_{t,abc_1}, v_{t,abc_2}, v_{t,abc_3}, i_{L,abc}, i_{t,abc_1}, i_{t,abc_2}, i_{t,abc_3}$ are basically 3×1 vectors which include the phase quantities. Every 3-phase variable x_{abc} in (3.1) can be converted to a $\alpha\beta$ reference frame system under balanced conditions. This conversion is accomplished by applying the following transformation ($abc\,to\,\alpha\beta$).

$$
x_{\alpha\beta} = x_a e^{j0} + x_b e^{j\frac{2\pi}{3}} + x_c e^{j\frac{4\pi}{3}} \tag{3.2}
$$

where $x_{\alpha\beta} \triangleq x_\alpha + j x_\beta$. Hence the dynamic model of the above system in the $\alpha\beta$

frame is

$$\begin{aligned}
\frac{dv_{\alpha\beta}}{dt} &= -\frac{1}{RC}v_{\alpha\beta} + \frac{1}{C}i_{t,\alpha\beta_1} - \frac{1}{C}i_{L,\alpha\beta} + \frac{1}{C}i_{t,\alpha\beta_2} + \frac{1}{C}i_{t,\alpha\beta_3} \\
\frac{di_{t,\alpha\beta_1}}{dt} &= -\frac{R_{t_1}}{L_{t_1}}i_{t,\alpha\beta_1} - \frac{1}{L_{t_1}}v_{\alpha\beta} + \frac{1}{L_{t_1}}v_{t,\alpha\beta_1} \\
\frac{di_{L,\alpha\beta}}{dt} &= \frac{1}{L}v_{\alpha\beta} - \frac{R_l}{L}i_{L,\alpha\beta} \\
\frac{di_{t,\alpha\beta_2}}{dt} &= -\frac{R_{t_2}}{L_{t_2}}i_{t,\alpha\beta_2} - \frac{1}{L_{t_2}}v_{\alpha\beta} + \frac{1}{L_{t_2}}v_{t,\alpha\beta_2} \\
\frac{di_{t,\alpha\beta_3}}{dt} &= -\frac{R_{t_3}}{L_{t_3}}i_{t,\alpha\beta_3} - \frac{1}{L_{t_3}}v_{\alpha\beta} + \frac{1}{L_{t_3}}v_{t,\alpha\beta_3}
\end{aligned} \tag{3.3}$$

Now (3.3) is transferred to a rotating frame which has its basis on

$$x_{\alpha\beta} = x_{dq}e^{j\theta} = (x_d + jx_q)e^{j\theta} \tag{3.4}$$

where $\theta(t) \triangleq \int_0^t \omega(\zeta)d\zeta + \theta_0$. $\theta(t)$ represents the phase angle of a reference vector $(x_\alpha^{ref} + jx_\beta^{ref})$ in the $\alpha\beta$ frame. The equations for the dq-frame can be written as [89]:

$$\begin{aligned}
\frac{dV_{dq}}{dt} + j\omega_0 V_{dq} &= -\frac{1}{RC}V_{dq} + \frac{1}{C}I_{t,dq_1} - \frac{1}{C}I_{L,dq} + \frac{1}{C}I_{t,dq_2} + \frac{1}{C}I_{t,dq_3} \\
\frac{dI_{t,dq_1}}{dt} + j\omega_0 I_{t,dq_1} &= -\frac{1}{L_{t_1}}V_{dq} - \frac{R_{t_1}}{L_{t_1}}I_{t,dq_1} + \frac{1}{L_{t_1}}V_{t,dq_1} \\
\frac{dI_{L,dq}}{dt} + j\omega_0 I_{L.dq} &= \frac{1}{L}V_{dq} - \frac{R_l}{L}I_{L,dq} \\
\frac{dI_{t,dq_2}}{dt} + j\omega_0 I_{t,dq_2} &= -\frac{1}{L_{t_2}}V_{dq} - \frac{R_{t_2}}{L_{t_2}}I_{t,dq_2} + \frac{1}{L_{t_2}}V_{t,dq_2} \\
\frac{dI_{t,dq_3}}{dt} + j\omega_0 I_{t,dq_3} &= -\frac{1}{L_{t_3}}V_{dq} - \frac{R_{t_3}}{L_{t_3}}I_{t,dq_3} + \frac{1}{L_{t_3}}V_{t,dq_3}
\end{aligned}$$

Table 3.1: Parameters of the microgrid system.

Quantity	Value
R_{t1} (series filter resistance in DG 1)	1.5 m Ω
L_{t1} (series filter inductance in DG 1)	300 μH
R_{t2} (series filter resistance in DG 2)	6 m Ω
L_{t2} (series filter inductance in DG 2)	900 μH
R_{t3} (series filter resistance in DG 3)	9 m Ω
L_{t3} (series filter inductance in DG 3)	1200 μH
VSC rated power	S_{base}=2.5 MVA
VSC terminal voltage (line-line)	V_{base}=600V
f_{sw} (PWM carrier frequency)	1980 Hz
R (Load nominal resistance)	76 Ω
L (Load nominal inductance)	111.9 mH
C (Load nominal capacitance)	62.86 μF
$q = \frac{L\omega_0}{R_L}$(Inductor quality factor)	120
f_0 (System frequency)	60 Hz
V_{dc} (DC bus voltage)	1500 V
Transformer voltage ratio (Y/Δ)	0.6 / 13.8 kV

3.3 Networked Control System

After formulating the above equations, considering the states as

$x_p = [V_d, V_q, I_{td_1}, I_{tq_1}, I_{Ld}, I_{Lq}, I_{td_2}, I_{tq_2}, I_{td_3}, I_{tq_3}]$,

the control vector as $u_p = [V_{td_1}, V_{tq_1}, V_{td_2}, V_{tq_2}, V_{td_3}, V_{tq_3}]$ and output vector as $y_p = [V_d, V_q, I_{td_2}, I_{tq_2}, I_{td_3}, I_{tq_3}]$, we can obtain the state-space model of the islanded system in the standard form

$$\dot{x}_p(t) = A_p x_p(t) + B_p u_p(t), \;\; y_p(t) = C_p x(t) \tag{3.5}$$

The matrices A_p, B_p and C_p are shown below.

$$A_p = \begin{bmatrix}
-\frac{1}{RC} & \omega_0 & \frac{1}{C} & 0 & -\frac{1}{C} & 0 & \frac{1}{C} & 0 & \frac{1}{C} & 0 \\
-\omega_0 & -\frac{1}{RC} & 0 & \frac{1}{C} & 0 & -\frac{1}{C} & 0 & \frac{1}{C} & 0 & \frac{1}{C} \\
-\frac{1}{L_{t1}} & 0 & -\frac{R_{t1}}{L_{t1}} & \omega_0 & 0 & 0 & 0 & 0 & 0 & 0 \\
0 & -\frac{1}{L_{t1}} & -\omega_0 & -\frac{R_{t1}}{L_{t1}} & 0 & 0 & 0 & 0 & 0 & 0 \\
\frac{1}{L} & 0 & 0 & 0 & -\frac{R_l}{L} & \omega_0 & 0 & 0 & 0 & 0 \\
0 & \frac{1}{L} & 0 & 0 & -\omega_0 & -\frac{R_l}{L} & 0 & 0 & 0 & 0 \\
-\frac{1}{L_{t2}} & 0 & 0 & 0 & 0 & 0 & -\frac{R_{t2}}{L_{t2}} & \omega_0 & 0 & 0 \\
0 & -\frac{1}{L_{t2}} & 0 & 0 & 0 & 0 & -\omega_0 & -\frac{R_{t2}}{L_{t2}} & 0 & 0 \\
-\frac{1}{L_{t_3}} & 0 & 0 & 0 & 0 & 0 & 0 & 0 & -\frac{R_{t_3}}{L_{t_3}} & \omega_0 \\
0 & -\frac{1}{L_{t_3}} & 0 & 0 & 0 & 0 & 0 & 0 & -\omega_0 & -\frac{R_{t_3}}{L_{t_3}}
\end{bmatrix}$$

$$B_p = \begin{bmatrix}
0 & 0 & 0 & 0 & 0 & 0 \\
0 & 0 & 0 & 0 & 0 & 0 \\
\frac{1}{L_{t1}} & 0 & 0 & 0 & 0 & 0 \\
0 & \frac{1}{L_{t1}} & 0 & 0 & 0 & 0 \\
0 & 0 & 0 & 0 & 0 & 0 \\
0 & 0 & 0 & 0 & 0 & 0 \\
0 & 0 & \frac{1}{L_{t2}} & 0 & 0 & 0 \\
0 & 0 & 0 & \frac{1}{L_{t2}} & 0 & 0 \\
0 & 0 & 0 & 0 & \frac{1}{L_{t_3}} & 0 \\
0 & 0 & 0 & 0 & 0 & \frac{1}{L_{t_3}}
\end{bmatrix}; C_p = \begin{bmatrix}
1 & 0 & 0 & 0 & 0 & 0 \\
0 & 1 & 0 & 0 & 0 & 0 \\
0 & 0 & 0 & 0 & 0 & 0 \\
0 & 0 & 0 & 0 & 0 & 0 \\
0 & 0 & 0 & 0 & 0 & 0 \\
0 & 0 & 0 & 0 & 0 & 0 \\
0 & 0 & 1 & 0 & 0 & 0 \\
0 & 0 & 0 & 1 & 0 & 0 \\
0 & 0 & 0 & 0 & 1 & 0 \\
0 & 0 & 0 & 0 & 0 & 1
\end{bmatrix}^T$$

For all practical purposes, we seek digital control and hence using appropriate sampling period $T_s = 0.1sec$ (arbitrarily chosen), we convert model (3.5) into the following discrete-time linear time-invariant model as:

$$x_p(k+1) = Ax_p + Bu_p, \;\; y_p = Cx_p \tag{3.6}$$

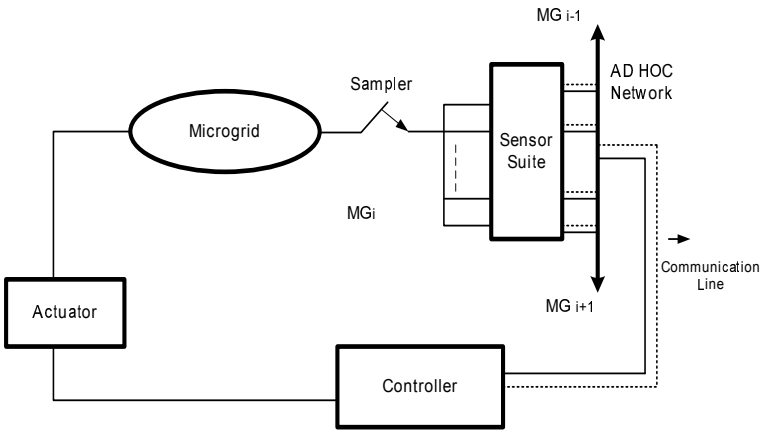

Figure 3.4: Microgrid networked controlled sos

We now consider the operation of SoS-NCS system under the effect of random communication delays, where the sensor is clock-driven and the controller and the actuator are event driven. See Fig. 3.4 where the solid line for wired connections and dotted line for wireless connections. For a more general case, we assume that the measurement after passing through the network exhibits a randomly varying communication delay and is described by

$$y_c(k) = y_p(k - \delta(k)\tau_k^m), \tag{3.7}$$

where τ_k^m is the *communication delay* and $\delta(k)$ is a stochastic binary variable

with $Prob\{\delta(k) = 1\} = p_k$ where p_k assumes discrete values. When the full state information is not available and the time delay occurs on the actuation side, it is desirable to design the following observer-based controller [121]:

$$\begin{aligned} \hat{x}(k+1) &= A\hat{x} + Bu_p(k) + L(y_c(k) - \hat{y}_c(k)) \\ \hat{y}_c(k) &= C\hat{x}(k - \delta(k)\tau_k^m), \qquad (3.8) \\ u_c(k) &= K\hat{x}(k), \quad u_p = K\hat{x}(k - \alpha(k)\tau_k^a) \qquad (3.9) \end{aligned}$$

where $\hat{x}(k) \in \Re^n$ is the estimate of the system (3.5), $\hat{y}_c(k) \in \Re^p$ is the observer output, and $L \in \Re^{n\times p}$ and $K \in \Re^{m\times n}$ are the observer and controller gains, respectively, and τ_k^a is the *actuation delay*. The stochastic binary variable $\alpha(k)$, mutually independent of $\delta(k)$, is also a Bernoulli distributed white sequence with $Prob\{\alpha(k) = 1\} = s_k$ where s_k assumes discrete values.

In this chapter, to reflect the actual operation of microgrids, we assume that τ_k^a and τ_k^m are time-varying and have the following bounded condition:

$$\tau_m^- \le \tau_k^m \le \tau_m^+, \;\; \tau_a^- \le \tau_k^a \le \tau_a^+ \qquad (3.10)$$

Define the estimation error by $e(k) = x_p(k) - \hat{x}(k)$. Then, it yields

$$\begin{aligned} x_p(k+1) &= Ax_p(k) + BKx_p(k - \alpha(k)\tau_k^a) - BKe(k - \alpha(k)\tau_k^a), \quad (3.11) \\ e(k+1) &= Ae(k) - LCe(k - \delta(k)\tau_k^m) \quad (3.12) \end{aligned}$$

In terms of $\xi(k) = [x_p^T(k) \quad e^T(k)]^T$, system (3.11) and (3.12) can be cast into the form:

$$\xi(k+1) = \mathsf{A}_j\xi(k) + \mathsf{B}_j\xi(k - \tau_k^m) + \mathsf{C}_j\xi(k - \tau_k^a) \quad (3.13)$$

where $\{\mathsf{A}_j,\ \mathsf{B}_j,\ \mathsf{C}_j,\ j = 1, ..., 4\}$ and j is an index identifying one of the following pairs $\{(\delta(k) = 1,\ \alpha(k) = 1),\ (\delta(k) = 1,\ \alpha(k) = 0),\ (\delta(k) = 0,\ \alpha(k) =$

$0),\ (\delta(k)=0,\ \alpha(k)=1)\}$:

$$
\begin{aligned}
\mathsf{A}_1 &= \begin{bmatrix} A & 0 \\ 0 & A \end{bmatrix},\ \mathsf{A}_2 = \begin{bmatrix} A+BK & -BK \\ 0 & A \end{bmatrix}, \\
\mathsf{A}_3 &= \begin{bmatrix} A+BK & -BK \\ 0 & A-LC \end{bmatrix},\ \mathsf{A}_4 = \begin{bmatrix} A & 0 \\ 0 & A-LC \end{bmatrix}, \\
\mathsf{B}_1 &= \begin{bmatrix} BK & -BK \\ 0 & 0 \end{bmatrix},\ \mathsf{B}_2 = \begin{bmatrix} 0 & 0 \\ 0 & 0 \end{bmatrix}, \\
\mathsf{B}_3 &= \begin{bmatrix} 0 & 0 \\ 0 & 0 \end{bmatrix},\ \mathsf{B}_4 = \begin{bmatrix} BK & -BK \\ 0 & 0 \end{bmatrix}, \\
\mathsf{C}_1 &= \begin{bmatrix} 0 & 0 \\ 0 & -LC \end{bmatrix},\ \mathsf{C}_2 = \begin{bmatrix} 0 & 0 \\ 0 & -LC \end{bmatrix}, \\
\mathsf{C}_3 &= \begin{bmatrix} 0 & 0 \\ 0 & 0 \end{bmatrix},\ \mathsf{C}_4 = \begin{bmatrix} 0 & 0 \\ 0 & 0 \end{bmatrix}
\end{aligned} \tag{3.14}
$$

Remark 3.3.1 *Following [121], we note from (3.14) that*

$$
\mathsf{A}_j + \mathsf{B}_j + \mathsf{C}_j = \begin{bmatrix} A+BK & -BK \\ 0 & A-LC \end{bmatrix}, j = 1, .., 4 \tag{3.15}
$$

The interpretation of this significant result is that $\mathsf{A}_j + \mathsf{B}_j + \mathsf{C}_j$ *represents the fundamental matrix of the delayed system (3.13), which must be independent of the mode of operation. This fact will help in simplifying the control design algorithm.*

The aim of the remaining part of the chapter is to *design an observer based feedback stabilizing controller in the form of (3.8) and (3.9) such that the closed loop system (3.13) is exponentially stable in the mean square.* Our approach is based on the concepts of switched time-delay systems [122]. For simplicity in exposition, we introduce

$$\begin{aligned}
\sigma_1(k) &= Prob\{\delta(k)=1,\ \alpha(k)=1\},\ \ \hat{\sigma}_1=[\sigma_1] \\
\sigma_2(k) &= Prob\{\delta(k)=1,\ \alpha(k)=0\},\ \ \hat{\sigma}_2=[\sigma_2] \\
\sigma_3(k) &= Prob\{\delta(k)=0,\alpha(k)=0\},\ \ \hat{\sigma}_3=[\sigma_3] \\
\sigma_4(k) &= Prob\{\delta(k)=0,\ \alpha(k)=1\},\ \ \hat{\sigma}_4=[\sigma_4]
\end{aligned} \tag{3.16}$$

where $[\sigma_i]$ is the expected value of $\sigma_i,\ i=1,..,4$.

3.4 Closed-Loop Stability Results

In this section, we will thoroughly investigate the stability analysis problem for the closed-loop system (3.13). First, let us deal with the stability analysis problem and derive a sufficient condition under which the closed-loop system (3.13) with the given controller (3.8) and (3.9) is exponentially stable in the mean square. Extending on [123], the following Lyapunov function candidate is

constructed to establish the main theorem:

$$
\begin{aligned}
V(\xi(k)) &= \sum_{i=1}^{5} V_i(\xi(k)) \qquad (3.17)\\
V_1(\xi(k)) &= \sum_{j=1}^{4} \xi^T(k) P \xi(k),\ P>0,\ \ V_2(\xi(k)) = \sum_{j=1}^{4} \sum_{i=k-\tau_k^m}^{k-1} \xi^T(i) Q_j \xi(i),\ Q_j = Q_j^T > 0\\
V_3(\xi(k)) &= \sum_{j=1}^{4} \sum_{i=k-\tau_k^a}^{k-1} \xi^T(i) Q_j \xi(i),\ \ V_4(\xi(k)) = \sum_{j=1}^{4} \sum_{\ell=-\tau_m^+ +2}^{-\tau_m^- +1} \sum_{i=k+\ell-1}^{k-1} \xi^T(i) Q_j \xi(i)\\
V_5(\xi(k)) &= \sum_{j=1}^{4} \sum_{\ell=-\tau_a^+ +2}^{-\tau_a^- +1} \sum_{i=k+\ell-1}^{k-1} \xi^T(i) Q_j \xi(i) \qquad (3.18)
\end{aligned}
$$

It is not difficult to show that there exist real scalars $\mu > 0$ and $\upsilon > 0$ such that

$$\mu \|\xi\|^2 \leq V(\xi(k)) \leq \upsilon \|\xi(k)\|^2 \qquad (3.19)$$

We now present the main results for system (3.13) to be exponentially stable in two theorems: **Theorem 1** concerns the conditions under which the closed-loop stability is guaranteed given that the controller gains are known and **Theorem 2** provides a way to determine these gains.

Theorem 1: *Let the controller and observer gain matrices K and L be given. The closed-loop system (3.13) is exponentially stable if there exist matrices $0 < P,\ 0 < Q_j^T = Q_j,\ j = 1,..,4$ and matrices R_i, S_i, and M_i, $i = 1, 2$, such that*

the following matrix inequality holds

$$\Lambda_j = \begin{bmatrix} \Lambda_{1j} & \Lambda_{2j} \\ \bullet & \Lambda_{3j} \end{bmatrix} < 0 \tag{3.20}$$

$$\Lambda_{1j} = \begin{bmatrix} \Psi_j + \Phi_{j1} & -R_1 + S_1^T & -R_2 + S_2^T \\ \bullet & -S_1 - S_1^T - \hat{\sigma}_j Q_j & 0 \\ \bullet & \bullet & -S_2 - S_2^T - \hat{\sigma}_j Q_j \end{bmatrix}$$

$$\Lambda_{2j} = \begin{bmatrix} -R_1 + M_1^T - \Phi_{j2} & -R_2 + M_2^T - \Phi_{j3} \\ -S_1 - M_1^T & 0 \\ 0 & -S_2 - M_2^T \end{bmatrix}$$

$$\Lambda_{3j} = \begin{bmatrix} -M_1 - M_1^T + \Phi_{j4} & \Phi_{j5} \\ \bullet & -M_2 - M_2^T + \Phi_{j6} \end{bmatrix} \tag{3.21}$$

where

$$\begin{aligned} \Psi_j &= -P + \hat{\sigma}_j(\tau_m^+ - \tau_m^- + \tau_a^+ - \tau_a^- + 2)Q_j + R_1 + R_1^T + R_2 + R_2^T \\ \Phi_{j1} &= (\mathsf{A}_j + \mathsf{B}_j + \mathsf{C}_j)^T \hat{\sigma}_j P(\mathsf{A}_j + \mathsf{B}_j + \mathsf{C}_j) \\ \Phi_{j2} &= (\mathsf{A}_j + \mathsf{B}_j + \mathsf{C}_j)^T \hat{\sigma}_j P\mathsf{B}_j \\ \Phi_{j3} &= (\mathsf{A}_j + \mathsf{B}_j + \mathsf{C}_j)^T \hat{\sigma}_j P\mathsf{C}_j,\ \Phi_{j5} = \mathsf{B}_j^T P\mathsf{C}_j \\ \Phi_{j4} &= \mathsf{B}_j^T \hat{\sigma}_j P\mathsf{B}_j,\ \Phi_{j6} = \mathsf{C}_j^T \hat{\sigma}_j P\mathsf{C}_j \end{aligned}$$

Proof: The proof follows parallel lines to [121] and therefore it is omitted.

Next, a solution to the problem of the observer-based stabilizing controller design is provided by the following theorem:

Theorem 2: *Let the delay bounds* $\tau_m^+,\ \tau_m^-,\ \tau_a^+,\ \tau_a^-$ *be given. Evaluate the quantities* $\hat{\sigma}_j,\ j = 1,..,4$. *Then the closed-loop system (3.13) is exponentially stable if there exist matrices* $0 < X_1,\ X_2,\ Y_1,\ Y_2,\ Z_1,\ 0 < \Xi_j,\ j = 1,..,4$ *and matrices* $\Pi_i,\ \Upsilon_i$ *and* $\Gamma_i,\ i = 1, 2,$ *such that the following matrix inequality holds*

for $j = 1, .., 4$*:*

$$\begin{bmatrix} \widehat{\Lambda}_{1j} & \widehat{\Lambda}_{2j} & \widehat{\Omega}_j \\ \bullet & \Lambda_{3j} & 0 \\ \bullet & \bullet & -\hat{\sigma}_j \widehat{X} \end{bmatrix} < 0 \tag{3.22}$$

$$\widehat{X} = \begin{bmatrix} X_1 & X_2 \\ X_2^T & X_2 \end{bmatrix} \tag{3.23}$$

$$\widehat{\Psi}_j = -\hat{X} + \hat{\sigma}_j(\tau_m^+ - \tau_m^- + \tau_a^+ - \tau_a^- + 2)\Xi_j + \Pi_1 + \Pi_1^T + \Pi_2 + \Pi_2^T$$

$$\widehat{\Lambda}_{1j} = \begin{bmatrix} \widehat{\Psi}_j & -\Pi_1 + \Upsilon_1^T & -\Pi_2 + \Upsilon_2^T \\ \bullet & -\Upsilon_1 - \Upsilon_1^T - \hat{\sigma}_j \Xi_j & 0 \\ \bullet & \bullet & -\Upsilon_2 - \Upsilon_2^T - \hat{\sigma}_j \Xi_j \end{bmatrix}$$

$$\widehat{\Lambda}_{2j} = \begin{bmatrix} -\Pi_1 + \Gamma_1^T & -\Pi_2 + \Gamma_2^T \\ -\Upsilon_1 - \Gamma_1^T & 0 \\ 0 & -\Upsilon_2 - \Gamma_2^T \end{bmatrix}, \quad \widehat{\Lambda}_{3j} = \begin{bmatrix} -\Gamma_1 - \Gamma_1^T & 0 \\ \bullet & -\Gamma_2 - \Gamma_2^T \end{bmatrix}$$

$$\widehat{\Omega}_j = \begin{bmatrix} \widehat{\Omega}_{1j} & 0 & 0 & -\widehat{\Omega}_{4j} & -\widehat{\Omega}_{5j} \end{bmatrix}$$

$$\widehat{\Omega}_{1j} = \begin{bmatrix} X_1 A^T + Y_1^T B^T - Y_1^T B^T Z_1 & X_2 A^T - Y_2^T \\ X_2 A^T & X_2 A^T - Y_2^T \end{bmatrix}, \ \forall \ j$$

$$\widehat{\Omega}_{4j} = \begin{bmatrix} Y_1^T B^T - Y_1^T B^T Z_1 & 0 \\ 0 & 0 \end{bmatrix}, \quad j = 1, 4 \tag{3.24}$$

$$\widehat{\Omega}_{5j} = \begin{bmatrix} 0 & -Y_2^T \\ 0 & -Y_2^T \end{bmatrix}, \quad j = 1, 2, \ \ \widehat{\Omega}_{4j} = 0, \ j = 2, 3, \ \ \widehat{\Omega}_{5j} = 0, \ \ j = 3, 4$$

where the gain matrices are given by

$$K = Y_1 X_1^{-1}, \;\; L = Y_2 X_2^{-1} C^{\dagger}$$

Proof: Define

$$\Omega_j = \begin{bmatrix} (\mathsf{A}_j + \mathsf{B}_j + \mathsf{C}_j) & 0 & -\mathsf{B}_j & -\mathsf{C}_j \end{bmatrix}^T$$

then matrix inequality (3.20) can be expressed as

$$\Lambda_j = \widetilde{\Lambda_j} + \Omega_j P \Omega_j^T < 0 \tag{3.25}$$

$$\widetilde{\Lambda}_j = \begin{bmatrix} \widetilde{\Lambda}_{1j} & \widetilde{\Lambda}_{2j} \\ \bullet & \widetilde{\Lambda}_{3j} \end{bmatrix} < 0$$

$$\widetilde{\Lambda}_{1j} = \begin{bmatrix} \Psi_j & -R_1 + S_1^T & -R_2 + S_2^T \\ \bullet & -S_1 - S_1^T - Q_j & 0 \\ \bullet & \bullet & -S_2 - S_2^T - Q_j \end{bmatrix}$$

$$\widetilde{\Lambda}_{2j} = \begin{bmatrix} -R_1 + M_1^T & -R_2 + M_2^T \\ -S_1 - M_1^T & 0 \\ 0 & -S_2 - M_2^T \end{bmatrix}$$

$$\widetilde{\Lambda}_{3j} = \begin{bmatrix} -M_1 - M_1^T & 0 \\ \bullet & -M_2 - M_2^T \end{bmatrix} \tag{3.26}$$

Setting $\widehat{X} = P^{-1}$, invoking Schur complements, we write matrix Λ_j in (3.25)

equivalently as

$$\begin{bmatrix} \widetilde{\Lambda}_{1j} & \widetilde{\Lambda}_{2j} & \Omega_j \\ \bullet & \widetilde{\Lambda}_{3j} & 0 \\ \bullet & \bullet & -\widehat{X} \end{bmatrix} < 0 \tag{3.27}$$

Applying the congruence transformation

$$T_j = diag[\widehat{X},\ \widehat{X},\ \widehat{X},\ \widehat{X},\ \widehat{X},\ I]$$

to matrix inequality in (3.27) and manipulating using (3.23) and

$$\begin{aligned} \Xi_j &= \widehat{X}Q_j\widehat{X},\ \Pi_j = \widehat{X}R_j\widehat{X},\ \Upsilon_j = \widehat{X}S_j\widehat{X}, \\ \Gamma_j &= \widehat{X}M_j\widehat{X},\ Z_1 = X_1^{-1}X_2. \end{aligned}$$

we readily obtain matrix inequality (3.22) subject (3.25).

Some remarks stand out:

Remark 3.4.1 *In this work, the $\widehat{X}$ matrix considered in* **Theorem 2** *is distinct from the one in [121] from several aspects. First, the $\widehat{X}$ matrix incorporates two different elements X_1 and X_2 unlike the $\widehat{X}$matrix in [121] which contains the same element X. This extension results in a distinct LMI term $\widehat{\Omega_j}$ given in (3.22). Second, the expression for calculating the controller and observer gains (K and L) is also different from [121]. This is done to present a more realistic approach in determining the controller and observer gains. Further, the*

computational results of this work would be less sensitive than that of [121] since the feedback gains are independent in our case but they are somehow coupled in [121].

Remark 3.4.2 *The selection of* $\widehat{X}$ *as given by (3.23) has the advantage of converting the solution of bilinear matrix inequalities to that of seeking the feasibility of linear matrix inequalities and hence avoiding iterative procedures. It should be noted that the LMI (3.22) depends of the average dropout patterns identified by (3.16), which is quite useful in illustrating different operating conditions of the communications network.*

Remark 3.4.3 *It is noted that the implementation of* **Theorem 2** *is on-line in nature as it requires calling random generators to pick-up numbers corresponding to the scalars* $\hat{\sigma}_1$, ..., $\hat{\sigma}_4$ *and to evaluate the probabilities in model (3.16) to compute the state and error trajectories. This represents a salient feature not shared by other methods for networked control design under unreliable communication links.*

Remark 3.4.4 *The networked control system model considered in this chapter is distinct from the one presented in [121]. The model represents a typical system of systems networked control model consisting of a sensor suite and an ad-hoc network for multiple subsystems. Moreover the illustrated example for the proposed control strategy is exclusively a microgrid system of systems.*

3.5 Application Example 1

The example considered here is a 3-subsystem SoS model of the microgrid with three distributed generation units and a load. The respective state space matrices are obtained by substituting the parameter values given in Table 3.1. The system is discretized at a sampling time $T = 0.1s$ and the simulations are carried out in MATLAB and SIMULINK. A screenshot of the control design implementation in simulink, used to carry out the simulation is shown in Fig. 3.5. The controller and observer gains can be obtained by using the relation $K = Y_1 X_1^{-1}$ and $L = Y_2 X_2^{-1} C^{\dagger}$ respectively. Where X_1, X_2, Y_1, Y_2 can be found by solving the LMI (3.22). The values of $\bar{\alpha}$ and $\bar{\delta}$ are set at 0.1 each i.e the probability of the measurement and actuation delay is taken as 0.1. The measurement delay is varied from $\tau_m^- = 1$ to $\tau_m^+ = 5$ and the actuation delay is varied from $\tau_a^- = 3$ to $\tau_a^+ = 9$.These numbers are chosen arbitrarily to vary the delays from a minimum value to a maximum value. The matrices K and L after solving the LMI (3.22) are

$$K = \begin{bmatrix} K_1 & K_2 \end{bmatrix}$$

$$K_1 = \begin{bmatrix} -0.0119 & 0.0002 & -0.0025 & -0.0002 & 0.0000 \\ 0.0010 & -0.0000 & 0.0001 & 0.0000 & 0.0000 \\ 0.0075 & -0.0001 & 0.0016 & 0.0002 & -0.0000 \\ -0.0042 & 0.0000 & -0.0308 & -0.0002 & -0.0221 \\ -0.2286 & 0.0074 & 0.0514 & 0.0017 & 0.2692 \\ 0.2442 & -0.0064 & -0.0055 & 0.0697 & -0.0026 \end{bmatrix}$$

$$K_2 = \begin{bmatrix} 0.0037 & -0.0002 & 0.0035 & -0.0002 & -0.0010 \\ -0.0001 & 0.0002 & -0.0000 & 0.0011 & -0.0000 \\ -0.0023 & 0.0001 & -0.0022 & 0.0001 & 0.0006 \\ -0.0029 & 0.0088 & 0.0020 & 0.0020 & -0.0154 \\ 0.3100 & -0.0279 & 0.0128 & -0.0097 & -0.0021 \\ 0.3061 & 0.0109 & 0.0021 & 0.0036 & 0.0040 \end{bmatrix}$$

$$L = \begin{bmatrix} -0.0166 & 0.0004 & -0.0010 & -0.0290 & -0.0034 & -0.0001 \\ -0.0301 & -0.0024 & -0.0025 & 0.0022 & 0.0006 & -0.0018 \\ 0.0351 & -0.0012 & 0.0003 & 0.0003 & -0.0008 & -0.0001 \\ 0.0015 & 0.0012 & 0.0012 & 0.0046 & 0.0005 & -0.0010 \\ 0.0071 & 0.0000 & -0.0001 & 0.0002 & -0.0003 & -0.0000 \\ -0.0829 & 0.0014 & 0.0182 & -0.3126 & 0.0903 & -0.0005 \\ 0.0723 & -0.0005 & 0.0042 & 0.0055 & 0.0059 & -0.0005 \\ 0.1060 & 0.0006 & 0.0025 & -0.0901 & 0.0101 & 0.0017 \\ -0.1834 & 0.0007 & -0.0167 & 2.2114 & -0.0582 & -0.0051 \\ 0.0103 & -0.0017 & 0.0032 & -0.0309 & 0.0097 & -0.0047 \end{bmatrix}$$

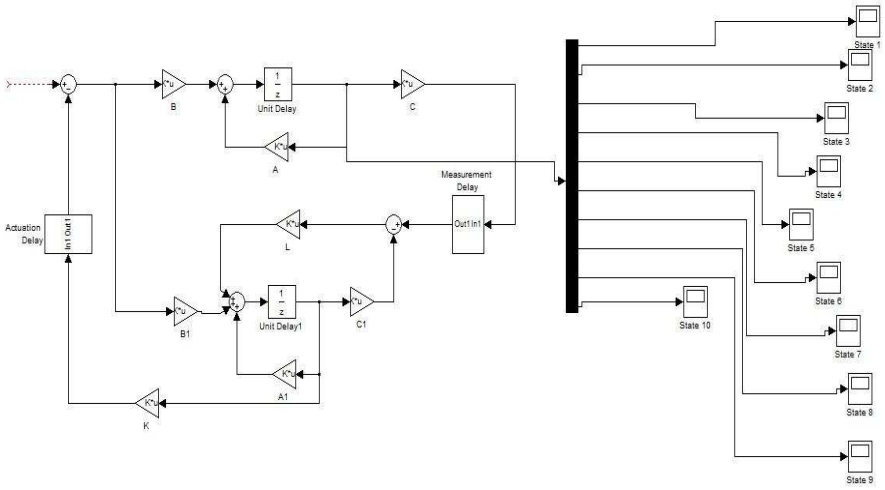

Figure 3.5: Simulink screenshot of the control design implementation

The NCS is modeled in such a way that delays are accommodated in both the measurement as well as the actuation channel. The delays are generated by

employing random number generators. The number obtained from the Uniform Random Number Generator is compared to a variable probability p_k explained earlier in the chapter. If the random generated number is less than p_k, then the output of the comparator is high meaning a delay has occurred. Otherwise, if the output of the comparator is low, there is no delay. This is accomplished by using the variable functional delay block in Simulink.

The figures shown above represent the state response of the microgrid system. Each state represents a typical dynamic of the system. The d-q components of currents of all the distributed generation units are controlled in addition to the load currents and load voltages of the islanded system.

The simulation results elucidate the effectiveness of the proposed control methodology. As evident from the graphs, the output feedback controller stabilizes the system at a reasonably less time with minimum overshoot and very less oscillations. Moreover, stabilization in presence of communication infractions such as packet dropouts and delays further explains the effectiveness of the controller.

Remark 3.5.1 *The state wise response of the microgrid system of systems is presented in Figures. 3.6-3.15. The controller designed for the network system of systems works efficiently to stabilize the system. It can be seen from the graphs that the system is stabilized at a considerably less time. Moreover, there is minimum overshoot and few oscillations which is an indication of the effectiveness of the proposed control strategy. This is a generalized statement explaining the controller response and as such no comparison can be made since this is the*

exclusive control methodology applied to the microgrid system considered in this chapter. Another important aspect of the control methodology is the ability of the controller to maintain the stability of the system in presence of communication infractions including non-stationary packet dropouts and time delays occurring in the measurement as well as the actuation channel which are inevitable in any network. Further it is to be noted that the regulation problem is addressed in this chapter for the microgrid system which explains all the states subsiding to zero. Also, the stability of the system is demonstrated in presence of delays and dropouts.

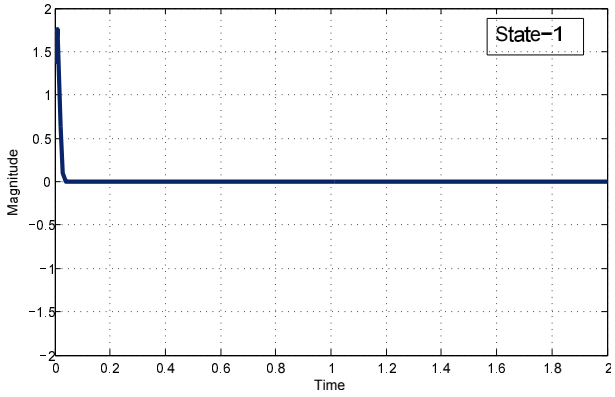

Figure 3.6: d component of load voltage

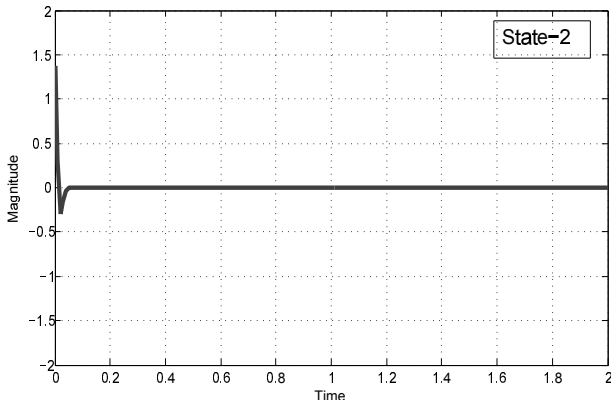

Figure 3.7: q component of load voltage

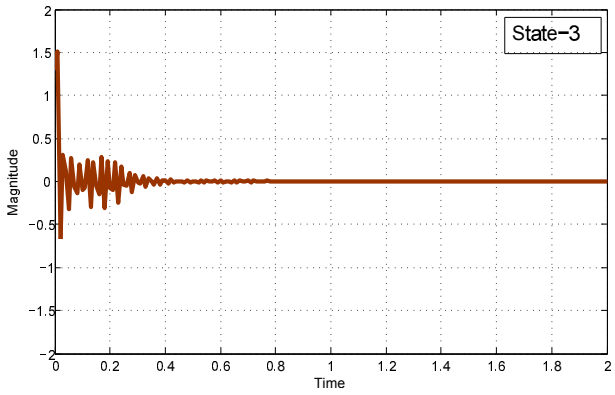

Figure 3.8: d component of DG1 current

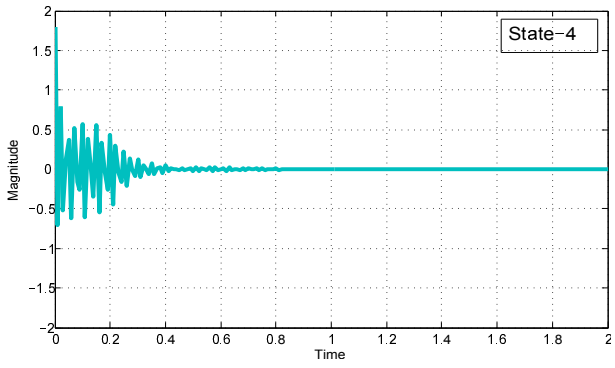

Figure 3.9: q component of DG1 current

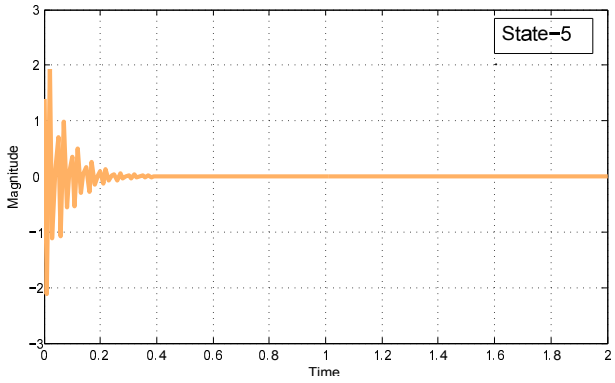

Figure 3.10: d component of load current

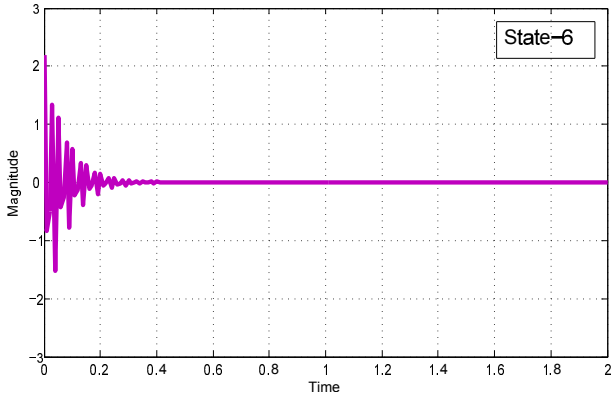

Figure 3.11: q component of load current

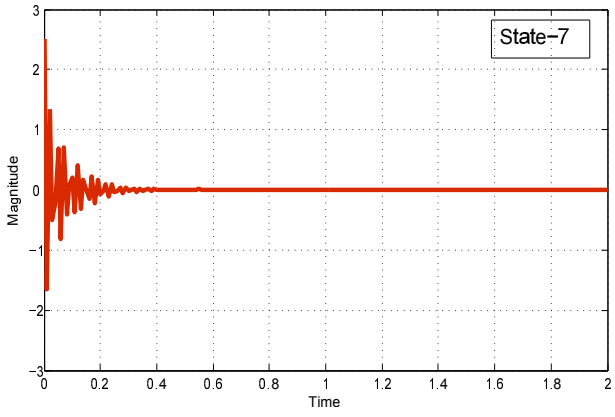

Figure 3.12: d component of DG2 current

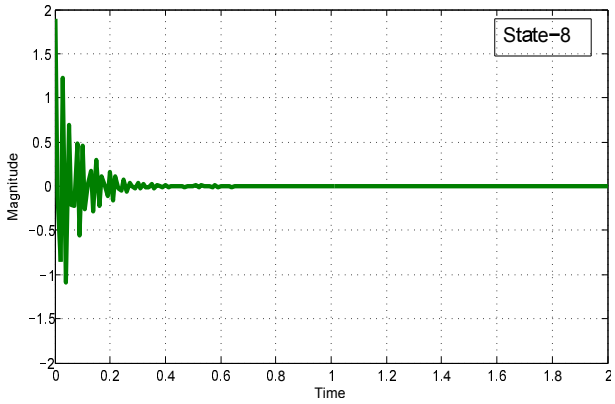

Figure 3.13: q component of DG2 current

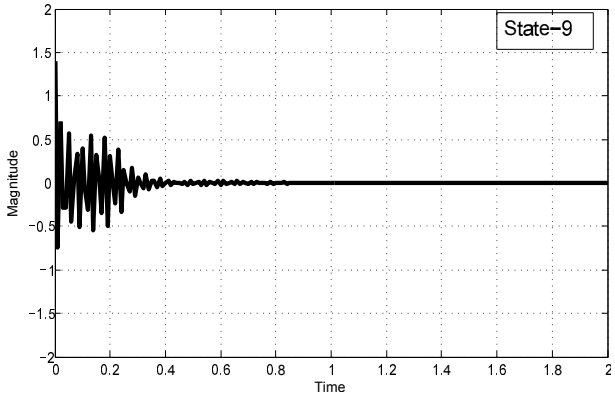

Figure 3.14: d component of DG3 current

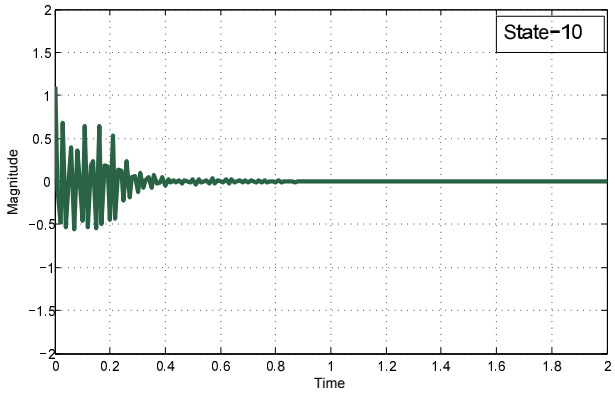

Figure 3.15: q component of DG3 current

Chapter 4

Networked Control Approach for Distributed Generation Systems

4.1 Introduction

The stability of its constituent systems is a major issue in microgrids. The inverters connected to these systems operate under imbalance conditions due to sensitive loads. This leads to switching harmonics, voltage and frequency variations in the microgrid system and disturbs the stability of the system. Therefore, in this chapter, a system of systems framework is proposed for organized

operation of the microgrid. A networked control system of systems controller is designed to stabilize the microgrid system when connected to load and in the presence of delays and packet dropouts. Hence two sets of microalternator and PV systems are considered as distributed generation units, which are eventually connected to a load and the main grid. Detailed modeling of both the microalternator and Photovoltaic (PV) system is presented in section 2. A combined framework of microalternator and PV system connected to a load and the main grid is proposed. A state space representation of the combined system is presented. The controller design explained in chapter 3 is implemented on the proposed framework and simulation results are shown for two sets of PV and microalternator systems. The effectiveness of the proposed framework and control strategy is discussed.

4.2 Modeling of the Microalternator-PV system

To model the microgrid system consisting of microalternator and photovoltaic system, we consider the separate modeling of microalternator and photovoltaic system initially. After modeling both these individual systems, we integrate them into a microgrid system which is connected to a load and the main grid. Two sets of such systems are considered eventually which form a system of systems structure for the microgrid system.

4.2.1 Microalternator

The swing equation of the alternator can be written as two first order differential equations [124]:

$$\frac{d\delta}{dt} = \omega_0(\omega - 1), \quad \frac{d\omega}{dt} = \frac{1}{2H}(P_m - P_e) \tag{4.1}$$

where δ and ω are rotor angle and rotor speed. P_m and P_e are mechanical power input and electrical power output of the generator. The internal voltage e'_q is given by

$$\frac{de'_q}{dt} = \frac{1}{T'_{do}}[E_{fd} - e'_q - (x_d - x'_d)i_{td}] \tag{4.2}$$

where x_d, x'_d and T'_{do} are the d-axis synchronous resistance, transient reactance and open circuit field constants respectively. e'_q is the voltage behind the transient reactance along q-axis. An IEEE type ST is used for the voltage regulator excitation.

$$\frac{dE_{fd}}{dt} = \frac{1}{T_A}[K_A(V_{tref} - V_t) - (E_{fd} - E_{fdo})] \tag{4.3}$$

where E_{fd} is the field voltage along d-axis, K_A and T_A are the gain and time constants of the exciter. Figure 4.1 shows a microalternator connected to the main grid.

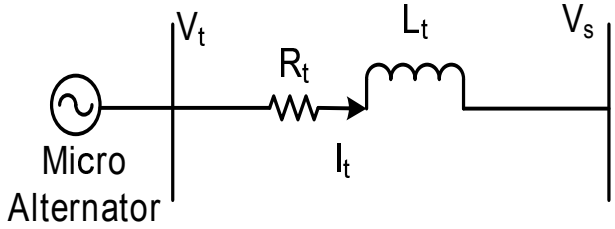

Figure 4.1: Microalternator connected to grid

The terminal voltage of the alternator is given as

$$V_t = V_s + (r_t + jx_t)i_t$$

In d-q terms it becomes

$$\begin{aligned} V_d + jV_q &= V_{sd} + jV_{sq} + (r_t + jx_t)(i_{td} + ji_{tq}) \\ x_q i_{tq} + j(e'_q - x'_d i_{td}) &= (V_{sd} + r_t i_{td} - x_t i_{tq}) + j(V_{sq} + r_t i_{tq} + x_t i_{td}) \end{aligned}$$

The real part can be written as

$$V_{sd} = (x_q + x_t)i_{tq} - r_t i_{td} \tag{4.4}$$

and the imaginary part can be written as

$$e'_q - V_{sq} = r_t i_{tq} + (x'_d + x_t)i_{td} \tag{4.5}$$

Substituting $x_1 = (x'_d + x_t)$ and $x_2 = (x_q + x_t)$ and solving for i_{td} and i_{tq}, we

obtain

$$\begin{aligned} i_{td} &= \frac{-r_t V_{sd} + (e'_q - V_{sq})(x_q + x_t)}{r_t^2 + (x'_d + x_t)(x_q + x_t)} \\ i_{tq} &= \frac{V_{sd}[(x'_d + x_t)(x_q + x_t)] + r_t(e'_q - V_{sq})(x_q + x_t)}{(x_q + x_t)[r_t^2 + (x'_d + x_t)(x_q + x_t)]} \end{aligned} \tag{4.6}$$

Hence, the terminal voltage and power output of the alternator are given as

$$\begin{aligned} V_t &= (V_d^2 + V_q^2)^{1/2} = ((x_q i_{tq})^2 + (e'_q - x'_d i_{td})^2)^{1/2} \\ P_e &= V_d i_{td} + V_q i_{tq} = (e'_q i_{tq}) + (x_q - x'_d) i_{td} i_{tq} \end{aligned} \tag{4.7}$$

By perturbing the above nonlinear equations around a normal operating point and letting $[\delta, \omega, e'_q, E_{fd}]$ as the states, we obtain the linearized state equations:

$$\begin{aligned} \Delta\dot{\delta} &= \omega_0 \Delta\omega \\ \Delta\dot{\omega} &= \frac{1}{2H}[-\Delta P_e] \\ \Delta\dot{e'_q} &= \frac{1}{T'_{do}}[\Delta E_{fd} - \Delta e'_q - (x_d - x'_d)\Delta i_{td}] \\ \Delta\dot{E_{fd}} &= \frac{K_A}{T_A}\Delta V_t - \frac{1}{T_E}\Delta E_{fd} \end{aligned} \tag{4.8}$$

along with the generator output current:

$$\Delta i_t = \Delta i_{td} + j\Delta i_{tq} \tag{4.9}$$

The first-order difference of i_{td} can be obtained from (4.6) as

$$\Delta i_{td} = \frac{-r_t}{r_t^2 + x_1 x_2}\Delta V_{sd} + \frac{x_2}{r_t^2 + x_1 x_2}(\Delta e'_q - \Delta V_{sq}) \tag{4.10}$$

Similarly obtaining the change in the q-axis generator output current is

$$\Delta i_{tq} = \frac{\Delta V_{sd}}{x_1} + \frac{r_t}{x'_d + x_t}(\Delta e'_q - \Delta V_{sq}) \tag{4.11}$$

Further algebraic manipulation yields

$$\Delta V_t = \frac{V_{do}}{V_{to}}\Delta V_d + \frac{V_{qo}}{V_{to}}\Delta V_q = \frac{V_{do}}{V_{to}}(x_q \Delta i_{tq}) + \frac{V_{qo}}{V_{to}}(\Delta e'_q - x'_d \Delta i_{td}) \tag{4.12}$$

$$\Delta P_e = e'_{qo}\Delta i_{tq} + i_{tqo}\Delta e'_q + (x_q - x'_d)[i_{tdo}\Delta i_{tq} + i_{tqo}\Delta i_{td}] \tag{4.13}$$

4.2.2 Photovoltaic system

A mathematical expression describing the I-V characteristics of a solar cell has been studied extensively. An equivalent model of a solar cell shown in figure 4.2 includes a photo diode, a shunt resistor depicting leakage current and a series resistor representing an internal resistance to current flow. The difference between photovoltaic current I_{ph} and sum of normal diode current I_D and leakage current in the shunt resistor I_{sh} gives the net output current from the PV cell.

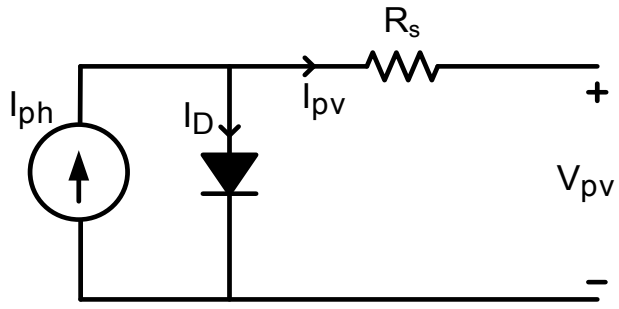

Figure 4.2: Model of PV cell

$$I_{pv} = I_{ph} - I_D - \frac{(V_{pv} + I_{pv}R_s)}{R_{sh}} \tag{4.14}$$

The diode current I_D is given as

$$I_D = I_s(e^{\frac{(V_{pv}+R_sI_{pv})}{nV_T}} - 1) \tag{4.15}$$

where I_{pv} is the cell current, V_{pv} is the cell voltage, I_s is the reverse saturation current(depends on temperature), n is the ideality factor, R_s is the series resistance, R_{sh} is the shunt resistance, $V_T(= \frac{kT}{q})$ is the thermal voltage, k is Boltzmann constant, T is working temperature of the cell and q is the charge of the electron.

The solar irradiation and the working temperature of the cell determines the photo current. At given cell temperature T, the photo current can be expressed as

$$I_{ph} = [I_{sc} + a(T - T_{ref})]G \tag{4.16}$$

where I_{sc} is the short current of the cell at 25^0C and $1kW/m^2$, a is the temperature coefficient of I_{sc}, T_{ref} is the reference temperature of the cell and G is the irradiation in kW/m^2.

The reverse saturation current also depends on temperature and can be expressed as

$$I_s = I_{sref}(\frac{T}{T_{ref}})^{\frac{3}{n}} e^{\frac{-qE_g}{nk}(\frac{1}{T}-\frac{1}{T_{ref}})} \tag{4.17}$$

where I_{sref} is the saturation current of the cell, E_g is the energy band gap of the semiconductor used in the solar cell.

The characteristic equation of the cell from the approximate model is given as

$$I_{pv} = I_{sc} - I_s[e^{q(\frac{V_{pv}+I_{pv}R_s}{nV_T})} - 1] \tag{4.18}$$

Because of the fact that the power generated by a solar cell is low, multiple solar cells are connected in series and parallel to generate power in the range of watts. Thus the characteristic equation of the photovoltaic array consisting of N_s series and N_p parallel modules can be derived from the PV cell equation mentioned above

$$I_{pv} = N_p I_{ph} - N_p I_s[e^{(\frac{V_{pv}}{N_s}+\frac{I_{pv}R_s}{N_p})/nV_T} - 1] \tag{4.19}$$

which is a nonlinear current voltage relationship of a PV array. Alternatively, it can be rewritten as

$$V_T = N_s[ln(\frac{N_p I_{ph} - I_{pv}}{N_p I_s} + 1)nV_T - \frac{I_{pv}R_s}{N_p}] \tag{4.20}$$

This can iteratively using Newton-Raphson algorithm [125] of the form

$$x_{n+1} \quad = \quad x_n - \frac{f(x_n)}{f'(x_n)}, \quad \overset{continues}{\longrightarrow} |\frac{x_{n+1} - x_n}{x_n}| \leq E_s \tag{4.21}$$

where E_s is a prescribed tolerance and x_n is the nth solution. Letting

$$x_n = V_{T,n}, \quad f(V_T) = V_T - N_s[nV_T * ln(\frac{N_p I_{ph} - I_{pv} - N_p I_s}{N_p I_s}) + \frac{I_{pv}R}{N_p}]$$

Since $f'(V_T) = 1$, the recursive formula (4.20) can be written as

$$V_{n+1} = N_s[nV_T * ln(\frac{N_p I_{ph} - I_{pv} - N_p I_s}{N_p I_s}) + \frac{I_{pv}R}{N_p}] \tag{4.22}$$

4.2.3 Power conditioning unit of PV system

:

The power conditioning unit (PCU) consists of devices needed to connect the PV array to the microgrid [126]. The significant components of the PCU are

1. *DC/DC Converter*

2. *DC link Capacitor*

3. *Inverter*

4. *Output filter circuit*

DC/DC Converter model:

The primary function of the DC/DC converter is to either increase or decrease the DC output voltage. Out of the various topologies of DC/DC converters, buck and boost converters are the more fundamental ones. Because the PV output voltage has be to stepped up, a boost converter is used in this case. A typical converter configuration is shown in Fig. 4.3. The boost converter steps up the DC voltage level. It consists of an inductor, a diode and a power electronic switch.

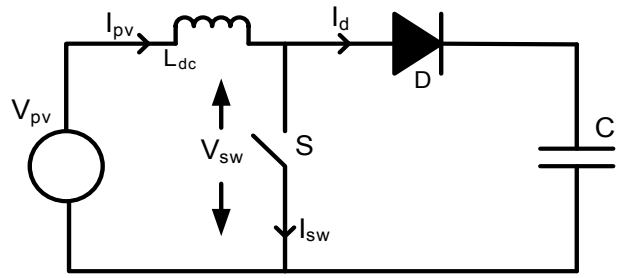

Figure 4.3: DC/DC converter configuration

The dynamics of the converter can be expressed as

$$V_{pv} = L_{dc}\dot{I}_{pv} + (1 - d_c)V_{dcp} \quad \longrightarrow \quad \dot{I}_{pv} = \frac{1}{L_{dc}}(V_{pv} - (1 - d_c)V_{dcp}) \qquad (4.23)$$

where L_{dc} is the inductance of the converter and d_c is the duty cycle defined as the ratio of ON period to the switching time period (T).

DC link capacitor model:

The DC link capacitor functions as an energy storage and filter for the DC voltage.

By applying KCL at the DC-link node, the dynamics of the DC link capacitor can be obtained as

$$\frac{dV_{dcp}}{dt} = \frac{1}{C_{dc}}(I_{dc1} - I_{dc2}) \tag{4.24}$$

where $I_{dc1} = (1 - d_c)I_{pv}$ and I_{dc2} is the input current to the inverter, which is derived later in this section. V_{dc} is the voltage across capacitor C_{dc}.

Inverter model:

The inverter is responsible for the conversion of the PV array DC output and giving it to the grid at an appropriate frequency. A voltage gain model of a voltage source inverter(VSI) operating in PWM mode is considered as shown in Fig. 4.4. The power on DC side of the inverter is given as

$$P_{dc} = V_{dcp}I_{dc2} \tag{4.25}$$

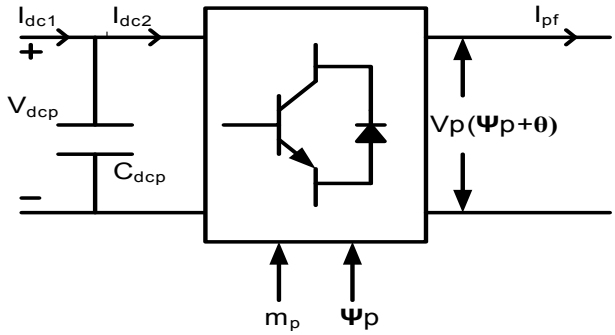

Figure 4.4: Inverter model

The instantaneous active power on the AC side of the inverter is expressed as

$$P_{ac} = Re[V_p I_{pf}^*] \tag{4.26}$$

where V_p and I_{pf} are the inverter output voltage and inverter output current respectively. In d-q terms, V_p and I_{pf} can be expressed as

$$V_p \;\; = \;\; V_{pd} + jV_{pq}, \quad I_{pf} = I_{pfd} + jI_{pfq}$$

Little algebra yields the power relations

$$P_{ac} = V_{pd}I_{pfd} + V_{pq}I_{pfq}, \quad P_{dc} = V_{pd}I_{pfd} + V_{pq}I_{pfq} \tag{4.27}$$

During its operation in PWM mode and referring to Fig. 4.4, the output voltage of the inverter can be written as

$$V_p = m_p + V_{dcp}\psi_p \tag{4.28}$$

where m_p is the modulation index and ψ_p is the phase angle of the inverter. In d-q terms, this becomes

$$V_{pd} = m_p * V_{dcp} * cos(\psi_p + \theta), \quad V_{pq} = m_p * V_{dcp} * sin(\psi_p + \theta) \tag{4.29}$$

Finally, we obtain the expression for I_{dc2} as

$$I_{dc2} = (I_{pfd} m_p cos(\psi_p + \theta) + I_{pfq} m_p sin(\psi_p + \theta)) \tag{4.30}$$

LC filter and coupling inductance model:

The purpose of using a low pass filter is attenuation of switching frequency ripple of the output voltage of a inverter. The filter is a T section of an RL circuit shunted by a capacitor. While the inductor blocks high frequency harmonics, the capacitor stops low frequency harmonics. Collectively, they block most of the harmonics, thereby reducing ripples from going through the system [127]. By applying KVL around the PV inverter and filter capacitor, we obtain a nonlinear relation as:

$$V_p = I_{pf} R_{pf} + L_{pf} \frac{dI_{pf}}{dt} + V_{cp} + (I_{pf} - I_p) R_{pdr} \tag{4.31}$$

where R_{pf} is the filter resistance, L_{pf} is the filter inductance, R_{pdr} is the damping resistance and V_{cp} is the capacitor voltage. Expressed in d-q frame, then (4.31)

can be written as

$$\begin{aligned}\frac{dI_{pfd}}{dt} &= \frac{-\omega_0 R_{pf}}{L_{pf}} I_{pfd} + \omega_0 \omega I_{pfq} + \frac{\omega_0 m_p V_{dcp} cos(\psi_p + \theta)}{L_{pf}} \\ &- \frac{\omega_0 V_{cpd}}{L_{pf}} - \omega_0 R_{pdr} I_{pcd} \qquad (4.32)\\ \frac{dI_{pfq}}{dt} &= \frac{-\omega_0 R_{pf}}{L_{pf}} I_{pfq} - \omega_0 \omega I_{pfd} + \frac{\omega_0 m_p V_{dcp} sin(\psi_p + \theta)}{L_{pf}} \\ &- \frac{\omega_0 V_{cpq}}{L_{pf}} - \omega_0 R_{pdr} I_{pcq} \qquad (4.33)\end{aligned}$$

By coupling the transmission line between microgrid and PV filter capacitor, we obtain a nonlinear equation as

$$V_{cp} = I_p R_p + L_p \frac{dI_p}{dt} + V_s - (I_{pf} - I_p) R_{pdr} \qquad (4.34)$$

Rewriting in d-q terms, we have

$$\begin{aligned}\frac{dI_{pd}}{dt} &= \frac{-\omega_0 R_p}{L_p} I_{pd} + \omega_0 \omega I_{pq} + \frac{\omega_0}{L_p}(V_{cpd} - V_{sd}) + \omega_0 R_{pdr} I_{pcd} \qquad (4.35)\\ \frac{dI_{pq}}{dt} &= \frac{-\omega_0 R_p}{L_p} I_{pq} + \omega_0 \omega I_{pd} + \frac{\omega_0}{L_p}(V_{cpq} - V_{sq}) + \omega_0 R_{pdr} I_{pcq} \qquad (4.36)\end{aligned}$$

where I_p is the coupling current, R_p is the coupling resistance and L_p is the coupling inductance. The voltage across the capacitor is given as

$$C_{pf} \frac{dV_{cp}}{dt} = (I_{pf} - I_p) \qquad (4.37)$$

where C_{pf} is the filter capacitor. Once again in d-q terms, we get

$$\frac{dV_{cpd}}{dt} = \frac{1}{C_{pf}}(I_{pfd} - I_{pd}) + \omega_0 \omega V_{cpq}, \quad \frac{dV_{cpq}}{dt} = \frac{1}{C_{pf}}(I_{pfq} - I_{pq}) + \omega_0 \omega V_{cpd} \quad (4.38)$$

Linearized model of the photovoltaic system:

A linearized model of the photovoltaic system includes a small signal model of characteristic equation of the PV array and power conditioning unit. The characteristic equation of the PV arrays is

$$V_{pv} = N_s[ln(\frac{N_p I_{ph} - I_{pv}}{N_p I_s} + 1)nV_T - \frac{I_{pv} R_s}{N_p}]$$

Making first-order changes of (4.20) with $V_T = V_{pv}$, we get

$$\Delta V_{pv} = K_{pv} \Delta I_{pv}, \quad K_{pv} = -N_s[\frac{nV_T}{N_p I_{ph} - I_{pvo} + N_p I_s} + \frac{R_s}{N_p}] \quad (4.39)$$

By linearization each of the components of the power conditioning unit, a small signal model is obtained. The linearized state equations are given as [126].

$$\begin{aligned} \Delta \dot{V}_{dcp} &= -\frac{1}{C_{dcp}}[-I_{pfd0} m_p sin(\psi_p + \theta)\Delta\psi_p + m_p cos(\psi_p + \theta)\Delta I_{pfd} \\ &+ I_{pfd0} cos(\psi_p + \theta)\Delta m_p \\ &+ I_{pfq0} m_p cos(\psi_p + \theta)\Delta\psi_p + m_p sin(\psi_p + \theta)\Delta I_{pfq} \\ &+ I_{pfq0} sin(\psi_p + \theta)\Delta m_p - (1 - d_c)\Delta I_{pv}] \end{aligned} \quad (4.40)$$

The PV inverter output filter current

$$\begin{aligned}\Delta\dot{I}_{pfd} &= \frac{-\omega_0 R_{pf}}{L_{pf}}\Delta I_{pfd} + \omega_0(\Delta I_{pfq} + I_{pfq0}\Delta\omega) + \frac{\omega_0}{L_{pf}}[m_p cos(\psi_p+\theta)\Delta V_{dcp} \\ &- m_p V_{dcp0} sin(\psi_p+\theta)\Delta\psi_p + V_{dcp0} cos(\psi_p+\theta)\Delta m_p] \\ &- \frac{\omega_0\Delta V_{cpd}}{L_{pf}} - \frac{\omega_0 R_{pdr}}{L_{pf}}(\Delta I_{pfd} - \Delta I_{pq}) \qquad (4.41)\end{aligned}$$

$$\begin{aligned}\Delta\dot{I}_{pfq} &= \frac{-\omega_0 R_{pf}}{L_{pf}}\Delta I_{pfq} - \omega_0(\Delta I_{pfd} + I_{pfd0}\Delta\omega) + \frac{\omega_0}{L_{pf}}[m_p sin(\psi_p+\theta)\Delta V_{dcp} \\ &+ m_p V_{dcp0} cos(\psi_p+\theta)\Delta\psi_p + V_{dcp0} sin(\psi_p+\theta)\Delta m_p] \\ &- \frac{\omega_0\Delta V_{cpq}}{L_{pf}} - \frac{\omega_0 R_{pdr}}{L_{pf}}(\Delta I_{pfq} - \Delta I_{pq}) \qquad (4.42)\end{aligned}$$

The PV output coupling inductance current

$$\begin{aligned}\Delta\dot{I}_{pd} &= -\frac{R_p}{L_p}\Delta I_{pd} + \omega_0(\Delta I_{pq} + I_{pq0}\Delta\omega) \\ &+ \frac{1}{L_p}(\Delta V_{cpd} - \Delta V_{sd}) + \frac{\omega_0 R_{pdr}}{L_p}(\Delta I_{pfd} - \Delta I_{pd}) \qquad (4.43) \\ \Delta\dot{I}_{pq} &= -\frac{R_p}{L_p}\Delta I_{pq} + \omega_0(\Delta I_{pd} + I_{pd0}\Delta\omega) \\ &+ \frac{1}{L_p}(\Delta V_{cpq} - \Delta V_{sd}) + \frac{\omega_0 R_{pdr}}{L_p}(\Delta I_{pfq} - \Delta I_{pq}) \qquad (4.44)\end{aligned}$$

The voltage across the filter capacitor

$$\Delta\dot{V}_{cpd} = \omega_0(\Delta V_{cpq} + V_{cpq0}\Delta\omega) + \frac{1}{C_{pf}}(\Delta I_{pfd} - \Delta I_{pd}) \tag{4.45}$$

$$\Delta\dot{V}_{cpq} = \omega_0(\Delta V_{cpd} + V_{cpd0}\Delta\omega) + \frac{1}{C_{pf}}(\Delta I_{pfq} - \Delta I_{pq}) \tag{4.46}$$

4.3 Integrated Microalternator-PV System Modeling

In the sequel, we consider a system where the microalternator and the PV system are the supply sources for a combined system. This eventually means that we have a microgrid with two distributed generation units. The modeling proceeds done in two parts. Initially both subsystems are modeled individually as presented in the earlier sections. An integrated modeling approach is presented here in this section from a novel view.

The microalternator-PV system is modeled to represent a system of systems, where two different subsystems are operating independently to achieve a common goal. There exists an integration between the two subsystems which is clearly evident from 4.5. It shows that both systems are connected through a common bus having voltage V_s. Eventually, the integrated system is connected to the main grid and a load.

In the end, the combined model consisting of both systems is considered for the

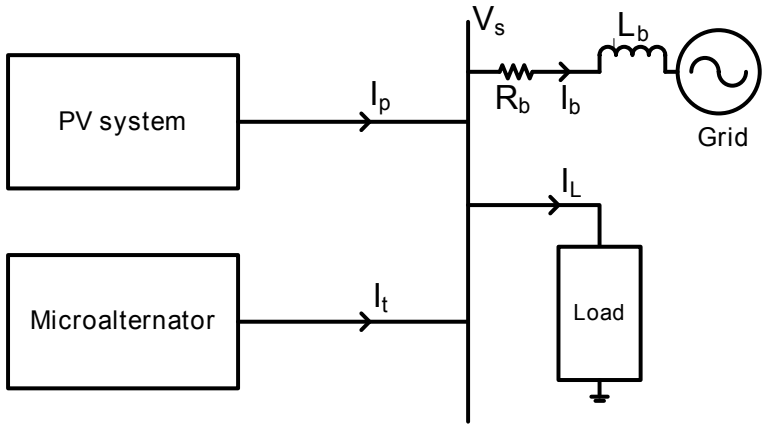

Figure 4.5: Combined system

networked control system (NCS) design implementation. For this reason, the state matrices shown are for the overall system. It is to be noted that the overall system matrices incorporate states and dynamics from both systems forming an integrated microalternator-PV system.

Figure 4.5 shows a microgrid system with a microalternator and PV generator along with a load connected to the main grid. All of these are connected through a common bus having voltage V_s. Microalternator and PV system dynamics have already been explained above. Both the systems had components of V_s along d-q axes. Now to get a closed form representation of the combined state model, V_{sd} and V_{sq} have to be expressed in terms of the selected states.For this we apply KCL at the common bus V_s, which gives

$$I_t + I_p = I_b + I_l$$

where I_t, I_p, I_b and I_l are microalternator output current, PV output current,

grid current and load current respectively. Considering the d-q components of these currents, we get

$$I_{td} + I_{pd} = I_{bd} + I_{ld} \tag{4.47}$$

$$I_{tq} + I_{pq} = I_{bq} + I_{lq} \tag{4.48}$$

Further, we express the non-state currents $(I_{td}, I_{tq}, I_{bd}, I_{bq}, I_{ld}, I_{lq})$ as functions of V_{sd} and V_{sq}. However, the microalternator output currents I_{td} and I_{tq} are already previously presented in terms of V_{sd} and V_{sq}.

Load current:

At the microgrid, the load is modeled as admittance $Y = g - jb$. The load current is $I_l = V_s Y$

$$I_{ld} + jI_{lq} = (V_{sd} + jV_{sq})(g - jb)$$

Equating real and imaginary parts, we get

$$I_{ld} = gV_{sd} + bV_{sq}, \quad I_{lq} = gV_{sq} - bV_{sd} \tag{4.49}$$

Grid current:

The main grid current I_b is given as

$$\begin{aligned} I_b &= \frac{V_s - V_b}{r_b + jx_b} \\ I_{bd} + jI_{bq} &= \frac{V_{sd} + jV_{sq} - (V_b sin\delta + jV_b cos\delta)}{r_b + jx_b} \end{aligned}$$

Equating real and imaginary parts

$$I_{bd} = \frac{(V_{sq} - V_b sin\delta)r_b + (V_{sq} - V_b cos\delta)x_b}{r_b^2 + x_b^2} \tag{4.50}$$

$$I_{bq} = \frac{(V_{sq} - V_b cos\delta)r_b + (V_{sq} - V_b sin\delta)x_b}{r_b^2 + x_b^2} \tag{4.51}$$

Standard manipulations yield the bus voltage components V_{sd} and V_{sq} as

$$V_{sd} = \frac{1}{\Theta_1}[z_b z_1 I_{pd} + z_b x_2 e'_q + V_b z_1 (r_b sin\delta + x_b cos\delta) - \Theta_2 V_{sq}] \tag{4.52}$$

$$V_{sq} = \Theta_4 I_{pd} + \Theta_5 e'_q + \Theta_6 I_{pq} + \Theta_7 V_b \tag{4.53}$$

where

$$\Theta_1 = [gz_b z_1 + z_1 r_b + r_t z_b], \quad \Theta_2 = [bz_b z_1 + x_b z_1 + x_2 z_b]$$

$$\Theta_3 = [x_b x_2 z_1 + bz_b x_2 z_1 + z_1 z_b - r_t^2 z_b], \quad \Theta_n = \Theta_2 \Theta_3 + \Theta_1^2 x_2$$

$$\Theta_4 = \frac{1}{\Theta_n}\Theta_3 z_b z_1, \quad \Theta_5 = \frac{1}{\Theta_n}(\Theta_3 z_b x_2 + z_b x_2 r_t \Theta_1)$$

$$\Theta_6 = \frac{1}{\Theta_n}(\Theta_1 x_2 z_1 z_b), \quad \Theta_7 = \frac{1}{\Theta_n}[z_1 \Theta_3 (r_b sin\delta + x_b cos\delta) + \Theta_1 x_2 z_1 (r_b cos\delta - x_b sin\delta)]$$

Linearized model of the combined system:

A linearized model of the combined system is obtained by expressing the linearized microgrid voltage components ($\Delta V_{sd}, \Delta V_{sq}$) along d-q axes in terms of the selected states. First-order analysis shows that

$$\Delta V_{sq} = \Theta_4 \Delta I_{pd} + \Theta_5 \Delta e'_q + \Theta_6 \Delta I_{pq} + \Theta_0 \Delta \delta \tag{4.54}$$

where

$$\Theta_0 = V_b[\frac{1}{Den}(z_1\Theta_3(r_b cos\delta_0 - x_b sin\delta_0) - \Theta_1 x_2 z_1(r_b sin\delta_0 + x_b cos\delta_0))]$$

Similarly, we also obtain

$$\begin{aligned} \Delta V_{sd} &= \frac{1}{\Theta_1}[z_b z_1 \Delta I_{pd} + z_b x_2 \Delta e'_q + V_b z_1(r_b cos\delta_0 - x_b sin\delta_0)\Delta\delta \\ &- \Theta_2(\Theta_4 \Delta I_{pd} + \Theta_5 \Delta e'_q + \Theta_6 \Delta I_{pq} + \Theta_0 \Delta\delta)] \end{aligned} \tag{4.55}$$

Finally, the values of ΔV_{sd} and Δv_{sq} are substituted in the linearized equations of the individual component models to obtain the closed-form equation. Selecting the states as $[\delta, \omega, e'_q, E_{fd}, I_{pv}, V_{dcp}, I_{pfd}, I_{pfq}, I_{pd}, I_{pq}, V_{cpd}, V_{cpq}]^T$ and the control input as $[m_p, \psi_p]$, we consequently obtain the state matrices for the combined microalternator-PV system.

$$A = \begin{bmatrix} A_1 & A_2 \end{bmatrix}$$

$$A_1 = \begin{bmatrix} 0 & \omega_0 & 0 & 0 & 0 & 0 \\ -\frac{P_{e1}}{2H} & 0 & -\frac{P_{e3}}{2H} & 0 & 0 & 0 \\ A_{(3,1)} & 0 & A_{(3,3)} & \frac{1}{T'_{do}} & 0 & 0 \\ \frac{K_A}{T_A}V_{t1} & 0 & \frac{K_A}{T_A}V_{t3} & \frac{-1}{T_A} & 0 & 0 \\ 0 & \omega_0 I_{pfq0} & 0 & 0 & \frac{k_{pv}}{L_{dc}} & \frac{(d_c-1)}{L_{dc}} \\ 0 & \omega_0 I_{pfd0} & 0 & 0 & \frac{(1-d_c)}{C_{dcp}} & 0 \\ -k_p D_1 & \omega_0 I_{pd0} & -k_p C_1 & 0 & k_{pf} & 0 \\ -k_p G & -\omega_0 I_{pq0} & -k_p C_1 & 0 & 0 & 0 \\ 0 & \omega_0 V_{cpq0} & 0 & 0 & 0 & 0 \\ 0 & -\omega_0 V_{cpq0} & 0 & 0 & 0 & 0 \\ 0 & 0 & 0 & 0 & 0 & 0 \\ 0 & 0 & 0 & 0 & 0 & 0 \end{bmatrix}$$

$$A_2 = \begin{bmatrix} 0 & 0 & 0 & 0 & 0 & 0 \\ P_{e1} & P_{e2} & 0 & 0 & 0 & 0 \\ e_{q1} & e_{q2} & 0 & 0 & 0 & 0 \\ 0 & 0 & 0 & 0 & 0 & 0 \\ 0 & 0 & 0 & 0 & 0 & 0 \\ m_p k_{pd1} & m_p k_{pd2} & 0 & 0 & 0 & 0 \\ -k_{pf} R_{eq} & \omega_0 & k_{pf} R_d & 0 & -k_{pf} & 0 \\ -\omega_0 & -k_{pf} R_{eq} & 0 & k_{pf} R_d & 0 & -k_{pf} \\ k_p R_d & 0 & A_{(9,9)} & A_{(9,10)} & k_p & 0 \\ 0 & k_p R_d & A_{(10,9)} & A_{(10,10)} & 0 & k_p \\ \frac{\omega_0}{C_{pf}} & 0 & -\frac{\omega_0}{C_{pf}} & 0 & 0 & \omega_0 \\ 0 & \frac{\omega_0}{C_{pf}} & 0 & -\frac{\omega_0}{C_{pf}} & -\omega_0 & 0 \end{bmatrix}$$

$$B = \begin{bmatrix} 0 & 0 \\ 0 & 0 \\ 0 & 0 \\ 0 & 0 \\ k_{pf}V_{dcp0}cos(\psi_p) & -k_{pf}V_{dcp0}m_p sin(\psi_p) \\ k_{pf}V_{dcp0}sin(\psi_p) & k_{pf}V_{dcp0}m_p cos(\psi_p) \\ 0 & 0 \\ 0 & 0 \\ 0 & 0 \\ 0 & 0 \\ 0 & 0 \\ \frac{(I_{pfd0}cos(\psi_P)+I_{pfq0}sin(\psi_P))}{C_{dcp}} & \frac{-m_p(I_{pfd0}sin(\psi_P)+I_{pfq0}cos(\psi_P))}{C_{dcp}} \end{bmatrix}$$

where

$$\begin{aligned} A_{3,1} &= \frac{-(x_d - x'_d)i_{td1}}{T'_{do}}, \quad A_{3,3} = \frac{-(x_d - x'_d)i_{td3}}{T'_{do}} \\ A_{9,9} &= -k_p(R_{eq1} + \Theta_{11}), \quad A_{9,10} = -\omega_0 - k_p(\frac{-\Theta_2\Theta_6}{\Theta_1}) \\ A_{10,9} &= -\omega_0 - k_p\Theta_4, \quad A_{10,10} = -k_p(R_{eq1} + \Theta_6) \\ \Theta_{11} &= (\frac{z_b z_1}{\Theta_1} - \frac{\Theta_2\Theta_4}{\Theta_1}) \end{aligned}$$

Table 4.1: Integrated system parameters [126]

Parameter	Value (p.u)	Parameter	Value (p.u)	Parameter	Value (p.u)
H	3	P_{e1}	0.02	P_{e2}	0.1
M	2.5	P_{e3}	0.15	C_{dcp}	1.1
ω_0	377	R_{eq}	0.1	C_{pf}	0.2
K_A	15	e_{q1}	0.04	R_{eq1}	0.2
T_A	0.03	e_{q2}	0.01	R_d	0.1
x_d	1.3	m_p	100	i_{pfq0}	0.67
x_q	0.47	$k_p = k_{pf}$	1885	i_{pfd0}	0.13
x'_d	0.3	k_{pd1}	0.08	r_t	0.1
T'_{do}	7	k_{pd2}	0.9	r_b	0.15
i_{td1}	0.28	k_{pv}	0.01	x_t	0.2
i_{td2}	0.08	d_c	0.6	x_b	0.265
L_{dc}	0.05				

4.4 Modeling of Networked Control System

Consider the microgrid with two sets of microalternator and PV system representing a system of systems (SoS)-NCS with random communication delays, where the sensor is clock driven and the controller and the actuator are event driven. The discrete-time linear time-invariant plant model is as follows:

$$x_p(k+1) = Ax_p + Bu_p, \quad y_p = Cx_p \tag{4.56}$$

where $x_p(k) \in \Re^n$ is the plant's state vector and $u_p(k) \in \Re^m$ and $y_p(k) \in \Re^p$ are the plant's control input and output vectors, respectively. A, B, and C are known as real matrices with appropriate dimensions. The microalternator-PV system containing A, B and C matrices is discretized at a sampling time of 0.01 seconds.

Table 4.2: Pattern of p_k

p_k	q_1	q_2	$\cdots$	q_{n-1}	q_n
$Prob(p_k = q)$	r_1	r_2	$\cdots$	r_{n-1}	r_n

For a more general case, we assume that the measurement after passing through the network exhibits a randomly varying communication delay and is described by [121]

$$y_c(k) = \begin{cases} y_p(k - \tau_k^m),\ \delta(k) = 1 \\ y_p(k),\ \delta(k) = 0 \end{cases} \tag{4.57}$$

where τ_k^m stands for *measurement delay*, the occurrence of which satisfies the Bernoulli distribution, and $\delta(k)$ is Bernoulli distributed white sequence exhibiting the occurrence of message (packet) dropouts. It order to capture the current practice of computer communication management that experiences different time-dependent operational modes, we let

$$Prob\{\delta(k) = 1\} = p_k$$

where p_k assumes discrete values, see Table II. Two particular classes can be considered:

Class 1: p_k has the probability mass function where $q_r - q_{r-1} =$ constant for $r = 2, ..., n$. This covers a wide range of cases including

1. If there is no information about the likelihood of different values, we use

the uniform discrete distribution, $r_i = 1/n,\ i = 1, 2, ..., n$,

2. If it is suspected that p_k follows a symmetric triangle distribution, we use the following function: i) For n even, $r_i = a + jd,\ j = 0, 1, ..., n/2$ and $r_i = a + (n-j)d,\ j = 0, 1, ..., n/2+1, n/2+2, ..., n,$ where $na + dn(n-1)/4 = 1$, ii) For n odd, $r_i = a + jd,\ j = 0, 1, ..., (n-1)/2$ and $r_i = a + (n-j)d,\ j = 0, 1, ..., (n+1)/2, (n+2)/2, ..., n,$ where $na + dn(n-1)^2/4 = 1$

3. If it is suspected that r_i is a decreasing linear function, we use $r_i = a - jd,\ j = 0, 1, ..., n$ where $na - dn(n-1)/2 = 1$

4. If it is suspected that r_i is a increasing linear function, we use $r_i = a - (n-j)d,\ j = 0, 1, ..., n$ where $na - dn(n-1)/2 = 1$

Class 2: $p_k = X/n,\ n > 0$ and $0 \leq X \leq n$ is a random variable that follows the Binomial distribution $\mathbf{B}(q, n),\ q > 0$, that is

$$\begin{aligned} Prob(p_k = (ax+b)/n) &= \begin{pmatrix} n \\ x \end{pmatrix} q^x (1-q)^{n-x},\ \ b > 0, \\ x &= 0, 1, 2, ..., n,\ \ an + b < n \end{aligned}$$

Remark 4.4.1 *It is significant to note that the case* $Prob\{\delta(k) = 1\} = \bar{\delta}$, *where* $\bar{\delta}$ *is a constant value, is widely used in majority of results on NCS. In this chapter, we focus on nonstationary dropouts.*

When the full state information is not available and the time delay occurs on the

actuation side, it is desirable to design the following observer-based controller [121]:

$$
\begin{aligned}
&Observer: \\
&\hat{x}(k+1) = A\hat{x} + Bu_p(k) + L(y_c(k) - \hat{y}_c(k)) \\
&\hat{y}_c(k) = \begin{cases} C\hat{x}(k),\ \delta(k) = 0 \\ C\hat{x}(k - \tau_k^m),\ \delta(k) = 1 \end{cases} \\
&Controller: \\
&u_c(k) = K\hat{x}(k) \\
&u_p = \begin{cases} u_c(k),\ \alpha(k) = 0 \\ u_c(k - \tau_k^a),\ \alpha(k) = 1 \end{cases}
\end{aligned}
\tag{4.58, 4.59}
$$

where $\hat{x}(k) \in \Re^n$ is the estimate of the system (5), $\hat{y}_c(k) \in \Re^p$ is the observer output, and $L \in \Re^{n \times p}$ and $K \in \Re^{m \times n}$ are the observer and controller gains, respectively, and τ_k^a is the *actuation delay*. The stochastic variable $\alpha(k)$, mutually independent of δ, is also a Bernoulli distributed white sequence with

$$Prob\{\alpha(k) = 1\} = s_k$$

where s_k assumes discrete values. By similarity, a particular class is that s_k has some probability mass function as in Table III, where $s_r - s_{r-1} =$ constant for $r = 2, ..., n$.

Table 4.3: Pattern of s_k

s_k	s_1	s_2	$\cdots$	s_{n-1}	s_n
$Prob(s_k = t)$	t_1	t_2	$\cdots$	t_{n-1}	t_n

For the stability analysis and controller design procedure, please see chapter 3, section 4. It has been omitted, because the same design has been employed to be implemented on the integrated microalternator-pv system presented earlier in this chapter.

4.5 Application Example 2

In this section, the microgrid system which is modeled as a networked control system of system is simulated. The output feedback controller design is implemented which stabilizes the system in presence of packet dropouts and delays. The parameter values given in Table 4.1 [126] are substituted in the state matrices A and B presented earlier in this chapter. Both the sets of PV-microalternator system are similar in nature but have different parameter values. There is no disturbance considered in this simulation, but the system is designed to incorporate packet dropouts and delays.

The controller and observer gains can be obtained by using the relation $K = Y_1 X_1^{-1}$ and $L = Y_2 X_2^{-1} C^{\dagger}$ respectively. Where X_1, X_2, Y_1, Y_2 can be found by solving the LMI (3.22). The values of $\bar{\alpha}$ and $\bar{\delta}$ are set at 0.1 each. The measurement delay is varied from 1 to 5 and the actuation delay is varied from 3 to 9.

The system is discretized at a sampling time of 0.01 seconds, chosen arbitrarily. The NCS is modeled in such a way that delays are accommodated in both the measurement as well as the actuation channel. The delays are generated by employing random number generators. The number obtained from the Uniform Random Number Generator is compared to a variable probability p_k explained earlier in the chapter. If the random generated number is less than p_k, then the output of the comparator is high meaning a delay has occurred. Otherwise, if the output of the comparator is low, there is no delay. This is accomplished by using the variable functional delay block in Simulink. Note that set 1 and set 2 represent two sets of microalternator-PV systems having distinct parameter values. A screenshot of the control design implementation in simulink is shown in Fig. 4.6.

The gain matrices for set 1 are

$$K = \begin{bmatrix} K_1 & K_2 \end{bmatrix}$$

$$K_1 = \begin{bmatrix} -0.0003 & -0.0002 & 0.0001 & -0.0002 & 0.0000 & 0.0001 \\ -0.0001 & -0.0016 & -0.0002 & 0.0004 & -0.0003 & -0.0001 \end{bmatrix}$$

$$K_2 = \begin{bmatrix} -0.0112 & 0.0001 & 0.0000 & -0.0006 & -0.0003 & 0.0000 \\ -0.0003 & -0.0001 & -0.0004 & -0.0001 & -0.0002 & -0.0067 \end{bmatrix}$$

$$L = \begin{bmatrix} -0.0076 & -0.0172 \\ -0.0172 & -0.0013 \\ 0.0041 & 0.0005 \\ -0.0244 & -0.0002 \\ 0.0121 & -0.0042 \\ 0.0061 & 0.0004 \\ -0.0069 & -0.0170 \\ -0.0489 & 0.0010 \\ -0.0039 & -0.0009 \\ -0.0002 & 0.0005 \\ 0.0156 & 0.0008 \\ -0.0015 & 0.0221 \end{bmatrix}$$

The gain matrices for set 2 are

$$K = \begin{bmatrix} K_1 & K_2 \end{bmatrix}$$

$$K_1 = \begin{bmatrix} -0.0007 & -0.0100 & 0.0028 & 0.0004 & 0.0003 & -0.0419 \\ -0.0005 & -0.0003 & 0.0000 & 0.0020 & -0.0002 & -0.0090 \end{bmatrix}$$

$$K_2 = \begin{bmatrix} 0.0000 & -0.0001 & 0.0016 & 0.0021 & 0.0023 & 0.0000 \\ 0.0000 & 0.0000 & -0.0012 & 0.0011 & 0.0000 & -0.0047 \end{bmatrix}$$

$$L = \begin{bmatrix} -0.0152 & -0.0036 \\ -0.0030 & -0.0003 \\ 0.0016 & -0.0025 \\ 0.0000 & 0.0005 \\ -0.0116 & 0.0010 \\ 0.0008 & 0.0002 \\ -0.0003 & -0.0001 \\ 0.0011 & -0.0126 \\ 0.0000 & 0.0003 \\ 0.0000 & -0.0124 \\ 0.0166 & -0.0008 \\ -0.0003 & 0.0003 \end{bmatrix}$$

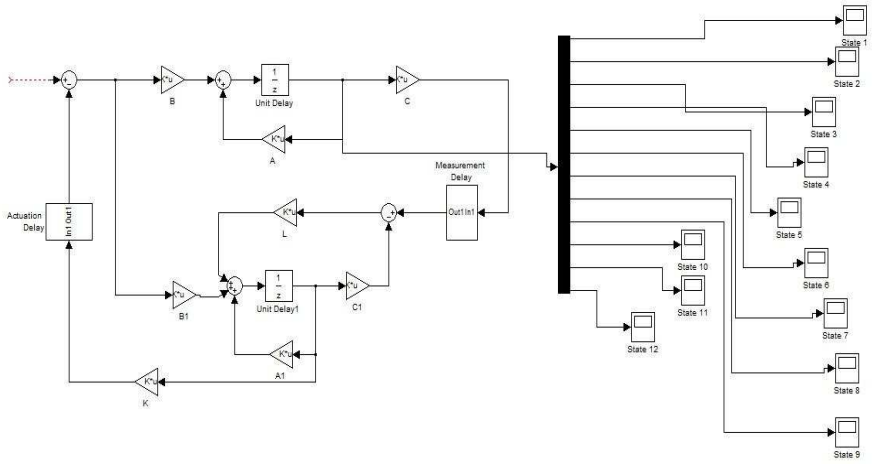

Figure 4.6: Simulink screenshot of the control design implementation

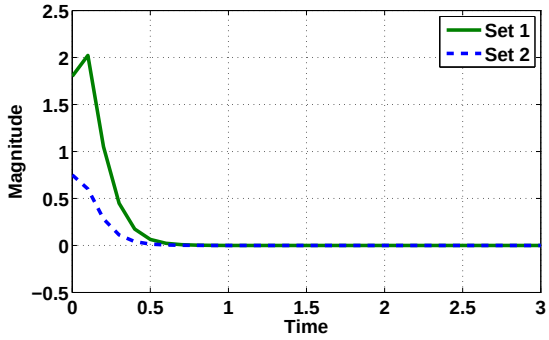

Figure 4.7: Rotor angle of the microalternator

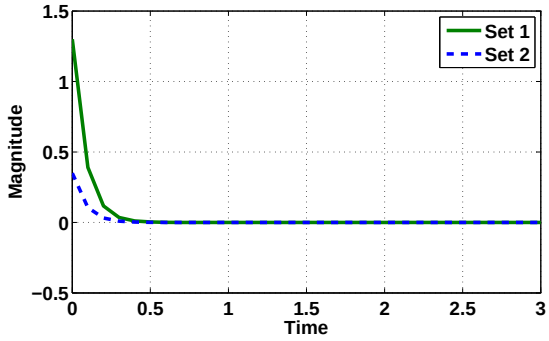

Figure 4.8: Rotor speed of the microalternator

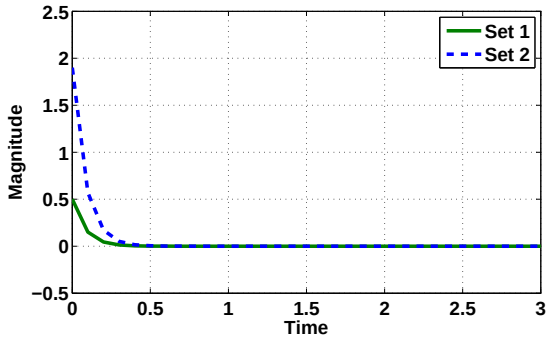

Figure 4.9: Internal voltage of microalternator along q-axis

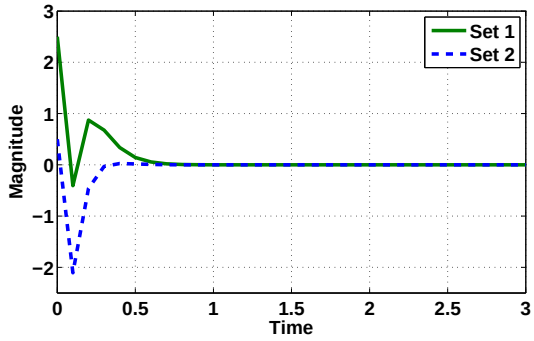

Figure 4.10: Field voltage of microalternator along d-axis

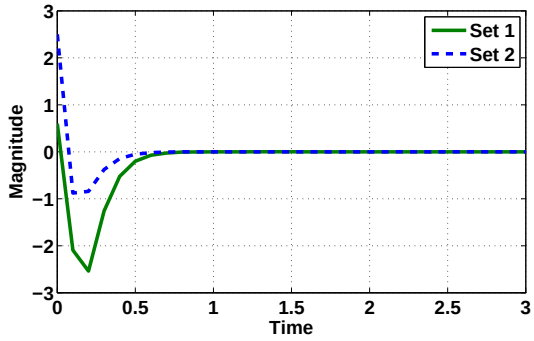

Figure 4.11: Photovoltaic cell current

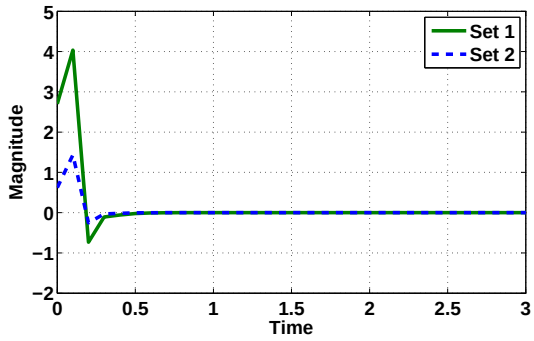

Figure 4.12: Voltage across DC-link capacitor

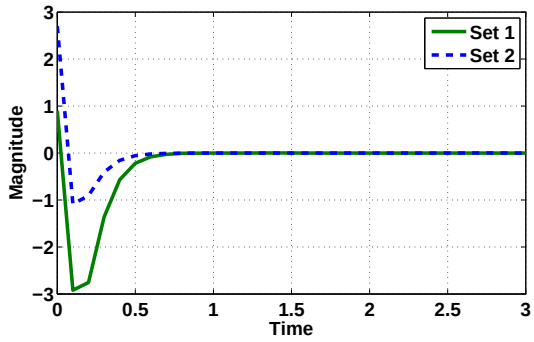

Figure 4.13: Inverter output current along d-axis

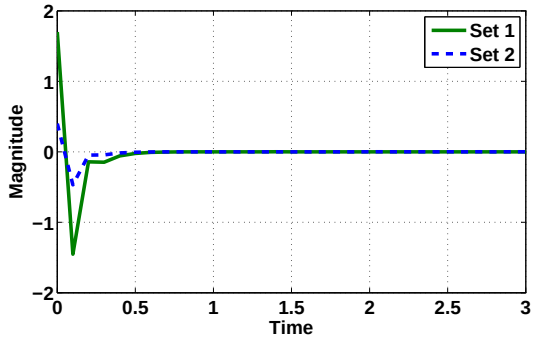

Figure 4.14: Inverter output current along q-axis

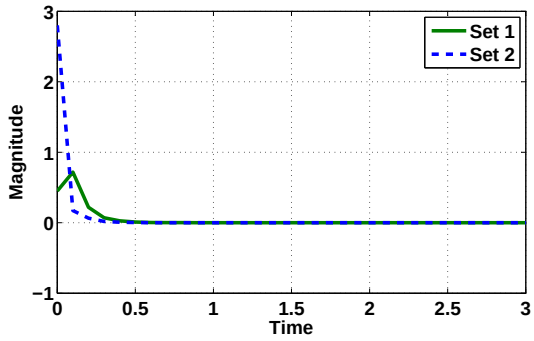

Figure 4.15: Coupling line current of the filter along d-axis

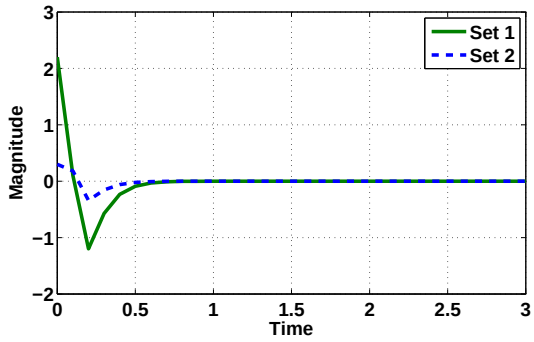

Figure 4.16: Coupling line current of the filter along q-axis

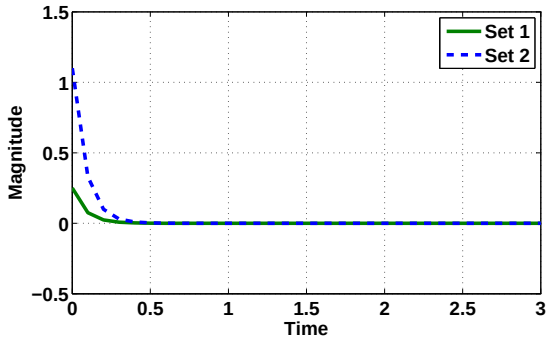

Figure 4.17: Capacitor voltage of the filter along d-axis

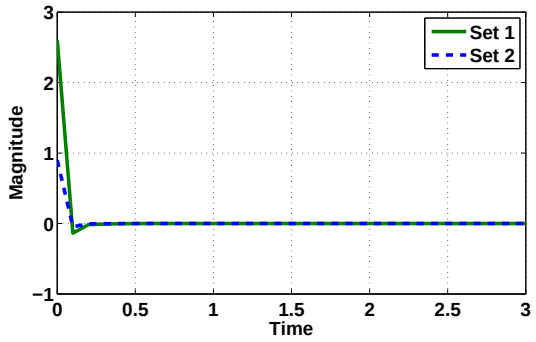

Figure 4.18: Capacitor voltage of the filter along q-axis

The figures shown above represent the state response of both sets of microalternator-PV system named as set 1 and set 2. Each state represents a typical dynamic of the system.

The simulation results elucidate the effectiveness of the proposed control methodology. Two sets of the microalternator-PV system are considered which have distinct parameter values. As evident from the graphs, the output feedback controller stabilizes the system in presence of delays and packet dropouts. It can be observed from the state-wise response that each state of both the sets possessing different values is stabilized by the controller at a reasonably less time with minimum overshoot and very less oscillations. Thus, the simulation results obtained significantly exhibit the controller responses for different parameter values. Moreover, stabilization in presence of communication infractions such as packet dropouts and delays further explains the effectiveness of the controller. It is also to be noted that the state response of both sets of microalternator-PV system is presented in one graph to demonstrate the ability of the controller to stabilize the system irrespective of the parameter values. Further, since the

model considered in this chapter is distinct from the one taken in chapter 3, a comparison cannot be made.

Chapter 5

Event Triggered Control of Wind Turbine With Control and Communication Optimization

5.1 Introduction

Networked Control Systems (NCSs) are now ubiquitous in the literature and have been investigated in detail in the past decade. They can be broadly classified into periodic and aperiodic systems. Majority of the networked control

systems are based on periodic schemes and substantial design methodologies are available. However, periodic networked control systems which are based on time triggering, tend to overload the communication channel by transmitting even if there is no requirement. This results in inefficient utilisation of network and increases communication cost. To overcome this issue, aperiodic schemes such as event triggering and self triggering can be employed. They considerably reduce the load on the communication channel by transmitting only when needed, thereby ensuring optimal performance of the NCS.

[128] presents a comprehensive review of aperiodic triggering for networked control systems. Theoretical results from numerous papers have been compiled and remarks on future extension have also been made. In [129], a model based predictive control based on event triggering is proposed for networked control systems. The effectiveness of the control methodology is demonstrated on a ball and beam system. In [130], the stabilization of quantized event triggered networked control systems is discussed. A networked control system is designed which considers plant uncertainty, quantization, packet losses and event triggering mechanism. Lyapunov functions and linear matrix inequalities are used to derive sufficient stabilization conditions. A review of periodic and aperiodic triggering schemes for networked control systems is provided in [131]. Considering the vast published literature, an attempt has been made to compare and analyze event, self and time triggering schemes for networked control systems. In [132], an event triggered scheduling based on an error-dependent scheme is proposed for multi-loop control systems which possess a common channel for data transmission. Packet dropouts are considered in the channel to demon-

strate its robustness. In [133], the H_∞ control problem is studied for networked control systems, where a Markovian jump system is used to describe the communication infractions such as delay and packet dropouts. Sufficient conditions are also derived to ensure stability of the system. A hybrid event triggered scheme for the intelligent control of microgrid based on multi agent systems is explained in [134].

Microgrids are gradually gaining a lot of popularity in the distributed generation domain. There has been an increasing interest in proposing control strategies for microgrids. Particularly, networked control has been receiving considerable attention. A robust networked control scheme for microgrids is presented in [50]. A distributed networked-based scheme is proposed for control of an islanded microgrid in [135]. The stability issue in networked microgrids has been addressed in [136]. In [58], a networked controlled model is presented for multi-inverter systems. A distributed scheme for detection and protection of networked control systems with applications to power systems is introduced in [137]. A distributed cooperative control based control methodology is proposed for the secondary level of microgrid control in [138]. The methodology is implemented through a communication network. Moreover, optimization techniques like the Particle Swarm Optimization (PSO) have also been used in microgrids for various purposes and applications.[139]-[141].

However, event triggering based networked control has not been addressed significantly in microgrids. Aperiodic networked control schemes, as mentioned earlier tend to utilize communication network efficiently and hence can be envisaged to enhance microgrid control design. Stability is a primary issue in microgrids

and networks need to be meticulously used in order to avoid unnecessary load on the channel. Thus, event triggering schemes can be employed for microgrid controller and communication design. Further, optimization techniques can be employed to optimize event sampling and system cost. This is what motivates us to design an event triggering based methodology for a wind turbine as a part of microgrid system coupled with controller design and optimization.

Thus we propose an optimized event triggering scheme and an LQG controller design for a wind turbine model in a microgrid system. An Asynchronous-sampled data system (ASDS) approach is used to model the event-triggered system. The communication channel is subject to delays. Also, PSO is employed to optimize the cost and event sampling. A comparative analysis is included to demonstrate the effectiveness of the algorithm.

5.2 Wind Turbine Model

With the advent of renewable energy technology, distributed energy resources like wind turbine systems have been in demand. While serving the evergrowing energy demand, it has managed to provide sustainable and economically viable solutions to the energy market all over the world [142]. A schematic of a typical wind turbine system is shown in fig.5.1.

However, wind turbine systems are difficult to model and control. For efficient analysis of wind turbine systems, the model must closely replicate the dynamic behavior of the system [143]. As can be seen from fig.5.1, there are three main

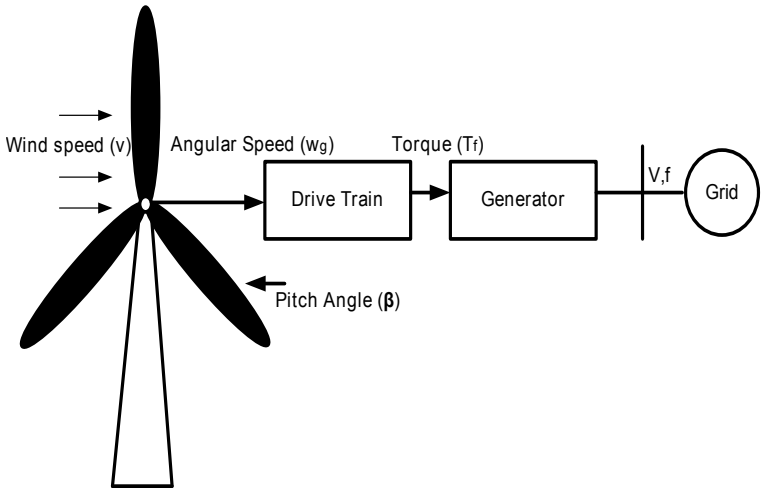

Figure 5.1: Wind turbine system

parts of a wind turbine system:

1. Aerodynamics
2. Drive Train
3. Generator

We now present the modeling equations of these parts. The aerodynamic part acts as a transfer of wind speed to effective rotor torque. A mean wind speed is considered as an input to obatin a simple aerodynamics model [144]. C_p curves are employed to model the aerodynamic transfer. The equation for rotor power is given as

$$P_r = C_p(\lambda, \beta)\frac{1}{2}\rho\pi R^2 v^3 \tag{5.1}$$

where $C_p(\lambda, \beta)$ is the power coefficient obtained from design data, ρ is air density, R is radius of rotor and v is wind speed. The variable λ is defined as

$$\lambda = \frac{\omega_r R}{v} \tag{5.2}$$

where ω_r is the rotor speed.

An electro-mechanical actuator is used to control the pitch angle. The actuator is modeled as a first order system having time constant τ_β.

$$\beta = \frac{1}{\tau_\beta}(\beta_r - \beta) \tag{5.3}$$

with β_r as reference input.

Now, the rotor torque, which is the output of the aerodynamic system is given as

$$T_r = \frac{P_r}{\omega_r} \tag{5.4}$$

.

In the drive train system of the wind turbine,there is a rotor having mass moment of inertia J_r, which is coupled to the generator with mass moment of inertia J_g through a gear transmission. The electro-mechanical torque of the generator is T_e. The equation of motion for relative angle of displacement in the secondary shaft, denoted by ξ is

$$J_v\ddot{\xi} = \frac{vJ_v}{J_r}(T_r - T_D) + \frac{J_v}{J_g}T_e - k\dot{\xi} - T_\xi \tag{5.5}$$

where

$$J_v = \frac{J_r J_g}{J_r + v^2 J_g}$$

In which, k is the damping of the flexible element. T_ξ is the static axis torque, given as

$$T_\xi = 10^4(100\xi^3 - 20\xi^2 + 2\xi) \tag{5.6}$$

The total friction of drive train is

$$T_D = C_1 + \frac{C_2}{\omega_r} + C_3\omega_r \tag{5.7}$$

where C_1, C_2 and C_3 are constants given in [144]. The generator speed ω is

$$J_g\dot{\omega}_g = T_\xi + k\dot{\xi} - T_e \tag{5.8}$$

ω_g is asynchronous generator angular speed. A sensor is used to measure the speed, whose dynamics are

$$\dot{\omega}_{gm} = \frac{1}{\tau_\omega}(\omega_g - \omega_{gm}) \tag{5.9}$$

where ω_{gm} is asynchronous generator measurement angular speed. Then the rotor speed can be computed as

$$\omega_r = \frac{(\xi + \omega_g)}{v} \tag{5.10}$$

and the mechanical torque is

$$T_m = k\dot{\xi} + T_\xi \tag{5.11}$$

Now, (5.1)-(5.11) represents the complete aero-mechanical system of the wind turbine. Linearizing these equations and choosing the state variables as $x^T = [\beta \ \xi \ \dot{\xi} \ \omega_g \ \omega_{gm}]^T$, gives the state space model of the wind turbine in standard form as [143]

$$\begin{aligned} \dot{x}(t) &= Ax(t) + Bu(t) + Ew(t) \\ y &= Cx(t) \end{aligned} \tag{5.12}$$

where $x \in \Re^N$ is the state vector, $u \in \Re^M$ is the input control vector, $w \in \Re^O$ is the disturbance and $y \in \Re^p$ is the output vector.

The state vector is taken as $x^T = [\beta \ \xi \ \dot{\xi} \ \omega_g \ \omega_{gm}]^T$ and the control input vector is taken as $u^T = [\beta_r]$. Where β is pitch angle, ξ is angular speed, ω_g is asynchronous generator angular speed and ω_{gm} is asynchronous generator measurement angular speed. β_r given in the control vector represents blade pitch angle. The details of linearization and modeling can be found in [144].

Table 5.1: Parameter values

Parameter.	**Value**
J_r	$350000kgm^2$
J_g	$32kgm^2$
R	$15m$
ρ	$1.25kg/m^2$
T_ω	$0.1s$
v	21.81
$C_1 = C_2$	$1000Nm$
$C_3 = k$	$100Nm$
τ_β	$0.2s$

The state space matrices, after substituting parameter values given in Table 5.1 are

$$A = \begin{bmatrix} -5 & 0 & 0 & 0 & 0 \\ 0 & 0 & 1 & 0 & 0 \\ -10.5 & -106667 & -3.38 & 23.5 & 0 \\ 0 & 993.84 & 3.12 & -23.5 & 0 \\ 0 & 0 & 0 & 10 & -10 \end{bmatrix}$$

$$B = \begin{bmatrix} 5 \\ 0 \\ 0 \\ 0 \\ 0 \end{bmatrix} \tag{5.13}$$

The C matrix is taken as unity.

5.3 Control Design

A continuous time LTI event-triggered control system is considered and shown in fig.5.2 which has communication in its feedback loop and incorporates random

bounded delays in it. The system is represented by

$$\begin{aligned} \dot{x}(t) &= Ax(t) + B_1u(t) + B_2w(t), \;\; x(0) = x_0, \\ y(t) &= Cx(t) + v(t), \end{aligned} \tag{5.14}$$

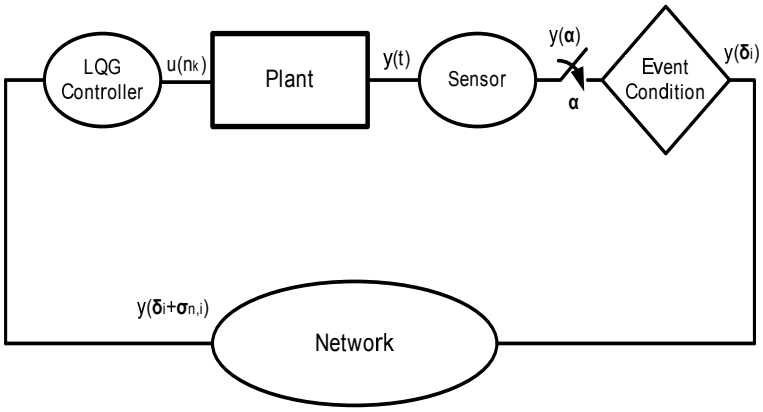

Figure 5.2: Event triggered system block diagram

where $A \in \mathbb{R}^{(n\times n)}$, $B_1 \in \mathbb{R}^{(n\times m)}$, $B_2 \in \mathbb{R}^{(n\times l)}$ and $C \in \mathbb{R}^{(q\times n)}$ are system matrices with appropriate dimensions. $x(t) \in \mathbb{R}^n$ is the state vector, $u(t) \in \mathbb{R}^m$ is the input vector and $y \in \mathbb{R}^q$ is the output vector. $w(t) \in \mathbb{R}^l$ represents Gaussian process noise and $v(t) \in \mathbb{R}^q$ repesents measurement noise.

After every $\alpha \in \mathbb{R}_+$ time units, periodic monitoring of plant state is done and comparison is carried out between costs of ET system and that of periodically triggered system. Only when the cost of aperiodic system is greater than a threshold (that is dependent on cost of periodic system), the occurrence of an event takes place. Following which, transmission of the state to the controller is

done at at δ_i, where $i \in \mathbb{Z}_{\{0,+\}}$. After going through a network-induced random time-delay, the transmission is received by the controller at ρ_j, where $j \in \mathbb{Z}_{\{0,+\}}$. Then, $\sigma_c \in \mathbb{R}_+$ units of time are taken by the controller to compute and estimate the state and controller output u. This will be applied at η_k, where $k \in \mathbb{Z}_{\{0,+\}}$ and $\eta_k = \rho_j + \sigma_c$. It is to be noted that $\Delta_i \triangleq \delta_i - \delta_{i-1}$ represents difference between successive events, while $\Theta_k \triangleq \eta_k - \eta_{k-1}$ denotes difference between corresponding successive updates from controller. A timing diagram is shown in fig.5.3, from which it can be understood that $i = j = k$ signifies translation to i-th event, following j-th corresponding reception and k-th control update.

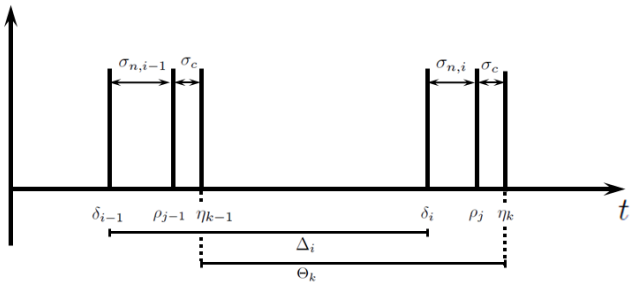

Figure 5.3: Timing diagram illustrating sampling times for ET systems with random transmission delays.

It is also to be noted that intervals between events are lower and upper bounded, meaning $\alpha \leq \Delta_i \leq \Gamma\alpha$, where $1 << \Gamma$. The reason behind introducing upper bound is to make sure latency is bounded. Therefore, the sampling period in worst case is $\Gamma\alpha$, $\overline{\Delta} \triangleq \Gamma\alpha$ and $\overline{\Theta} \approx \Gamma\alpha$ because of random delay.

Assumption 5.3.1 *The following assumptions are made*

1. $\delta_0, \rho_0, \eta_0 = 0$,
2. *All states are available for measurement,*
3. *The computational delay* σ_c *is constant,*
4. *The received states are time-stamped, i.e.,* δ_i *is received along with* i*-th transmission of the state,*
5. *The delay* $\sigma_{n,i} + \sigma_c$ *is less than* Δ_i*, which implies* $\delta_i < \eta_k$, $\forall i = k$*, and*
6. Θ_k/Δ_i *is irrational for all* i, k .

Remark 5.3.1 *Because the network-induced delay is of random nature, the last assumption becomes realistic and makes the below ratio irrational*

$$\frac{\Theta_k}{\Delta_i} = 1 + \frac{\sigma_{n,i} - \sigma_{n,i-1}}{\Delta_i}$$

Now, the objective is two pronged. While one being optimal control of the plant (5.14) having network-induced and computational delays $\sigma_{n,i}$ and σ_c, the other is employing an event triggered scheme to conserve communication bandwidth. The aforementioned objectives are accomplished by using an asynchronous sampled-data system (ASDS) approach to model the event triggered closed-loop system having delays, followed by corresponding LQG controller design.

5.3.1 ET LQG Controller

The plant (5.14) can be considered as a dual-rate ASDS, owing to the sampling scheme mentioned above. This is because, at the sensor node, usually the sampling interval is distinct from the control update i.e.,$\Delta_i \neq \Theta_k \ \forall i = k$. Assuming all states are availbale for measurement, this leads to

$$\begin{aligned} \dot{x}(t) &= Ax(t) + B_1 u(t) + B_2 w(t), \quad x(0) = x_0, \\ y(\delta_i) &= x(\delta_i) + v(\delta_i), \\ u(t) &= u_{\eta_k} = f(\hat{x}(\delta_i)), \quad \forall t \in [\eta_k, \eta_{k+1}), \end{aligned} \tag{5.15}$$

where $f(.) : \mathbb{R}^n \rightarrow \mathbb{R}^m$ is a causal mapping that optimizes a particular cost function.

In [145], a solution is presented for optimal control of ASDS. The sampling and hold times for the sensor and conroller respectively are considered to be disproportionate i.e., $\delta_i \neq \eta_k$. For the cost function minimization, the controller was shown to depend on estimated state η_k using state information at δ_i. Fixed sampling and hold rates were assumed. However, in this case, sampling time is considered aperiodic. This means the control application time is also aperiodic. Consequently, the sampling and hold times are taken as event and control update instants.

Assumption 5.3.2 *It is assumed for all i, k that,*

1. *The discrete-time (DT) systems (C, A_{Δ_i}) are detectable,*

2. *The DT systems* $(A_{\Theta_k}, B_{\Theta_k})$ *are stabilizable,*

3. *System* (5.15) *is stabilizable and detectable,*

where $A_a = e^{A(a)}$ and $B_a = \int_0^a A_s B_1 ds$ are the discretized system matrices for any time-interval a.

Consider $\hat{x}_\tau$, x_τ, and u_τ to represent the estimated state, sampled-state, and control input at time τ, respectively, and $Q_\tau \in \mathbb{R}^{n\times n} > 0$ and $R_\tau \in \mathbb{R}^{m\times m} > 0$ represents the state and input weighting matrices at τ, then the controller that minimizes following discrete cost function

$$J_\Theta = \sum_{k=0}^{K-1} \frac{1}{K\eta_k} \mathsf{E}\left[x_{\eta_k}^T Q_{\eta_k} x_{\eta_k} + u_{\eta_k}^T R_{\eta_k} u_{\eta_k} dt \right], \tag{5.16}$$

is expressed as

$$\begin{aligned} u_{\eta_k} &= -(R_{\eta_k} + B_{\Theta_k}^T P_k B_{\Theta_k})^{-1} (B_{\Theta_k}^T P_k A_{\Theta_k}) \hat{x}_{\eta_k}, \\ &= -K_{\eta_k} \hat{x}_{\eta_k}, \end{aligned} \tag{5.17}$$

where, the state estimate $\hat{x}_{\eta_k}$ is

$$\begin{aligned} \hat{x}_{\eta_k} &= A_{\eta_k - \delta_i} \hat{x}_{\delta_i} + B_{\eta_k - \delta_i} u_{\eta_{k-1}}, \ \forall k = i, \\ \hat{x}_{\eta_0} &= x_0. \end{aligned} \tag{5.18}$$

Q_{η_k} and R_{η_k} are described as

$$\begin{aligned} Q_{\eta_k} &= \int_{\eta_{k-1}}^{\eta_k} [A_{s-\eta_{k-1}}^T A_{s-\eta_{k-1}}] ds, \\ R_{\eta_k} &= \int_{\eta_{k-1}}^{\eta_k} [B_{s-\eta_{k-1}}^T B_{s-\eta_{k-1}}] ds, \end{aligned} \tag{5.19}$$

and $\{P_k\}$ is expressed as the unique positive semi-definite solution of DT Riccati equation

$$\begin{aligned} P_k = A_{\Theta_k}^T [P_{k+1} - P_{k+1} B_{\Theta_k} (R_{\eta_k} + B_{\Theta_k}^T P_{k+1} B_{\Theta_k})^{-1} \\ B_{\Theta_k}^T P_{k+1}] A_{\Theta_k} + Q_{\eta_k}, \\ P_K = 0. \end{aligned} \tag{5.20}$$

Observing (5.18), it can be noted that the estimated state for time instant η_k is dependent on the state estimate for δ_i, which is represented as

$$\hat{x}_{\delta_i} = \hat{x}_{\delta_i^-} + S_i [I + S_i]^{-1} \big(y_{\delta_i} - \hat{x}_{\delta_i^-} \big), \tag{5.21}$$

where

$$\begin{aligned} \hat{x}_{\delta_i^-} &= A_{\delta_i - \eta_{k-1}} \hat{x}_{\eta_{k-1}} + B_{\delta_i - \eta_{k-1}} u_{\eta_{k-1}}, \\ \hat{x}_{\delta_0^-} &= x_0, \end{aligned} \tag{5.22}$$

and $\{S_i\}$ is the solution of following Riccati equation

$$\begin{aligned} S_i &= A_{\Delta_i} S_{i-1} A_{\Delta_i}^T - A_{\Delta_i} S_{i-1} [I + S_{i-1}]^{-1} S_{i-1} A_{\Delta_i}^T + W_{\delta_i}, \\ S_0 &= 0, \end{aligned} \tag{5.23}$$

with $W_{\delta_i} = \int_{\delta_{i-1}}^{\delta_i} A_{\delta_i - t} B_2 B_2^T A_{\delta_i - t}^T dt$. The time-varying controller described in (5.17) is rigorous in computation, which means it translates to a larger σ_c. The solution of (5.20) needs knowledge of P_{k+1}, which is difficult to find offline because of aperiodic triggering. Hence, a worst-case system is considered from a control perspective to cope up with problems mentioned above. This system has a control update interval $\overline{\Theta}$ $\forall k$, where optimization is carried out over a finite horizon. Thus, this gives (5.16) as

$$J_\Theta = \lim_{K\to\infty} \sum_{k=0}^{K-1} \frac{1}{K\eta_k} \mathsf{E}\left[x_{\eta_k}^T Q_{\overline{\Theta}} x_{\eta_k} + u_{\eta_k}^T R_{\overline{\Theta}} u_{\eta_k} \right]. \tag{5.24}$$

The above asumption enables a designer to calculate a constant control gain offline,

$$K_{\overline{\Theta}} = (R_{\overline{\Theta}} + B_{\overline{\Theta}}^T P B_{\overline{\Theta}})^{-1} (B_{\overline{\Theta}}^T P A_{\overline{\Theta}}), \tag{5.25}$$

such that

$$u(t) = -K_{\overline{\Theta}} \hat{x}(\eta_k), \;\; \forall t \in [\eta_k, \eta_{k+1}), \tag{5.26}$$

Along with ARE

$$P = A_{\overline{\Theta}}^T [P - P B_{\overline{\Theta}} (R_{\overline{\Theta}} + B_{\overline{\Theta}}^T P B_{\overline{\Theta}})^{-1} B_{\overline{\Theta}}^T P] A_{\overline{\Theta}} + Q_{\overline{\Theta}}. \tag{5.27}$$

For maintaining estimation accuracy, (5.18), (5.21), (5.22), and (5.23) are used. The computational time is further reduced by offline computation of the integral in (5.23) at interval α, i.e., W_α. Also, in course of real-time estimation, the num-

ber of α-spaced intervals in Δ_i are multiplied to obtain W_{δ_i}. In the forthcoming part, the cost of aperiodic system is proven to be lesser than or equal to the cost of worst-case system.

Theorem 5.3.1 *If the system* (5.15) *is implemented using controller* (5.26) *with the Assumptions 5.3.1 and 5.3.2, then the value of the cost*

$$J_\Theta = \sum_{k=0}^{K-1} \frac{1}{K\eta_k} E\Big[x_{\eta_k}^T Q_{\overline{\Theta}} x_{\eta_k} + u_{\eta_k}^T R_{\overline{\Theta}} u_{\eta_k} dt\Big], \tag{5.28}$$

for the ET system is less than (or at most equal to) the cost paid for the system with worst-case sampling period $\overline{\Theta}$*, i.e.,*

$$\begin{aligned} &J_\Theta \leq \\ &\overline{J} \triangleq \frac{1}{K\overline{\Theta}} E \sum_{k=0}^{K-1} \Big[x_{\eta_k}^T Q_{\overline{\Theta}} x_{\eta_k} + u_{\eta_k}^T R_{\overline{\Theta}} u_{\eta_k} dt\Big]. \end{aligned} \tag{5.29}$$

5.4 Event Condition

As stated earlier, periodic monitoring of the plant is done. The cost of event triggered system $J_\Theta(p\alpha)$, where $p \in \mathbb{Z}_{\{0,+\}}$, is compared with periodic system's

cost at every period. The periodic system is given as

$$\begin{aligned} x((p+1)\alpha) &= Ax(p\alpha) + B_1 u(p\alpha), \\ y(p\alpha) &= x(p\alpha) + v(p\alpha), \\ u(p\alpha) &= -(R_\alpha + B_\alpha^T P B_\alpha)^{-1}(B_\alpha^T P A_\alpha)\hat{x}(p\alpha), \\ &= -K_\alpha \hat{x}(p\alpha), \end{aligned} \tag{5.30}$$

and the cost is

$$J_d^*(p\alpha) = \mathsf{E}[x_{p\alpha}^T P_\alpha x_{p\alpha}], \tag{5.31}$$

where P_α is the solution of the following DT ARE

$$P_\alpha = A_\alpha^T[P_\alpha - P_\alpha B_\alpha(R_\alpha + B_\alpha^T P_\alpha B_\alpha)^{-1} B_\alpha^T P_\alpha]A_\alpha + Q_\alpha, \tag{5.32}$$

The measurement noise $v(p\alpha)$ is zero-mean white Gaussian having variance $V\ \forall p$. $J_d^*(p\alpha)$, which is the cost evolution is simulated and saved in the ET setup offline. If $J_\Theta(p\alpha)$ is greater than $J_d^*(p\alpha)$-dependent threshold, transmission of state to controller takes place at δ_i. i.e.,

$$\delta_i = \{t | i \in \mathbb{Z}_{\{0,+\}} \wedge J_\Theta(p\alpha) \geq \gamma J_d^*(p\alpha)\}, \tag{5.33}$$

In the above equation, $\gamma \geq 1$ signifies what amount of control cost the designer is willing to compromise for decrease in communication cost. The value of γ is directly proportional to Δ_i.

The event condition (5.33) has to be amended to incorporate a threshold, since

it does not yield large event-intervals when the system's cost is near origin. The modified equation is

$$\delta_i = \{t | i \in \mathbb{Z}_{\{0,+\}} \wedge J_\Theta(p\alpha) \geq \gamma J_d^*(p\alpha) + \epsilon\}, \tag{5.34}$$

where $\epsilon \in \mathbb{R}_+$.

After considerable simulations, it is deduced that ϵ should be selected $10 - 20\%$ lower than W, which is variance of process noise. Another significant point is that when the value of cost goes below ϵ, the transmission occurs at $\overline{\Delta}$. Thereby increasing cost and using bandwidth inefficiently. Hence, the aforementioned modification justifies itself through efficient bandwidth usage and good system response.

5.4.1 Optimization of γ Using Particle Swarm Optimization

As can be seen from (5.34), the event condition incorporates a parameter γ, other than a constant ϵ and two costs coming from the system. For an event to occur, $J_\Theta(p\alpha) \geq \gamma J_d^*(p\alpha) + \epsilon$ must be satisfied. Since the costs are generated by the system during simulation and epsilon being a fixed constant, we are left only with γ as a variable that can be manipulated. It is worth noting that, the event condition now depends directly on the value of γ. The value of γ will

decide how often the event condition is met and the frequency of transmission. Since our objective here is to reserve communication bandwidth by transmitting only when needed i.e., (only when an event occurs), it becomes incumbent to keep a check on the event condition and minimize the event rate for the efficient utilization of communication network.

In the initial stages, a trial and error methodology was employed for selecting an appropriate value of γ. However, the trial and error method is cumbersome and it is difficult to set a typical value of γ for different systems having peculiar dynamics and system response. Hence, optimization techniques had to be implemented for obtaining optimized values of γ after every α. Out of the many optimization techniques available, the Particle Swarm Optimization (PSO) technique was used, owing to its simplicity and efficiency. A cost function was formulated which had to be minimized by optimizing γ after every α. This would ensure minimization of the cost function with an optimal value of γ, thereby optimizing the event rate and preserving the communication bandwidth.

The formulated cost function is given as

$$J_{opt}(p\alpha) = W_1(\gamma(p\alpha)J_p(p\alpha) + \epsilon) + \frac{W_2}{\gamma(p\alpha)} \tag{5.35}$$

From the above equation, it can be observed that it is similar to (5.34), except that two weights ($W_1 and W_2$) are added. These weights are introduced to emphasize on the control and communication costs. Since both are inversely related, the second term in (5.35) is added. This gives the designer flexibility

to trade off between control and communication costs. In this study, however we have placed equal emphasis on both control and communication. The event condition in (5.34) is modified to (5.35), which forms the objective function of the PSO. The functions thus served by the PSO algorithm are:

1. Optimize γ.
2. Minimize the objective function (5.35) subject to γ, such that the event rates are reduced.
3. Carry out optimization after every period (α).
4. Implement the algorithm within a time constraint of 24 milli seconds as imposed by the practical limitation of the network. This was done to make the algorithm suitable for application to real time networks.

5.4.2 Particle Swarm Optimization

Particle Swarm Optimization (PSO) is a stochastic, population based optimization technique developed by Kennedy and Eberhart [146]. This algorithm is inspired by group communication in animals. Social behavior of animals like bird flocking and fish schooling forms the basis for this technique. PSO has emerged as a popular technique and has been used in a variety of applications. PSO is considered advantageous over its conventional counterparts because it is easy to understand and implement. It is more robust since it employs probability transition rules. It guarantess convergence to the optimal solution, no

matter where the search is initiated in the search space. Also, it does not get trapped in local minima because it is a population based algorithm [147].

5.4.3 PSO Algorithm and Analysis

Intially, a swarm consisting of n particles is considered. Each particle in the swarm represents a potential solution to the minimization problem. Every particle while flying in the multidimensional search space, keeps updating its position based on its own experience and that of other particles. The position update equation of each particle is given by

$$x_{t+1}^{i} = x_{t}^{i} + v_{t+1}^{i} \tag{5.36}$$

where x_i denotes the position of ith particle at time t and x_i denotes the velocity of ith particle at time t. Every particle is initially randomized to compute the fitness function together. This yields a personal best(best value of each particle) and a global best(best value of particle in the entire swarm). A loop is run to find an optimal solution. First the velocities of the particles are updated based on the personal best and global best values. The velocity update equation is

given by

$$\begin{aligned} v_{t+1}^{i} &= wv_{i}^{t} + c_1 * rand * (p_{best} - x_{t}^{i}) \\ &+ c_2 * rand * (g_{best} - x_{t}^{i}) \end{aligned} \tag{5.37}$$

where w is a weighting factor, c_1 and c_2 are positive constants. p_{best} is the personal best value and g_{best} is the global best value.

The PSO algorithm is based on the velocity and position update equations mentioned above. It is fairly simple and easy to implement. The steps involved in the algorithm can be enumerated as follows

1. Set number of iterations, swarm size and the constant values.
2. Intialize the position and velocity vectors.
3. For every particle, the fitness function is computed. The best value among the swarm is selected as global best (g_{best}) and the personal best of every particle is updated as (p_{best}).
4. Velocity and position of the particles are updated based on the equations mentioned earlier.
5. Each particle is evaluated based on the updated position. If the cost function of a particular particle at this instant is less than the global best, then the individual best of each particle is updated as global best.
6. Finally, the minimum value is searched among the global best. This is the minimized value of the fitness function.

As mentioned earlier, the simulation time was a crucial factor in our application. The time constraint was stringent as imposed by the practical limitations of the network and the alloted time could not exceed 24 *milliseconds*. Hence an analysis had to performed to blend the optimization technique to suit the problem constraints. The simulation time depends on several factors and hence meticulous selection of various parameters was incumbent to ensure minimal operational time and effective optimization. The factors involved in the algorithm which could possibly affect simulation time were:

1. Number of iterations
2. Swarm size
3. Correction factors (c_1 and c_2)
4. Inertia (w)
5. Initial values (of position and velocity)

A thorough analysis of the PSO algorithm was carried out, carefully studying the impact of each parameter on the simulation time and minimization. Various objective functions were considered and the algorithm was implemented on single as well as multi variable objective functions. After considerable analysis and test runs, the optimum values were noted that would suit our application and provide optimized values within the prescribed time. Hence general guidelines could be formulated that were tailor made for our application. The ideal number

of iterations and swarm size were found to be $20 - 40$. The values of inertia were determined to be between $0.5 - 1$ and that of correction factor to be in the range $1 - 2$. Initial velocity was set at 0. This analysis proved instrumental in choosing ideal parameter values, thereby avoiding complexity in the final simulation where the controller design is coupled with the optimization. The results of PSO are shown in Table 5.2, which is included in the next section.

5.5 Application Example 3

The controller design coupled with the event triggering scheme is applied to the linearized model of the wind turbine given in (5.13). The simulations are carried out in two stages. First without optimization and then with optimization. In the latter stage, the PSO algorithm is implemented with the event triggering scheme and a comparative analysis is presented. After every period, i.e.,$\alpha = 0.02$ seconds, the event condition is checked. The network is subject to delays having upper bound of $10ms$. The simulation run-time for both stages is 40 seconds. In the first stage, the value of ϵ is taken as 0.003 and that of γ is 10. The value of γ is chosen on basis of trial and error and will be optimized in the next stage. The controller gain for both cases is given as

$$K = \begin{bmatrix} 9.077 & -8.755 & -6.924 & -0.193 & -0.151 \end{bmatrix} \tag{5.38}$$

First, we present the simulation results without optimization. Figure 5.4 shows the reponse of the system after the applied control methodology and event sampling. As can be observed, all states are regulated by the controller in presence of measurement and process noise. This demonstrates the effectiveness of the proposed controller. Now, fig.5.5 shows the sampling intervals for the event condition in (5.34). Further, in fig.5.6, normalized cost curves are shown. One of them is the cost of event triggered system, while the other is a curve representing the comparison between the cost of event triggered system and the costs of other periodic systems.

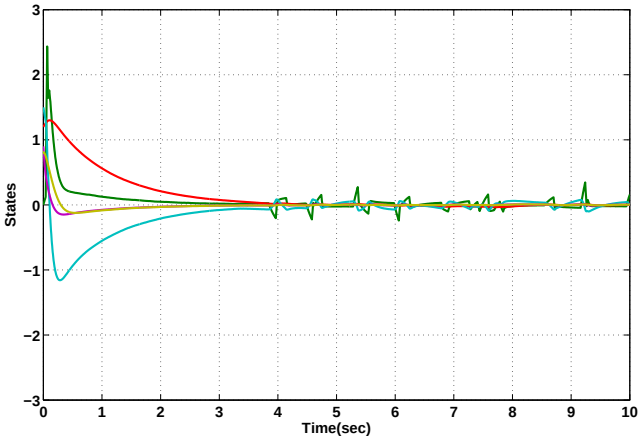

Figure 5.4: State response of the system

Next, we present the simulation results with optimization. Figure 5.7 depicts the system response in presence of measurement and process noise. The controller regulates all the states towards zero. Needless to say, the optimization algorithm does not affect the system stability at all. In fig.5.8, the sampling intervals and events are shown. Figure 5.9 shows the normalized cost curves as explained

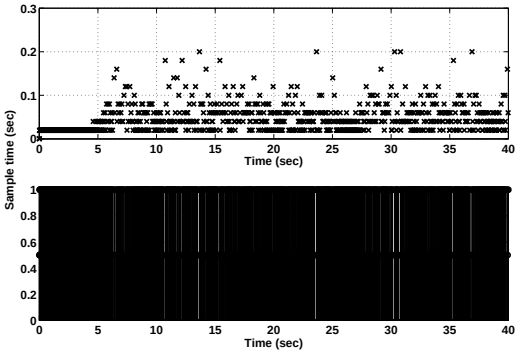

Figure 5.5: Sampling intervals and events

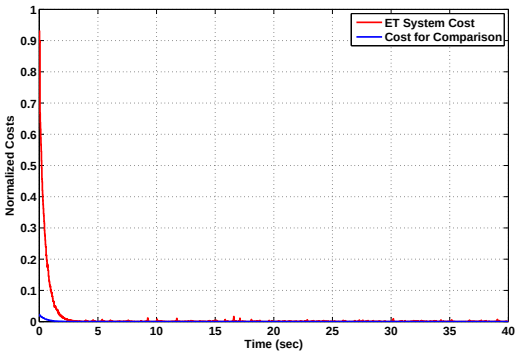

Figure 5.6: Normalized cost curves

above. A comparison between the event triggered system's cost and the costs of other periodic systems is illustrated. Lastly, optimized gamma (γ) over the simulation time is shown in fig.5.10. The value of (γ) is optimized for every period (α). Unlike the constant value of (γ) considered in the first part (without optimization), the optimized (γ) allows the system to attenuate the number of events occuring during sampling and eventually decreases event rate.

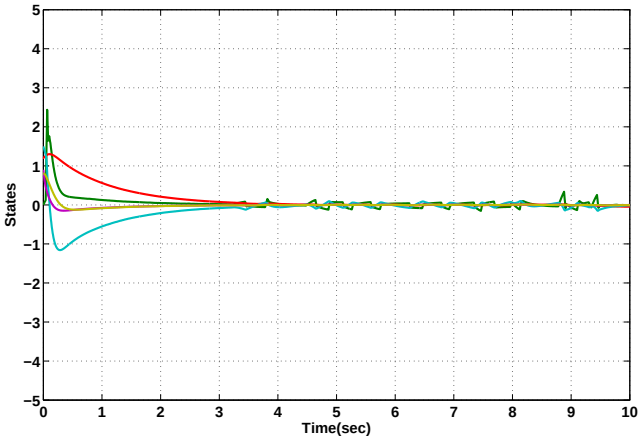

Figure 5.7: State response of the system

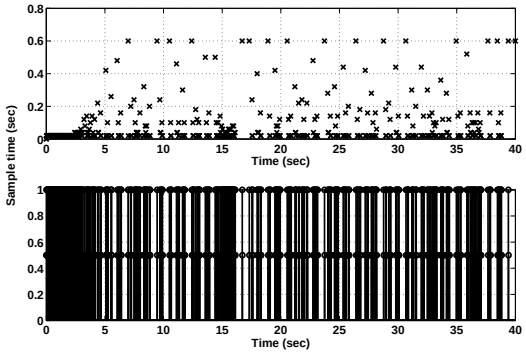

Figure 5.8: Sampling intervals and events

A major difference is observed in the number of events and event rate of the event

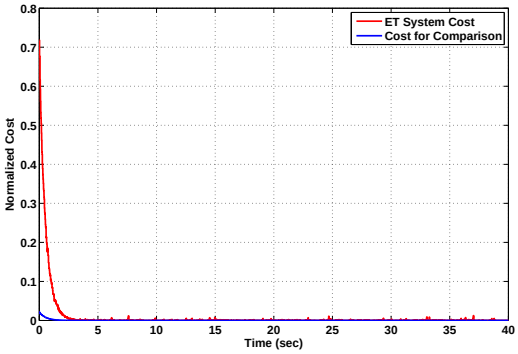

Figure 5.9: Normalized cost curves

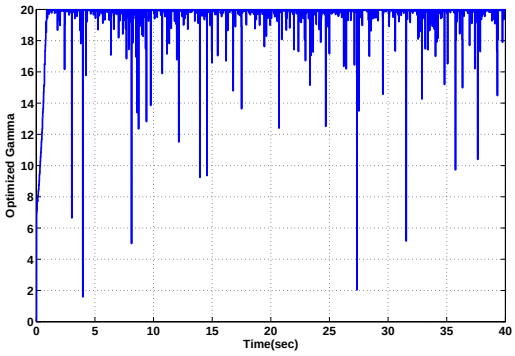

Figure 5.10: Optimized gamma (γ)

Table 5.2: Comparative analysis

Parameter	**Without PSO**	**With PSO**
Number of Events	950	514
Event Rate	32.13	17.13
Worst-case System Cost	0.018	0.02
ET System Cost	3.08×10^{-4}	3.05×10^{-4}

sampled system. The application of PSO algorithm has resulted in a drastic drop in number of events and event rate while making very less or negligible change in the system costs. Table 5.2 demonstrates a comparative analysis of event rates, number of events and system costs for both stages, with and without optimization. It is evident from the table that the event rate is reduced to 17.13 from 32.13, which is quite significant. Another remarkable observation is that there is very less change in the costs of the system. This signifies, for a very little increase in cost, the number of events have been reduced drastically, thereby preserving bandwidth and utilizing the communication network efficiently. The obtained results justify the addition of PSO in the event sampling scheme.

Chapter 6

Conclusion and Future Work

To conclude the work presented in this thesis, we have devised networked control methodologies comprising of both periodic and aperiodic schemes for application to microgrid from an intelligent System of Systems perspective. The stability and control of networked microgrid systems suffering from packet dropouts and delays has been the primary concern of this research.

To begin with, an in depth survey of microgrid architectures and models was done followed by a review of SoS applications. The characteristics of SoS were contrasted with those of a microgrid and the resemblance was portrayed. Further, a framework was proposed for the efficient and organized operation of the microgrid. Then, detailed mathematical modeling of various components of microgrid was presented including wind turbine, solar cell and alternator. Various control methodologies available for microgrids were enlisted. Out of the enlisted

control paradigms, we have focussed on the networked control approach.

In the next part of the thesis, the networked control of microgrid system of systems was presented. For this, the microgrid system consisting of three distributed generation units was modeled as a networked control system of systems having three subsystems. The network was subjected to both measurement and actuation delays and non-stationary packet dropouts. A thorough stability analysis was carried out by employing Lyapunov-Krasovski functions. After which, an output feedback controller was designed for the stabilization of the system in presence of communication infractions. An LMI based approach was adopted for the controller design and further explained by relevant theorems. The control design was implemented on the microgrid system modeled as an RLC network with three generations units representing subsystems in a SoS. Simulation results were depicted to demonstrate the controller performance.

In the next part of the thesis, a combined microalternator-PV system was considered to represent a microgrid system. The detailed dynamic modeling of both constituent systems was presented followed by modeling of the combined system. Two sets of these combined systems having distinct parameter values were considered for the controller implementation. The controller design explained earlier was applied to this combined system. Effectiveness of the controller was demonstrated through simulation. The controller successfully managed to stabilize both sets of the combined system in presence of non stationary dropouts and time delays in quick time with very less oscillations.

In the last part of the thesis, an event triggered scheme was employed for the control of a linear wind turbine system of a microgrid. The inherent advantage

of aperiodic schemes, which is transmitting only when needed and hence preserving communication bandwidth and avoiding overburdening of the channel, prompted us to apply this scheme on a wind system. The wind system was considered as an event triggered system with computational and network delays in the communication channel. An Asynchronous-sampled data system (ASDS) approach was used to design an LQG controller for the event triggered system. Also, Particle Swarm Optimization (PSO) was employed to optimize the event sampling rate. A cost function was formulated for the PSO algorithm and empirical analysis was carried out to customize the algorithm for this application. Futher, a comparative analysis was also done to highlight and justify the significance of the optimization technique. The event sampling optimization and controller performance was elucidated by simulation results and graphs.

Control of microgrids is still a topic of interest and hence has potential for future research. With respect to this thesis work, the directions for further research and extensions include:

- Applying self triggering networked control schemes to microgrid would be an interesting research option. The fact that very little attention has been paid to aperiodic networked control schemes for microgrid control, makes it an open area of future research.
- Including distributed generation sources like fuel cells and hybrid energy vehicles to model a microgrid system could also be an extension to this work.

- The packet loss procedure described in chapter 3 could be replaced by Markov process. Also, different types of communication infractions in the network could be introduced and its impact could be studied.

- Different optimization algorithms can be employed to optimize the event sampling rate, as mentioned in chapter 5.

Bibliography

[1] R. H. Lasseter, "Microgrids and distributed generation", *J. Energy Engineering*, American Society of Civil Engineers, vol. 133, pp. 144–149, 2007.

[2] A. Arulampalam, M. Barnes, A. Engler, A. Goodwin and N. Jenkins, "Control of power electronic interfaces in distributed generation Microgrids", *Int. J. Electronics*, vol. 91, pp. 503–523, 2004.

[3] N. Hatziargyriou, H. Asano, R. Iravani and C. Marnay, "Microgrids: an overview of ongoing research and development and demonstration projects", *Proc. IEEE Power and Energy Magazine*, pp. 78–94, 2007.

[4] G. A. Pagani and M. Aiello, "Towards decentralization: A topological investigation of the medium and low voltage grids", *IEEE Trans. Smart Grid*, vol. 2, pp. 538–547, 2011.

[5] T. L. Vandoorn, B. Renders, L. Degroote, B. Meersman, and L. Vandevelde, "Active load control in islanded microgrids based on the grid voltage", *IEEE Trans. Smart Grid*, vol. 2, pp. 139–151, 2011.

[6] Q. Yang, J. A. Barria, and T. C. Green, "Advanced power electronic conversion and control system for universal and flexible power management", *IEEE Trans. Smart Grid*, vol. 2, pp. 231–243, 2011.

[7] A. Bidram, and A. Davoudi, "Hierarchical structure of microgrids control system", *IEEE Trans. Smart Grid*, vol. 3, pp. 1963-1976, 2012.

[8] M. E. Elkhatib, R. El-Shatshat, and M. M. A. Salama, "Novel coordinated voltage control for smart distributed networks with DG", *IEEE Trans. Smart Grid*, vol. 2, pp. 598–605, 2011.

[9] M. Henshaw, C. Siemieniuch, M. Sinclair, S. Henson, V. Barot, M. O. Jamshidi, D. Delaurentis, C. Ncube, S. L . Lim, and H. Dogan, "Systems of systems engineering: a research imperative", *IEEE Int. Conf. System Science and Engineering*, Hungary, pp. 389–394, 2013.

[10] M. Jamshidi, *System of Systems Engineering: Principles and Applications*, Taylor Francis CRC Publishers, Boca Raton, USA, 2008.

[11] M. Jamshidi, "System of systems engineering- new challenges for the 21'st century", *IEEE System Magazine*, pp. 6–7, 2002.

[12] M. W . Maier, "Architecting principles for systems-of-systems", *Systems Engineering*, vol. 1 , no. 4, pp. 267–284, 1998.

[13] Z. Xiao, J. Wu and N. Jenkins, "An overview of microgrid control", *Intelligent Automation and Soft Computing*, vol. 16, no. 2, pp. 199–212, 2010.

[14] J. M. Guerrero, J. C. Vasquez, J. Matas, L. G. de Vicuna, and M. Castilla, "Hierarchical control of droop-controlled AC and DC microgrids A general approach toward standardization", *IEEE Trans. Ind. Electron.*, vol. 58, no. 1, pp. 158–172, 2011.

[15] A. Kim, M. Kim, E. Puchaty, M. Sevcovic and D. Delaurentis, "A system-of-systems framework for the improved capability of insurgent tracking missions involving unmanned aerial vehicles", *Proc. IEEE 5th Int. Conf. System of Systems Engineering*, pp. 1–6, 2010.

[16] E. T. Rafael, "A top-down, hierarchical, system-of-systems approach to the design of an air defense weapon", *Dissertation* , Georgia Institute of Technology,.2006.

[17] D. S. Soban and D. N. Mavris, "The need for a military system effectiveness framework: The system of systems approach", *American Institute of Aeronautics and Astronautics* pp. 1–11, 2001.

[18] E. Altamiranda and E. Colina, "A system of systems engineering approach for intelligent control and supervision of subsea production systems", *Proc. IEEE/MTS Ocean*, pp. 1–7, 2013.

[19] A. Alfieri, M. Cantamessa, F. Montagna and E. Raguseo, "Usage of SoS methodologies in production system design", *Computers and Industrial Engineering*, vol. 64(2), pp. 562–572, 2013.

[20] J. Q. Liu, H. Nishimura and H. Umehara, "On applying the method of "system of systems" in robustness analysis and autonomous control of

dynamics-aware internet architecture", *Proc. IEEE Int. Systems Conf. (SysCon)*, pp. 1–6, 2012.

[21] E. Grigoroudis, V. S. Kouikoglou and Y.A.Phillis, "A system-of-systems approach for improving healthcare systems", *World Automation Congress*, pp. 1–6, 2012.

[22] Y. Hata, S. Kobashi and H. Nakajima, "Human health care system of systems", *IEEE Systems Journal*, vol. 3, no.2, pp. 231–238, 2009.

[23] M. Mane, W. A. Crossley and Nusawardhana, "System-of-systems inspired aircraft sizing and airline resource allocation via decomposition", *Journal of Aircraft*, vol. 44, no. 4, pp. 1222–1235, 2007.

[24] K. Tsilipanos, I. Neokosmidis and D. Varoutas, "A system of systems framework for the reliability assessment of telecommunications networks", *IEEE Systems Journal*, vol. 7, no. 1, pp. 114–124, 2013.

[25] K. W. Hipel, "Tackling climate change: A system of systems engineering perspective", *Proc. IEEE Int. Conf. System Science and Engineering*, pp. 11–12, 2013.

[26] N. Wenger, A. Antoniev and Dr. A. Gorod, "The international space station: Applying system of systems methodology", *Proc. 8th Int. Conf. System of Systems Engineering*, pp. 235–242, 2013.

[27] A. W. Colombo, S. Karnouskos and T. Bangemann, "A system of systems view on collaborative industrial automation", *Proc. IEEE Int. Conf. on Industrial Technology*, pp. 1968–1975, 2013.

[28] *European Research Project Microgrids* [Online]. Available: http://Microgrids.power.ece.ntua.gr.

[29] *European Research Project More Microgrids* [Online]. Available: http://Microgrids.power.ece.ntua.gr.

[30] M. Prodanovic and T. C. Green, "High-quality power generation through distributed control of a power park microgrid", *IEEE Trans. Industrial Electronics*, vol. 53, no. 5, pp. 1471–1482, 2006.

[31] E. Jones, C. Fitzer and M. Barnes, "Investigation of microgrids", *Proc. the 3rd IET Int. Conf. Power Electronics, Machines and Drives*, pp. 510–514, 2006.

[32] D. Georgakis and S. Papathanassiou, "Operation of a prototype microgrid system based on micro-sources equipped with fast acting power electronics interfaces", *IEEE 35th Annual Power Electronics Specialists Conference,* vol. 4, pp. 2521–2526, Germany, 2004.

[33] E. Planas, A. Gil-de-Muro, J. Andreu, I. Kortabarria and I. M. de Algeria, "General aspects, hierarchical controls and droop methods in microgrids: A review", *Renewable and Sustainable Energy Reviews*, vol. 17, pp. 147–159, 2013.

[34] O. Palizban, K. Kauhaniemi and J. M. Guerrero, "Microgrids in active network managementPartI: Hierarchical control, energy storage, virtual power plants, and market participation", *Renewable and Sustainable Energy Reviews*, vol. 36, pp. 428–439, 2014.

[35] M. Barnes, J. Kondoh, H. Asano, J. Oyarzabal, G. Ventakaramanan, R. Lasseter, N. Hatziargyriou and T. Green, "Real-world microGrids - An overview", *Proc. IEEE Int. Conf. System of Systems Engineering*, pp. 1–8, 2007.

[36] R. Zamora and A. K. Srivastava, "Controls for microgrids with storage: Review, challenges, and research needs", *Renewable and Sustainable Energy Reviews*, vol. 14, no. 7, pp. 2009–2018, 2010.

[37] M. A. Pedrasa and T. Spooner, "A Survey of techniques used to control microgrid generation and storage during island operation", *Australian Universities Power Engineering Conference*, 2006.

[38] S. Baudoin, I. Vechiu and H. Camblong, "A review of voltage and frequency control strategies for islanded microgrid", *Proc. IEEE 16th Int. Conf. System Theory, Control and Computing (ICSTCC)*, pp. 1–5, 2012.

[39] J. B. Almada, R. P. S. Leao, F. F. D. Montenegro, S. S. V. Miranda and R.F. Sampaio, "Modeling and simulation of a microgrid with multiple energy resources", *Proc. IEEE Eurocon*, pp. 1150–1157, 2013.

[40] A. S. Dobakhshari, S. Azizi and A. M. Ranjbar, "Control of microgrids: Aspects and prospects", *Proc. IEEE Int. Conf. Networking, Sensing and Control*, pp. 38–43, 2011.

[41] M. S. Mahmoud, S. A. Hussain and M. A. Abido, "Modeling and control of microgrid: An overview", *J. the Franklin Institute*, vol. 351(5), pp. 2822–2859, 2014.

[42] S. A. Kale, P. P. Jagtap and J. B. Helonde, "Role of micro sources within microgrid", *Proc. IEEE 4th Int. Conf. Emerging Trends in Engineering and Technology*, pp. 174–179, 2011.

[43] H. Liang, B. J. Choi, W. Zhuang and X. Shen, "Stability enhancement of decentralized inverter control through wireless communications in microgrids", *IEEE Trans. Smart Grid*, vol. 4, no. 1, pp. 321–331, 2013.

[44] W. D. Zheng and J. D. Cai, "A multi-agent system for distributed energy resources control in microgrid", *Proc. IEEE 5th Int. Conf. Critical Infrastructure (CRIS)*, pp. 1–5, 2010.

[45] J. Oyarzabal, J. Jimeno, J. Ruela, A. Engler and C. Hardt, "Agent based microgrid management system", *Proc. IEEE Int. Conf. Future Power Systems*, pp. 1–6, 2005.

[46] K. D. Brabandere, K. Vanthournout, J. Driesen, G. Deconinck and R. Belmans, "Control of microgrids", *Proc. IEEE Power Engineering Society General Meeting*, pp. 1–7, 2007.

[47] P. Piagi and R. H. Lasseter, "Autonomous control of microgrids", *Proc. IEEE Power Engineering Society General Meeting (PES)*, 2006.

[48] Y. A. R. I. Mohamed and A. A. Radwan, "Hierarchical control system for robust microgrid operation and seamless mode transfer in active distribution systems", *IEEE Trans. Smart Grid*, vol. 2, no. 2, pp. 352–362, 2011.

[49] A. Mehrizi-Sani and R. Iravani, "Potential-function based control of a microgrid in islanded and grid-connected modes", *IEEE Trans. Power Systems*, vol. 25, no. 4, pp. 1883–1891, 2010.

[50] Q. Shafiee, J. M. Guerrero and J. C. Vasquez, "Distributed secondary control for islanded microgrids A novel approach", *IEEE Trans. Power Electronics*, vol. 29, no. 2, pp. 1018–1031, 2014.

[51] G. Diaz, C. Gonzalez-Moran, J. Gomez-Aleixandre and A. Diez, "Complex-valued state matrices for simple representation of large autonomous microgrids supplied by PQ and Vf generation", *IEEE Trans. Power Systems*, vol. 24, no. 4, pp. 1720–1730, 2009.

[52] A. Bidram, A. Davoudi, F. L. Lewis and J. M. Guerrero, "Distributed cooperative secondary control of microgrids using feedback linearization", *IEEE Trans. Power Systems*, vol. 28, no. 3, 3462–3470, 2013.

[53] P. H. Divshali, A. Alimardani, S. H. Hosseinian and M. Abedi, "Decentralized cooperative control strategy of microsources for stabilizing au-

tonomous VSC-based microgrids", *IEEE Trans. Power Systems*, vol. 27, no. 4, 1949–1959, 2012.

[54] A. Yazdani and R. Iravani, "A unified dynamic model and control for the voltage-sourced converter under unbalanced grid conditions", *IEEE Trans. Power Delivery*, vol. 21, no. 3, pp. 1620–1629, 2006.

[55] N. Pogaku, M. Prodanovic and T. C. Green, "Modelling, analysis and testing of autonomous operation of an inverter based microgrid", *IEEE Trans. Power Electron*, vol. 22, no. 2, pp. 613–625, 2007.

[56] A. J. del Real, A. Arce and C. Bordons, "Hybrid model predictive control of a two-generator power plant integrating photovoltaic panels and a fuel cell", *Proc. 46th IEEE Conf. Decision and Control*, pp. 5447–5452, 2007.

[57] D. L. Peters, A. R. Mechtenberg, J. W. Whitefoot and P. Y. Papalambros, "Model predictive control of a microgrid with plug - in vehicles: error modeling and the role of prediction horizon", *Proc. ASME Dynamic Systems and Controls Conference*, 2011.

[58] W. Zheng, H. Ma and X. He, "Modeling, analysis and implementation of real time network controlled parallel multi-inverter systems", *Proc. IEEE 7th Int. Conf. Power Electronics and Motion Control*, pp. 1125–1130, 2012.

[59] Li, Y. Wei and C. N. Kao, "An accurate power control strategy for power-electronics-interfaced distributed generation units operating in a low-voltage multi-bus microgrid", *IEEE Trans. Power Electronics*, vol. 24, no. 12, pp. 2977–2988, 2009.

[60] M. Nagahara, Y. Yamamoto, S. Miyazaki, T. Kudoh and N. Hayashi, "H-infinity control of microgrids involving gas turbine engines and batteries", *Proc. IEEE 51st Annual Conf. Decision and Control (CDC)*, pp. 4241–4246, 2012.

[61] A. Nejati, A. Nobakhti and H. Karimi, "Multivariable control strategy for autonomous operation of a converter-based distributed generation system", *Proc. IEEE/PES Power Systems Conference and Exposition (PSCE)*, pp. 1–8, 2011.

[62] J. A. P Lopes, A. G. Madureira and C. C. L. M Moreira, "A view of microgrids", *WIREs Energy Environ*, vol 2, no. 1, pp 86–103, 2012.

[63] R. H. Lasseter, A. Akhil, C. Marnay, J. Stephens, J. Dagle, R. Guttronmson, A. S. Meliopoulous, R. Yinger and J. Eto, "White paper on integration of distributed energy resources- the CERTS microgrid concept", Available Online: http://certs.lbl.gov/pdf/50829-app.pdf.

[64] D. Yubing, G. Yulei, L. Qingmin, W. Hui, "Modelling and simulation of the microsources within a microgrid", *IEEE Int. Conf. Electrical Machines and Systems ICEMS*, pp. 2667–2671, 2008.

[65] Y. Zhu, K. Tomsovic, "Development of models for analyzing load - following performance of microturbines and fuel cells", *Electric Power Systems Research*, vol. 62(1), pp. 1–11, 2002.

[66] G. Stavrakakis, G. Kariniotakis. "A general simulation algorithm for the accurate assessment of isolated diesel-wind turbines systems-part I:a gen-

eral multi-machine power system model",.*IEEE Trans. Energy Conversion*, vol. 10(3), pp. 577–583, 1995.

[67] S. Roy, O. Malik, G. Hope. "An adaptive control scheme for speed control of diesel driven power-plants", *IEEE Trans. Energy conversion*, vol. 6(4), pp. 605–611, 1991.

[68] N. Hatziargyriou N, G. Kariniotakis G, "Modelling of microsources for security studies", *Proc. the 2004 CIGRE SESSION*, Paris, France, 2004.

[69] G. Kariniotakis, "DA1-digital models for microsources", *Microgrids Project Deliverable DA1*, 2003.

[70] F. Mohamed, "Microgrid Modelling and Simulation", *PhD Thesis, Helsinki University of Technology*, Finland, 2006.

[71] F. Katiraei, M. R. Iravani and P. W. Lehn, "Microgrid autonomous operation during and subsequent to islanding process", *IEEE Trans. Power Delivery*, vol. 20, no. 1, pp. 248–257, 2005.

[72] H. Karimi, H. Nikkhajoei and R. Iravani, "Control of an electronically-coupled distributed resource unit subsequent to an islanding event", *IEEE Trans. Power Delivery*, vol. 23, no. 1, pp. 493–501, 2008.

[73] F. D. Kanellos, A. I. Tsouchnikas and N. D. Hatziargyriou, "Micro-grid simulation during grid-connected and islanded modes of operation", *Proc. Int. Conf. Power Systems Transients (IPST)*, Canada, 2005.

[74] A. K. Saha, S. Chowdhury, S. P. Chowdhury and P. A. Crossley, "Modelling and simulation of microturbine in islanded and grid-connected mode as distributed energy resource", *Proc. IEEE Power and Energy Society General Meeting*, pp. 1–7, Pittsburgh, 2008.

[75] R. H. Lasseter, P. Paigi, "Microgrids: a conceptual solution", *35th Annual IEEE Power Electronics Specialists Conference*, Germany 2004.

[76] J.H. Watts, "Microturbines: a new class of gas turbine engines", *Gas Turbine News in Brief*, vol. 39 (1), pp. 5–11, 1999.

[77] M. Nagpal, A. Moshref, G.K. Morison and P. Kundur, "Experience with testing and modeling of gas turbines", *Proc. of the IEEE/PES 2001 Winter Meeting*, Ohio, USA, pp. 652–656, 2001.

[78] J. C. H. Phang, D. S. H. Chan, J. R. Phillips, "Accurate analytical method for the extraction of solar cell model parameters",*Electronic Letters*, vol. 20, no. 10, pp. 406–408, 1984.

[79] R. J. Wai and W. H. Wang, "Grid connected photovoltaic generation system", *IEEE Trans. Circuits and Systems 1: Regular Papers* vol. 55, pp. 953–964, 2008.

[80] M. A. Eltawil and Z. Zhao, "Grid-connected photovoltaic power systems: technical and potential problems- A review", *Renewable and Sustainable Energy Reviews*, vol. 14, pp 112–129, 2010.

[81] R. Mukund, *Wind and solar power systems*, CRC Press, LLC, Florida, 1999.

[82] N. Jenkins, R. Allan, P. Crossley, D. Kirschen and G. Strbac, "Embedded generation", *The Institution of Electrical Engineers*, UK, 2000.

[83] T. Ackermann, *Wind Power in Power Systems*, John Wiley and Sons,Ltd, Royal Institute of Technology, Stockholm, Sweden, 2005.

[84] G. N. Kariniotakis, N. L. Soultanis, A. I. Tsouchnikas, S. A. Papathanasiou and N. D. Hatziargyriou, "Dynamic modeling of microgrids", *IEEE Int. Conf. Future Power Systems*, 2005.

[85] M. H. Ashourian , M. A. A. Zin , A. S. Mokhtar, S. J. Mirazimi and Z. Muda, "Controlling and modeling power-electronic interface DERs in islanding mode operation microgrid", *Proc. IEEE Symposium on Industrial Electronics and Applications (ISIEA)*, pp. 161–166, 2011.

[86] X. Zhang, J. Liu, T. Liu and L. Zhou, "A novel power distribution strategy for parallel inverters in islanded mode microgrid", *Proc. 25th Annual IEEE Applied Power Electronics Conference and Exposition (APEC)*, pp. 2116–2120, 2010.

[87] P. K. Ray, S. R. Mohanty and N. Kishor, "Dynamic modeling and control of renewable energy based hybrid system for large band wind speed variation", *Proc. IEEE PES Innovative Smart Grid Technologies Conference Europe (ISGT Europe)*, pp. 1–10, 2010.

[88] N. S. Jayalakshmi and D. N. Gaonkar, "Performance study of isolated hybrid power system with multiple generation and energy storage units", *Proc. Int. Conf. Power and Energy Systems (ICPS),*, pp. 1–5, 2011.

[89] M. Babazadeh and H. Karimi, "Robust decentralized control for islanded operation of a microgrid", *Proc. IEEE Power and Energy Society General Meeting*, pp. 1–8, 2011.

[90] R. Moradi, H. Karimi and M. Karimi-Ghartemani, "Robust decentralized control for islanded operation of two radially connected DG systems", *Proc. IEEE Int. Sym. Industrial Electronics (ISIE)*, pp. 2272–2277, 2010.

[91] S. M. A. Shabestary, M. Saeedmanesh, A. Rahimi-Kian and E. Jalalabadi, "Real-time frequency and voltage control of an islanded mode microgrid", *Proc. The 2nd Iranian Conference on Smart Grids (ICSG),*, pp. 1–6, 2012.

[92] M. Jamshidi, "Control of System of Systems", *Proc. 7th IEEE Int. Conf. Industrial Informatics*, pp. 1–16, 2009.

[93] A. H. Etemadi, E. J. Davison and R. Iravani, "A Decentralized robust control strategy for multi-der microgridsPart I: fundamental concepts", *IEEE Trans. Power Delivery*, vol. 27, no. 4, pp. 1843–1853, 2012.

[94] A. H. Etemadi and R. Iravani, "Eigenvalue and robustness analysis of a decentralized voltage control scheme for an islanded multi-der microgrid", *IEEE Trans. Power Delivery*, vol. 27, no. 4, pp. 1–8, 2012.

[95] C. L. Chen, J. S. Lai, D. Martin and Y. S. Lee, "State-space modeling, analysis, and implementation of paralleled inverters for microgrid applications", *Proc. 25th IEEE Applied Power Electronics Conference and Exposition (APEC)*, pp. 619–626, 2013.

[96] M.Zhu, H. Li and X. Li, "Improved state-space model and analysis of islanding inverter-based microgrid", *Proc. IEEE Int. Sym. Industrial Electronics (ISIE)*, pp. 1–6, 2013.

[97] J. C. Vasquez, J. M. Guerrero, J. Miret, M. Castilla and L. G. D. Vicuna, "Hierarchical control of intelligent microgrids", *IEEE Industrial Electronics Magazine*, pp. 23–29, 2010.

[98] A. L. Dimeas and N. D. Hatziargyriou, "Operation of a multi-agent system for microgrid control", *IEEE Trans. Power Systems*, vol. 20, no. 3, pp. 1447–1455, 2005.

[99] M. A. Joordens and M. Jamshidi, "Consensus control for a system of underwater swarm robots", *IEEE Systems Journal*, vol. 4, no. 1, pp. 65–73, 2010.

[100] J. A. Fax and R. M. Murray, "Information flow and cooperative control of vehicle formations", *IEEE Trans. Automatic Control*, vol. 49, no. 9, pp. 1465–1476, 2004.

[101] R. Olfati-Saber and R. M. Murray, "Consensus protocols for networks of dynamic agents", *Proc. American. Control Conference*, pp. 951–956, 2003.

[102] Z. Lin, M. Broucke and B. Francis, "Local control strategies for groups of mobile autonomous agents", *IEEE Trans. Automatic Control*, vol. 49, no. 4, pp. 622–629, 2004.

[103] W. Ren and R. W. Beard, "Formation feedback control for multiple spacecraft via virtual structures", *Proc. IET Control Theory Appl.*, vol. 151, no. 3, pp. 357–368, 2004.

[104] E. S. Kazerooni and K. Khorasani, "Optimal consensus seeking in a network of multiagent systems: an LMI approach", *IEEE Trans. Systems, Man, and Cybernetics–Part B: Cybernetics*, vol. 40, no. 2, pp. 540–547, 2010.

[105] D. Wu, T. Dragicevic, J. C. Vasquez, J. M. Guerrero and Y. Guan, "Secondary coordinated control of islanded microgrids based on consensus algorithms", *Proc. IEEE Energy Conversion Congress and Exposition*, pp. 4290–4297, 2014.

[106] D. He, D. Shi and R. Sharma, "Consensus-based distributed cooperative control for microgrid voltage regulation and reactive power sharing", *Proc. IEEE PES Innovative Smart Grid Technologies*, pp. 1–6, 2014.

[107] W. Zhang, M. Branicky and S. Phillips, "Stability of networked control systems", *IEEE Control Systems Magazine*, vol 21, no. 1, pp. 84–99, 2001.

[108] J. A. P. Lopes, C. L. Moreira, and A. G. Madureira, "Defining control strategies for analyzing microgrids islanded operation", *Proc. IEEE Russia Power Tech*, pp. 1–7, 2005.

[109] F. Katiraei and M. R. Iravani, "Power management strategies for a microgrid with multiple distributed generation units", *IEEE Trans. Power Systems*, vol. 21, pp. 1821–1831, 2006.

[110] D. J. Lee and L. Wang, "Small-signal stability analysis of an autonomous hybrid renewable energy power generation/energy storage system part I: Time-domain simulations", *IEEE Trans. Energy Conversion*, vol. 23, no. 1, pp. 311–320, 2008.

[111] A. M. O. Haruni, A. Gargoom, M. E. Haque and M. Negnevitsky, "Dynamic operation and control of a hybrid wind-diesel stand alone power systems", *Proc. 25th Annual IEEE Applied Power Electronics Conference and Exposition (APEC)*, pp. 162–169, 2010.

[112] G. K. Kasal and B. Singh, "Voltage and frequency controllers for an asynchronous generator-based isolated wind energy conversion system", *IEEE Trans. Energy Conversion*, vol. 26, no. 2, pp. 402–416, 2011.

[113] Y. Xia, G. P. Liu, M. Fu and D. Rees, "Predictive control of networked systems with random delay and data dropout", *IET Control Theory Appl.*, vol. 3, pp. 1476–1486, 2009.

[114] H. Zhang, Y. Shi and J. Wang, "Observer-based tracking controller design for networked predictive control systems with uncertain markov delays", *Int. J. Control*, vol. 86, no. 10, pp. 1824–1836, 2013.

[115] Y. Shi, J. Huang and B. Yu, "Robust tracking control of networked control systems: Application to a networked DC motor", *IEEE Trans. Industrial Electronics*, vol. 60, no. 12, pp. 5864–5874, 2013.

[116] S. Liu, T. Li, L. Xie, M. Fu and J. F. Zhang, "Continuous-time and sampled-data-based average consensus with logarithmic quantizers", *Automatica*, vol. 49, no. 11, pp. 3329–3336, 2013.

[117] L. Cheng, Y. Wang, Z. G. Hou, M. Tan and Z. Cao, "Sampled-data based average consensus of second-order integral multi-agent systems: Switching topologies and communication noises", *Automatica*, vol. 49, no. 5, pp. 1458–1464, 2013.

[118] S. Liu, T. Li and L. Xie, "Distributed consensus for multiagent systems with communication delays and limited data rate", *SIAM J. Control and Optimization*, vol. 49, no. 6, pp. 2239–2262, 2011.

[119] L. Cheng, Z. G. Hou and M.Tan, "A mean square consensus protocol for linear multi-agent systems with communication noises and fixed topologies", *IEEE Trans. Automatic Control*, vol. 59, no. 1, pp. 261–267, 2014.

[120] W. Liu, W. Gu, W. Sheng, X. Meng, Z. Wu and W. Chen, "Decentralized multi-agent system-based cooperative frequency control for autonomous microgrids with communication constraints", *IEEE Trans. Sustainable Energy*, vol. 5, no. 2, pp. 446–456, 2014.

[121] M. S. Mahmoud, S. Z. Selim, P. Shi and M. H. Baig, "New results on networked control systems with non-stationary packet dropouts", *IET Control Theory Appl.*, vol. 6, no. 15, pp. 2442–2452, 2012.

[122] M. S. Mahmoud, *Switched Time-Delay Systems*, Springer-Verlag, New York, 2010.

[123] M. S. Mahmoud and Y. Xia, "Robust stability and stabilization of a class of nonlinear switched discrete-time systems with time-varying delays", *J. Opt. Theory and Appl.*, vol. 143, pp. 329–355, 2009.

[124] Y. N. Yu *Electric power system dynamics*, Academic Press, New York, 1983.

[125] V. Quaschning and R. Hanitsch, "Numerical simulation of current-voltage characteristics of photovoltaic systems with shaded solar cells", *Solar Energy*, vol. 56, pp. 513–520, 1996.

[126] M. T. Hussain, "Modeling and control of a microgrid including photovoltaic and wind generation", *M.Sc Thesis, King Fahd University of Petroleum and Minerals*, Saudi Arabia, 2012.

[127] N. Mahamad, C. M. Hadzer and S. Masri, "Application of LC filter in harmonics reduction", *Proc.National Power and Energy Conference*, Malaysia, 2004.

[128] M. S. Mahmoud and A. M. Memon, "Aperiodic triggering mechanisms for networked control systems", *Information Sciences*, vol. 296, pp. 282–306, 2015.

[129] X. Yin, D. Yue and S. Hu, "Model-based event-triggered predictive control for networked systems with communication delays compensation", *Int. J. Robust and Nonlinear Control*, vol. 25, no. 5, 2014.

[130] F. L. Qu, Z. H. Guan, D. X. He and M. Chi, "Event-triggered control for networked control systems with quantization and packet losses", *J. of the Franklin Institute*, vol. 352, no. 3, pp. 974–986, 2015.

[131] Q. Hong and H. Zhang, "An introduction to event-based control for networked control systems", *Proc. IEEE Int. Conf. System Science and Engineering (ICSSE)*, pp. 190–195, 2014.

[132] M. H. Mamduhi, D. Tolic A. Molin and S. Hirche, "Event-triggered scheduling for stochastic multi-loop networked control systems with packet dropouts", *Proc. IEEE Conf. Decision and Control*, pp. 2776–2782, 2014.

[133] H. Wang, P. Shi, C. C. Lim and Q. Xue, "Event-triggered control for networked markovian jump systems", *Int. J. Robust and Nonlinear Control*, vol. 25, no. 5, 2014.

[134] C. X. Dou, B. Liu and J. M. Guerrero, "Event-triggered hybrid control based on multi-agent system for microgrids", *IET Generation, Transmission and Distribution*, vol. 8, no. 12, pp. 1987–1997, 2014.

[135] A. Kahrobaeian and Y. A. R. I. Mohamed, "Networked-based hybrid distributed power sharing and control for islanded microgrid systems", *IEEE Trans. Power Electronics*, vol. 30, no. 2, pp. 603–617, 2015.

[136] A. K. Singh, R. Singh and B. C. Pal, "Stability analysis of networked control in smart grids", *IEEE Trans. Smart Grid*, vol. 6, no. 1, pp. 381–390, 2015.

[137] A. Teixeira, H. Sandberg and K. H. Johansson, "Networked control systems under cyber attacks with applications to power networks", *Proc. American Control Conference*, pp. 3690–3696, USA, 2010.

[138] A. Bidram, A. Davoudi, F. L. Lewis and Z. Qu, "Secondary control of microgrids based on distributed cooperative control of multi-agent systems", *IET Generation, Transmission and Distribution*, vol. 7, no. 8, pp. 822–831, 2013.

[139] G. Coath, M. A. Dabbagh and S. A. Halgamuge, "Particle swarm optimization for reactive power and voltage control with grid-integrated wind farms", *Proc. IEEE Power Engineering Society General Meeting*, pp. 303–308, 2004.

[140] J. Mitra, S. Patra and S. Ranade, "Reliability stipulated microgrid architecture using particle swarm optimization", *Proc. 9th Int. Conf. Probabilistic Methods Applications Power Systems*, pp. 1–7, Sweden, 2006.

[141] I. Y. Chung, W. Liu, D. A. Cartes and K. Schoder, "Control parameter optimization for microgrid system using particle swarm optimization", *Proc. IEEE ICSET*, pp. 837–842, 2008.

[142] P. M. M. Bongers, "Experimental robust control of a flexible wind turbine system", *Proc. American Control Conference*, vol. 3, pp. 3214–3218, 1994.

[143] H. Zhihong, Z. Yuan and X.Chang, "State estimation for wind turbine system based on kalman filter", *IEEE 2nd Int. Sym. Systems and Control in Aerospace and Astronautics (ISSCAA)*, pp. 1–3, 2008.

[144] M. Steinbuch, "Dynamic modelling and robust control of a wind energy conversion system", *PhD Thesis, Delft University of Technology*, 1989.

[145] M. F. Sagfors and H. T. Toivonen, "H_∞ and LQG control of asynchronous sampled-data systems", *Automatica*, vol. 33, no. 9, pp. 1663–1668, 1997.

[146] J. Kennedy and R. Eberhart, "Particle Swarm Optimization", *Proc. IEEE International Conference on Neural Networks*, pp. 1942–1948, Australia, 1995.

[147] B. Panigrahi, A. Abraham and S. D. Eds, *Computational Intelligence in Power Engineering*, Springer-Verlag, Germany, 2010.

Vitae

- **Name:** Mohammed Saif ur Rahman.
- **Date/Place of Birth:** 5th October 1989 / Hyderabad, India.
- Received Bachelor of Engineering (BE) degree in Electronics & Instrumentation Engineering from Osmania University in 2011.
- Joined King Fahd University of Petroleum and Minerals in January 2012 in Systems Engineering Department (Automation and Control).
- **Contact details**: +966540394513
- **Present Address:** Department of Systems Engineering, King Fahd University of Petroleum and Minerals, P.O. Box 8656, Dhahran 31261, Saudi Arabia.
- **E-mail Address:** saif.rahman02@gmail.com